VASCULAR SMOOTH MUSCLE PRECURSOR CELL BEHAVIOR

IN NON-UNIFORM STRETCH ENVIRONMENTS

A Dissertation

by

WILLIAM JAMES RICHARDSON

Submitted to the Office of Graduate Studies of
Texas A&M University
in partial fulfillment of the requirements for the degree of

DOCTOR OF PHILOSOPHY

Approved by:

Chair of Committee,	James E. Moore Jr.
Committee Members,	Roland R. Kaunas
	Duncan J. Maitland
	Michael R. Moreno
	Emily Wilson
Head of Department,	Gerard L. Cote

December 2012

Major Subject: Biomedical Engineering

ABSTRACT

Cells in the body respond to mechanical loads in ways that are crucial to normal and disease physiology. Understanding these processes is difficult due to the complex mechanical environment *in vivo.* In this research, we have developed several cell-stretching devices capable of subjecting cell cultures to non-uniform stretch distributions in order to investigate pathological responses of vascular smooth muscle cells to physiologic stretches. 10T1/2 cells were cyclically stretched with these devices for 24 hours upon silicone membranes, PDMS tubes, and within 3D PEGDA hydrogels. After stretching, altered cell behaviors were measured, including orientation, proliferation (quantified by BrdU incorporation), and gene expression (quantified by real-time, RT-PCR).

Cells demonstrated marked changes in orientation, proliferation, and mRNA expression, which all varied with cellular location in the non-uniform environment. More specifically, increased orientation, increased proliferation, and more dramatically altered mRNA expression were found in regions of high, uniaxial stretch, relative to regions of low, near-equibiaxial stretch. These findings demonstrate the capabilities of graded stretch distributions to produce graded cell responses, indicating potentially localized smooth muscle cell behavior in a diseased artery. The novel devices employed herein will hopefully improve our understanding of these complicated cellular pathways, ultimately allowing for improved treatment or prevention of vascular disease.

DEDICATION

For my wife…

an ever-deep well of courage and comfort,

who has sacrificed much more than I have to complete this work

And for my daughter…

who inspires me to cure diseases, in hopes that she'll live forever

ACKNOWLEDGMENTS

This work could not have been completed without the significant efforts of many. Firstly, I owe much to my chair, advisor, and mentor, Jimmy Moore. With an ever-open door and an obvious care for my ultimate success, Professor Moore has generously provided invaluable counsel, guidance, motivation, opportunity, and perspective. His impact on this work and on my career is immeasurable, for which I will always be indebted. I also owe great acknowledgment to my committee members, Dr. Roland Kaunas, Dr. Michael Moreno, Dr. Duncan Maitland, and Dr. Emily Wilson. With broad expertise, this committee has greatly improved the quality of my work by sharing their ideas, critiques, and equipment whenever requested. I have learned much from the insightful discussions and impactful courses shared with these outstanding faculty members.

Many technical challenges were overcome with assistance from colleagues within the Department of Biomedical Engineering as well as the A&M Health Science Center. Specifically, I am grateful to Dr. Daisuke Mori for contributions to stretching device conception and formulation, Mrs. Shiva Yazdani-Beioky for help with initial device protocols, Mr. David Howell for assistance with cell culture and RT-PCR techniques, Dr. Rick Metz for assistance running preliminary RT-PCR samples, Ms. Mary Beth Browning and Dr. Elizabeth Cosgriff-Hernandez for guidance and training with PEGDA

hydrogel manufacturing, Mr. Dennis van der Voort for help with PDMS tube manufacturing as well as PEGDA hydrogel protocol formulation, and Mr. Sean Brocklehurst for assistance with cell culture and image analysis.

My past and present labmates are also worthy of acknowledgment for their contributions to this work and impact on my life. In particular, Dr. Joao Soares, Dr. Clark Meyer, Dr. Lucas Timmins, Dr. Ellie Rahbar, Mr. Franck Diaz, Mr. John Wilson, Mr. Mohammad Jafarnejad, Mrs. Samira Jamalian, and Dr. Danika Hayman all deserve much recognition in this regard.

On a more personal note, I am deeply grateful for the incredible love and support of all my family, who for many years have strengthened, encouraged, motivated, and challenged me to pursue what is good and do what is right. Finally, I must also acknowledge how honoring and humbling it is to spend my work exploring the intricate mechanisms of nature. Reveling in such wonder and awe has, for me, been worshipful to my gracious Creator.

TABLE OF CONTENTS

LIST OF FIGURES

FIGURE Page

LIST OF TABLES

1. INTRODUCTION

1.1 PROBLEM AND SIGNIFICANCE

Mechanical stimuli are well-established regulators of cell function in many processes of health and disease across many tissue types. Musculoskeletal, ocular, pulmonary, cardiac, vascular, neural, and embryonic tissues are all exposed to various mechanical loads including pressures, extensions, and shear due to fluid flow. The mechano-sensitivity of cells within these tissues is vital to their proper functioning, and deviation from normal mechanical loading is often correlated to the onset and progression of many diseases.

In the case of arterial walls, biomechanical cues are known to provide critical signals to modulate behavior in both normal and disease conditions. All cell types within the vessel (endothelial, smooth muscle, and fibroblast) are sensitive to their mechanical environment and can respond to physical loads in a number of ways including alignment, proliferation, apoptosis, protein expression, migration, and phenotype modulation (both differentiation and de-differentiation)[1; 2]. Alterations in these behaviors are significant contributors to arterial disease progression. For instance, during aneurysm development, cells remodel the artery's bulging wall in an adaptive way (via matrix-metalloproteinases, collagen synthesis and other mechanisms), seemingly in an attempt to maintain a preferred mechanical environment[3]. In the case of

atherosclerosis, a key step in the disease's development is the migration of smooth muscle cells (SMCs) from the media to the intima and subsequent proliferation and matrix synthesis[4]. A similar process occurs in response to interventional therapies such as balloon angioplasty and stenting[5]. In both the atherogenic and restenotic cases of intimal thickening, biomechanical stimuli such as blood flow patterns and intramural stress components are suspected as major contributors[6-9].

Cardiovascular disease (CVD) is the leading cause of mortality worldwide, responsible for 30% of deaths globally[10]. In the U.S., it results in 830,000 deaths every year (34.3% of total mortality) and costs the country an estimated $500 billion[11]. Moreover, CVD is not just an issue in the developed world; low and middle-income countries are over-represented in mortality figures, accounting for more than 80% of CVD-related deaths[10]. In our pursuit of treating and preventing these diseases, understanding how mechanical signals are detected, interpreted, and responded to by arterial cells is an important task.

Decades of studies have sought to elucidate the disease-related responses of vascular cells to the altered mechanical loads associated with disease development. The vast majority of these studies have simplified mechanical stimuli in attempts to isolate their effects on proliferation, protein synthesis, etc. Such setups include the application of shear stress over an endothelial cell (EC) monolayer in a parallel plate flow chamber (e.g., Levesque et al.), or the uniaxial and biaxial stretching of SMC on elastic substrates (e.g.,

Leung et al. and Cheng et al., respectively)[12-14]. These and many other investigations have revealed much important detail of cell mechanosensing ability and mechanisms. But despite the work in this area, many underlying processes are still poorly understood, and some significant features of *in vivo* mechanics remain without any previous investigation. One such feature is the presence of stretch gradients through the thickness of the artery wall.

The mechanical environment of an artery is complex due to heterogeneous and anisotropic material undergoing large deformations. The primary loads on the artery include flow-induced wall shear stress acting on the endothelium, axial tension acting throughout the wall due to longitudinal stretching and tethering, and pressure-induced hoop stresses acting in the radial and circumferential directions within the wall. As with any thick-walled incompressible tube, internal pressurization generates a higher degree of radial deformation at the inner radius compared to the outer radius. This results in gradients of both circumferential and radial stresses/stretches through the artery wall[15]. Residual stresses are known to exist in arteries, and these have been shown to homogenize the distribution of stresses in idealized, straight artery models[16]. However, non-uniform distributions still exist at particular locations within the vasculature, even when considering residual stresses. For example, inner radius stress in the later wall of the carotid sinus was estimated to equal four times that of the outer radius[17]. Interestingly, this ratio of inner radius to

outer radius stress positively correlated with intimal thickening in the carotid region[7].

Not only do stress gradients exist across the artery wall in normal conditions, several disease states have been predicted to exacerbate the non-uniform distribution. For example, higher pressures due to hypertension generate greater stretching of the intima compared to the adventitia[18]. Also, the development of atherosclerotic plaque can introduce heightened stress concentrations at the inner arterial wall[19]. Many interventional treatments for diseased vessels (e.g., balloon angioplasty and stenting) have also been predicted to magnify transmural non-uniformity of stress components[20-23]. Thus, it is clear that artery stresses are not always constant through the wall thickness and an increased degree of non-uniformity is correlated to several disease conditions. This finding has justified the investigation of cell behavior in the presence of such non-uniformity to reveal potential mechanobiological responses that may be contributing to pathologic developments.

1.2 EXPERIMENTAL STRATEGY

It is widely evident that the complex mechanical environment of an artery is intimately involved in disease progression. However, a gap remains in our understanding of the precise signals and mechanisms underlying this process. There is a dire need to improve this understanding if we hope to develop more

effective strategies to treat and prevent disease. In this research, we hope to elucidate cellular behavior in non-uniform stretch environments and its potential role in arterial disease progression, particularly atherosclerosis. Further, we hope our enhanced understanding will ultimately prove useful to improving the design of implantable devices or pharmaceutical targeting of molecular signaling cascades identified to be involved in these processes.

In order to investigate cell behavior in the presence of non-uniform stress distributions, we have developed a novel device capable of stretching cells in 2D and 3D circular constructs with tunable spatial gradients in circumferential and radial stretch components. The device design is based upon previous computational work done by our lab as well as Humphrey and colleagues solving the finite deformation problem for a circular elastomeric membrane with either a central defect or central fixation[24; 25]. When such membranes are radially deformed, circumferential and radial stretches are generated. The addition of either a defect or a fixation at the center of the membrane generates gradients in these stretch components across the radial direction (For detailed theory explanation, see Appendix 1).

The proposed study will be the first to apply controlled, physiologic-like stretch gradients to vascular cells, providing urgently needed insight into the cellular responses to altered mechanical environments as seen *in vivo*. An overall guiding hypothesis for this work is that subjecting vascular cells to the non-uniform stretch environments representative of disease-prone vessels will

lead to disease-related cell responses, and elucidate the spatial localization of these responses within the non-uniform stretch distribution. In this doctoral work, we seek to investigate cell orientation, proliferation, and phenotype modulation behaviors. Specifically, we hypothesize the following: 1) 10T1/2 cells will alter their alignment to a varying degree across the stretch gradient, with maximal alignment tendency in inner regions of high, uniaxial stretch and little alignment tendency in outer regions of near-equibiaxial stretch; 2) 10T1/2 cells will show increased proliferation rates to a varying degree across the stretch gradient; and 3) 10T1/2 cells will alter expression of mRNAs related to contractile-synthetic phenotype modulation to a varying degree across the stretch gradient. Understanding these pathological processes will enable a more accurately targeted treatment (either through implantable device design or pharmaceutical delivery) to inhibit or reverse disease progression.

1.3 SECTION SUMMARIES

The methods and findings of this project are divided into three main sections: stretching device capabilities and preliminary results; cellular orientation response; and cellular phenotype modulation response. These constitute Sections II, III, and IV, respectively, and each represent individual journal publications. That being the case, further introduction and discussion pertinent to the respective topics are included within each section. After these

three primary sections, the work will be concluded with additional discussion of overall significance, project limitations, and future directions of the research. Below are abstracts for the primary findings of the three results sections.

1.3.1 Section 2: Experimental Device and Preliminary Results

Herein, we present a cell-stretching device capable of subjecting cells to controllable gradients in biaxial stretch via radial deformation of circular elastomeric membranes. By including either a defect or a rigid fixation at the center of the membrane, various gradients are generated. Capabilities of the device were quantified by tracking marked positions of the membrane while applying various loads, and experimental feasibility was assessed by conducting preliminary experiments with 3T3 fibroblasts and 10T1/2 cells subjected to 24 hours of cyclic stretch. Quantitative real-time PCR was used to measure changes in mRNA expression of a profile of genes representing the major smooth muscle phenotypes. Genes associated with the contractile state were both upregulated (e.g., calponin) and downregulated (e.g., α-2-actin), and genes associated with the synthetic state were likewise both upregulated (e.g., SKI-like oncogene) and downregulated (e.g., collagen III). In addition, cells aligned with an orientation perpendicular to the maximal stretch direction.

1.3.2 Section 3: Orientation Response of 10T1/2 Mesenchymal Cells

Cellular orientation has long been known to alter in response to mechanical stretch. Herein, we investigated 10T1/2 orientation response in the presence of stretch gradients by employing two *in vitro* cell-stretching devices capable of subjecting cells to cyclic, non-uniform stretches upon the surface of either a circular elastomeric membrane, or a cylindrical PDMS tube. After 24 hours of cyclic stretch, cells on both devices showed marked changes in long-axis orientation, with tendencies to align parallel to the direction of minimal deformation. The degree of this response varied depending on location within the stretch gradients. These results demonstrated the feasibility of conducting cell mechanobiology investigation with the two novel devices, while also highlighting the experimental capabilities of non-uniform mechanical environments for this type of studies. Such capabilities include data collection for mechanobiological dose-response curves, signal threshold identification, and potential spatial targeting for drug delivery.

1.3.3 Section 4: Phenotype Modulation of 10T1/2 Mesenchymal Cells

Smooth muscle cell phenotype modulation contributes to neointimal formation during atherosclerosis and restenosis development. This process of cell dedifferentiation from a contractile to a proliferative, synthetic state has been shown to be related to mechanical loading conditions. Herein, we subjected

10T1/2 murine mesenchymal cells to non-uniform stretch environments representative of the arterial wall. After 24 hrs of cyclic stretch, cells on an elastomeric membrane demonstrated varied proliferation (assessed by BrdU incorporation) depending on location upon the membrane, with maximal proliferation occurring in a region of high, uniaxial stretch. Cells seeded in 3D PEGDA hydrogel constructs were also subjected to the non-uniform stretching regimen and demonstrated marked changes in mRNA expression of several phenotype-related proteins when compared to non-stretched controls. The results indicate that stretching induces a sort of 'hybrid' phenotype with contractile and synthetic markers being both upregulated and downregulated. Interestingly, expression of some mRNAs showed significantly different levels between different locations upon the stretched membrane. Along with the proliferation results, these data demonstrate the capability of non-uniform stretching devices to induce heterogeneous cell responses, potentially indicative *of in vivo* behaviors.

2. EXPERIMENTAL DEVICE AND PRELIMINARY RESULTS

2.1 INTRODUCTION

Mechanical loads can play crucial regulatory roles for both normal and diseased arterial cell functions. In order to develop adequate treatments for pathology, there is thus a need to connect specific mechanical stimuli to disease-related cell responses. This task is difficult partly due to the complex mechanical environment within the arterial wall. In an effort to identify the effects this loading has on arterial cells of all types, researchers over the past few decades have effectively employed a variety of experiments that sought to isolate mechanical stimuli. In general, those experiments subjected cells to a simplified mechanical load such as shear stress over an endothelial cell monolayer in a parallel plate flow chamber (e.g., Levesque and Nerem[12]), or uniform stretch (either uniaxial or equibiaxial) of smooth muscle cells (SMCs) and fibroblasts on elastic substrates (e.g., Leung et al.[13] and Lee et al.[26], respectively).

Previous research has led to a much improved understanding of cell mechanobiological behaviors. Such cell behaviors include alignment, proliferation, apoptosis, protein expression, migration, and phenotype modulation (both differentiation and de-differentiation)[1; 2]. Many of these behaviors are significant as they play key roles during disease progression. For

instance during atherosclerosis development, smooth muscle cells migrate from the media to the intima wherein they settle, undergo a phenotype shift, and proliferate (intimal hyperplasia)[4]. This process can also occur after interventions with angioplasty or stenting (termed restenosis in these cases), resulting in treatment failure[27].

A particular mechanical signal that has remained largely unaddressed in past mechanobiological studies is a gradient in stretch, rather than simply stretch magnitude. Applying internal pressure to a thick-walled incompressible tube results in a greater degree of stretching at the internal surface than the external. It is true that arteries are known to possess residual stresses, which act to homogenize the distribution of circumferential stress in idealized, straight artery models[16]. Still, this mechanism does not fully equalize stress distributions in all arteries. In the lateral wall of the carotid sinus, for example, inner wall stress is predicted to be four times that of the outer wall, even in the presence of residual stresses[17]. Intriguingly, the ratio of inner to outer wall stress correlated positively with early intimal thickening in this region[7].

A number of arterial pathology conditions can also exacerbate stress gradients therein. For example, higher pressures in hypertensive arteries generate greater stretching of the intima compared to the adventitia[18]. Also, interventions aimed at restoring flow to blocked vessels (e.g., balloon angioplasty and stenting) are predicted by numerous groups to magnify transmural gradients in stress[20-23]. Thus, despite compensatory mechanisms

such as residual stress, artery stresses are not always uniform across the wall, and a higher degree of non-uniformity (i.e., steeper gradient) is linked to conditions with altered cell behavior. We suppose that these gradients might be detected by arterial cells which respond in ways that contribute to disease progression and treatment failure. It should be noted that other tissues can exhibit non-uniform stress- and stretch-fields as well, for example skin after the introduction of a defect or a rigid fixation such as a suture[24; 25].

The notion that spatial distribution of mechanical signals can affect cell behavior has long been suggested, at least as early as Leung and colleagues[13] who, in concluding their landmark paper, identified “frequency, amplitude, or pattern of stress” as potential mechanical inputs for cell behavior. Supporting this hypothesis is the now well-known behavior of durotaxis, in which cells sense a gradient in stiffness of the substrate to which they are adhered, and preferentially migrate toward stiffer regions[28]. If cells possess the molecular machinery necessary to detect a gradient in substrate stiffness, then it would seem that the same or similar machinery might potentially be equipped to detect a gradient not in stiffness but in stress or stretch. This idea is further supported by the work of Raeber *et al.*, who noted fibroblast migration rates to be greatest in regions of the steepest strain gradient[29]. Despite suggestions that non-uniformity might play a role in mechanobiology, no study, to our knowledge, has decisively shown whether stretch gradients can act as a sufficient cue to modulate cell behavior.

Herein, we present the design and testing of a device capable of stretching cells on elastomeric membranes with tunable spatial gradients in stretch components. The device subjects cells to a non-uniform, biaxial stretch field by radially deforming a circular membrane with either a central defect or fixation boundary condition. Assessing cell behaviors within various regions of the non-uniform fields will help illuminate the effects of stretch gradients on disease-related cell behavior – a necessary task for a complete understanding of disease pathogenesis and important to the development of adequate treatment methods for cardiovascular disease, the leading cause of mortality in the United States[11].

2.2 METHODS

2.2.1 Device Design and Construction

The cell-stretching device (Fig. 2.1 and Fig. 2.2) uses a platen-displacement technique, as employed by others[26; 30], to radially deform circular, elastomeric membranes. A membrane with diameter of 80mm is cut from 0.25mm silicone sheeting, (Specialty Manufacturing Inc., Saginaw, WI) and clamped at its circumference to a Delrin ring. The ring suspends the membrane over a stationary, Teflon disc with rounded edges to facilitate smooth indentation. A stepper motor (Anaheim Automation, Anaheim, CA) is used to vertically displace the ring via a central post connector, which stretches the

membrane over the disk with uniform radial deformation. The stepper motor is controlled by SMC50WIN software (Anaheim Automation) that allows programming of precise levels of static or cyclic stretching. Excluding the motor, the stretching mechanism is enclosed in a Lexan box and incubated to maintain cell culture medium at 37°C and 5% CO_2. All device components can be sterilized by autoclave or UV exposure, and the assembled device fits on top of an inverted microscope for viewing through a coverslip mounted in the bottom of the culture box. By suspending the membrane over a stationary disc, cells can be kept in a constant focal plane for observation at any stretch level.

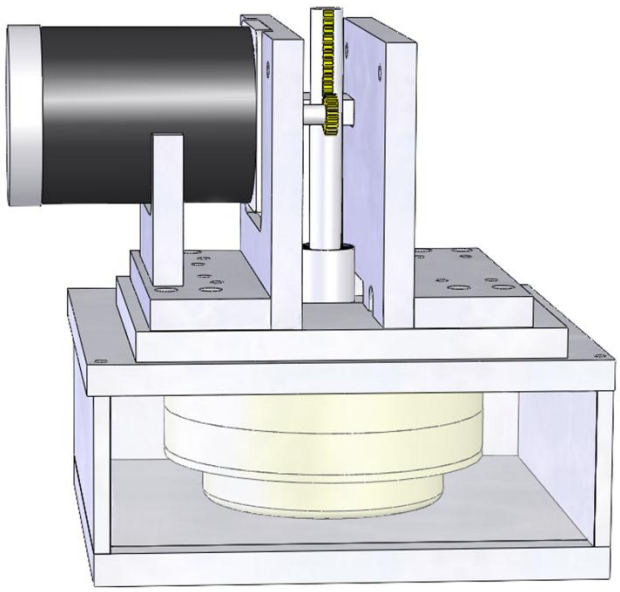

Fig. 2.1. Schematic of stretching device.
A computer-controlled stepper motor drives radial deformation of a circular membrane via stretching over an indenter disk. The assembly can be mounted on an inverted microscope for imaging through a coverslip in the bottom of the box.

To generate stretch gradients, a circular defect (hole) or fixation was placed at the center of the membrane. The production of non-uniform stretch environments in this way is based upon previous computational work done by our lab as well as Humphrey and colleagues[24; 25]. When circular elastomeric membranes are radially deformed, circumferential and radial stretches are generated. The addition of either a defect or a fixation at the center of the membrane generates gradients in these stretch components along the radial direction. The magnitude and shape of the stretch profile depend upon the size and type of the central boundary condition as well as the stretch imposed the outer circumference (based on the degree of vertical displacement, in our case). Defects are added to membranes using metal punches, and fixations are added by securing rigid rubber washers to the membranes' centers using Loctite 4206 medical device adhesive (Henkel Loctite Corp., Rocky Hill, CT).

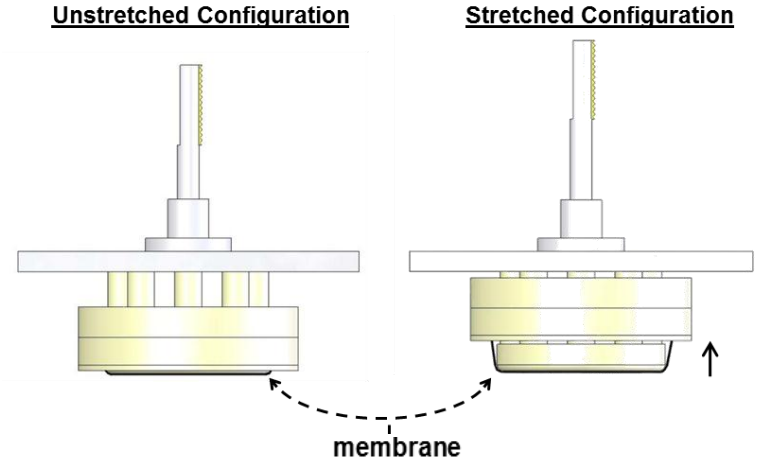

Fig. 2.2. Membrane deformation schematic.
The membrane's outer circumference is clamped and vertically displaced. This action radially deforms the cell-seeded membrane while holding it at a constant focal plane for imaging.

2.2.2 Membrane Stretch Characterization

Stretch profiles were characterized by tracking fiduciary markers on a membrane deformed by a range of motor displacements. Four cases were analyzed with varying boundary conditions: 2.8mm defect, 8.0mm defect, 2.2mm fixation, and 6.8mm fixation. The images were analyzed with ImageJ software (NIH), and positions calculated based on coordinates of the microscope stage and pixel coordinates within the image. Circumferential and radial stretch ratios were calculated as r/R (current/ original radial position) and Δr/ΔR, respectively. The resulting stretch data were used to find mechanical properties of the silicone membranes. Material parameters were estimated by fitting the data with the Mooney-Rivlin strain energy constitutive model in Eq. 2.1:

$$W = c_1(I_1 - 3) + c_2(I_2 - 3) \qquad \text{Eq. 2.1}$$

where W is the strain energy, I_1 and I_2 are the first and second invariants of the Right-Cauchy Green deformation tensor, and c_1 and c_2 are material parameters. The fitting procedure varied these parameters while iteratively solving the finite deformation problem as done previously[24], until a least squared error was achieved. Error was defined as the sum of the differences between experimental and theoretical circumferential stretch values at all loadings for both the small and large defect cases.

2.2.3 Cell Culture and Imaging

To demonstrate device feasibility for cell mechanobiology investigation, preliminary studies with fibroblasts and smooth muscle precursor cells were performed. Both NIH 3T3 mouse fibroblasts (ATCC CRL-1658) and mouse 10T1/2 cells (ATCC CCL-226) were grown and maintained in Dulbecco's modified Eagles medium with 10% fetal bovine serum, and 1% antibiotic-antimycotic (Invitrogen, Carlsbad, CA; Atlas Biologicals, Fort Collins, CO). 10T1/2 cells are a mesenchymal SMC line, traditionally used for phenotype studies due to the experimental ease of controlling their differentiation into mature SMCs[31]. Cultures were maintained at 37°C and 5% CO_2.

Membranes with the large defect boundary condition were coated for a period of 2 hours with bovine fibronectin (Sigma-Aldrich, St. Louis) diluted in PBS (Invitrogen) to a concentration of 50μg mL^{-1}. Cells were labeled with DiI lipid stain according to manufacturer's protocol (Invitrogen), seeded at a density of 10^4 cm^{-2}, and allowed to adhere for 24 hours. Subsequent to cell attachment, membranes were cyclically stretched for 24 hrs at 1Hz and a medium-level loading (4% circumferential stretch at outer edge achieved by 5.0 mm vertical displacement of the clamped ring). A Nikon TE-2000 Inverted Fluorescent Microscope equipped with a Nikon C-FL FITC HYQ filter set (Nikon Instruments, NY) was used to image the cells at 40x magnification.

2.2.4 Preliminary Cell Response Analysis: Gene Expression

The ultimate goal of this research is to link particular mechanical stimuli to specific cell behaviors. Thus, we need to demonstrate the ability to measure such behaviors during and after stretching with the device while maintaining cell viability. In addition to imaging cells, gene expression for a variety of phenotype-related proteins was quantified using quantitative reverse-transcription polymerase chain reaction (RT-PCR) with primers to a number of genes representing various aspects of smooth muscle phenotypes (Table 2.1). Subsequent to 24 hrs of stretching, membranes were cut into two concentric circles representing the inner and outer regions of the membrane. RNA from stretched cells in each region was collected separately by lysing and scraping using the RNEasy kit (Qiagen) with one column DNase digestion. Primers were designed using Primer Express software (ABI) using GeneBank annotated sequences. Real time RT-PCR was performed with 2X SYBR® Green Mastermix (ABI). Expression levels were calculated using a $\Delta\Delta$Ct method with results normalized to GAPDH levels. The expression of a set of genes representing the differentiated phenotype (e.g. alpha smooth muscle actin, gamma smooth muscle actin, caldesmon, smoothelin), and the synthetic/proliferative phenotype (e.g. pro-collagen I, pro-collagen III, biglycan, c-Fos, Egr-1, PDGF β, SKI-like oncogene) were quantified for each region.

Gene expression experiments were repeated for a total of 5 runs, in addition to 5 control runs (i.e., cells cultured without stretch). For statistical

analysis, a two-tailed, paired student's t-test was conducted on ΔΔCT values comparing stretched cell expression to unstretched cell expression. Statistical significance was defined as $p < 0.05$.

Table 2.1. Gene descriptions and primer sequences for RT-PCR analysis.

Gene Name	Function	Primer Sequence
Biglycan	Extracellular matrix component involved in deposition of collagen, cell adhesion, activation of growth factors.	F: 5' – CGC CCT GGT CTT GGT AAA CA – 3' R: 5' – TTC CGC AGA GGG CTA AAC G – 3'
Caldesmon	Calmodulin- and actin-binding protein that plays an essential role in the regulation of cell contraction.	F: 5' – AAC AAG TCA CCT GCT CCC AAG – 3' R: 5' – GAA GTG ACC TAT CCA CAG ATT GC – 3'
Calponin	Calcium binding protein that inhibits the ATPase activity of myosin in smooth muscle.	F: 5' – CGA TCC CAA GTA CTG CCT GAA – 3' R: 5' – TTG TGC GGG TGG TGA TTG – 3'
Early growth response 1	DNA binding domain that functions as a transcriptional regulator.	F: 5' – GCC GAG ATG CAA TTG ATG TCT – 3' R: 5' – TGT CCA TGG TGG GTG AGT GA – 3'
FBJ osteosarc. oncogene	An immediate early gene encoding a nuclear protein involved in signal transduction.	F: 5' – GGG AGG CCT TAC CTG TTC GT – 3' R: 5' – CAG ATG TGG ATG CTT GCA AGT C – 3'
Inhibitor of DNA binding 1	Inhibits transcriptional activation ability of basic HLH proteins playing a role in cell growth and differentiation.	F: 5' – TGC TAC TCA CGC CTC AAG GA – 3' R: 5' – GGA TCT CCA CCT TGC TCA CTT T – 3'
Inhibitor of DNA binding 2		F: 5' – CGC TGA CCA CCC TGA ACA C – 3' R: 5' – TCG ACA TAA GCT CAG AAG GGA AT – 3'
Integrin, alpha V	Joins with beta 3 to form a fibronectin receptor participating in cell-surface mediated signaling.	F: 5' – CGA CAT TGA CGG GCC AAT – 3' R: 5' – CGC CGC TGT GTC ATT CTT TT – 3'
Integrin, beta 3	Beta unit of a fibronectin receptor to participate in cell-surface mediated signaling.	F: 5' – CGC ATC CCA TTT GCT AGT GTT – 3' R: 5' – GTC GGT GCC AAT GTG ACA GT – 3'
Plasminogen Activator Inh.	Inhibitor of fibrinolysis.	F: 5' – GGC ACA GTG GCG TCT TCC T – 3' R: 5' – TGC CGA ACC ACA AAG AGA AAG – 3'
Platelet derived growth factor	Mitogenic factor for cells of mesenchymal origin.	F: 5' – AGC TCG GGT GAC CAT TCG – 3' R: 5' – TCA TGG GTG TGC TTA AAC TTT CG – 3'
pro-Collagen 1	Fibril-forming collagen found in most connective tissues abundant in bone, cornea, dermis and tendon.	F: 5' – CCC CGG GAC TCC TGG ACT T – 3' R: 5' – GCT CCG ACA CGC CCT CTC TC – 3'
pro-Collagen 3	A fibrillar collagen found in extensible connective tissues such as skin, lung, intestine and vasculature.	F: 5' – CCT GGA GCC CCT GGA CTA ATA G – 3' R: 5' – GCC CAT TTG CAC CAG GTT CT – 3'
SKI-like oncogene	Negative regulator of TGFβ signaling. Binds to nuclear Smad complexes, repressing transcriptional activities.	F: 5' – ATA CAC CAT CGG GAA TGG AA – 3' R: 5' – CAT GAT CTT CCC CTT GTC GT – 3'
SMAD family member 1	Signal transducer and transcriptional modulator that mediates BMP signaling.	F: 5' – CCT GTG GCT TCC GTC TCT TG – 3' R: 5' – AAT AGT TGG TCA CAG AGG TCA AGT – 3'
SMAD family member 5	Receptor regulated SMAD involved in BMP signaling.	F: 5' – CAC GCT TTT GGT ATC TAC TGA CTT – 3' R: 5' – ATT TCT CTT CCT CGT CAC CTT GT – 3'
Smooth muscle Actin alpha 2	Found in muscle tissues and are a major constituent of the contractile apparatus.	F: 5' – ACG AAC GCT TCC GCT GC – 3' R: 5' – GAT GCC CGC TGA CTC CAT – 3'
Smooth muscle Actin gamma 2	Component of the cytoskeleton that acts as a mediator of internal cell motility.	F: 5' – GCC CTG GAT TTC GAG AAT GA – 3' R: 5' – CCA TCA GGC AAC TCG TAG CTT – 3'
Smoothelin	Structural protein found only in contractile smooth muscle cells. It associates with stress fibers.	F: 5' – CGA GAG CCG AAG CAA TGT GG – 3' R: 5' – CGC TCG GTT TTG GTA ACT GTG – 3'
Snail homolog 1	Zinc finger transcriptional repressor downregulating expression of ectodermal genes within the mesoderm.	F: 5' – CAC CCT CAT CTG GGA CTC TC – 3' R: 5' – CTT CAC ATC CGA GTG GGT TT – 3'
Transgelin	A transformation and shape-change sensitive actin cross-linking/gelling protein.	F: 5' – GAG GGA TCG AAG CCA GTG AA – 3' R: 5' – TGA GCC ACC TGT TCC ATC TG – 3'
Tropomyosin 1	An actin-binding protein involved in contractile system of muscle cells and cytoskeleton of non-muscle cells.	F: 5' – TGC TGA CCG GAA GTA TGA AG – 3' R: 5' – TCA AGT TGT TCG TCA CCG TT – 3'

2.3 RESULTS

2.3.1 Device Capabilities

To analyze the stretch environments produced by the device, marked positions on membranes were tracked and measured before and after deformation. The results match very closely to the curves predicted by the model solutions, and the membranes follow the expected behavior as predicted previously[24; 25] (Fig. 2.3). For the defect cases, circumferential stretch ratio is greater than radial stretch ratio with the maximum difference occurring at the center edge. As radial position increases, circumferential stretch decreases (quickly at first, then more gradually) while radial stretch increases (in like manner) so that the outer edge is nearly equibiaxial. For the fixation cases, the same trend occurs but with the stretch components reversing places (i.e., radial stretch is greater and decreases with radial position; circumferential stretch is lesser and increases with position).

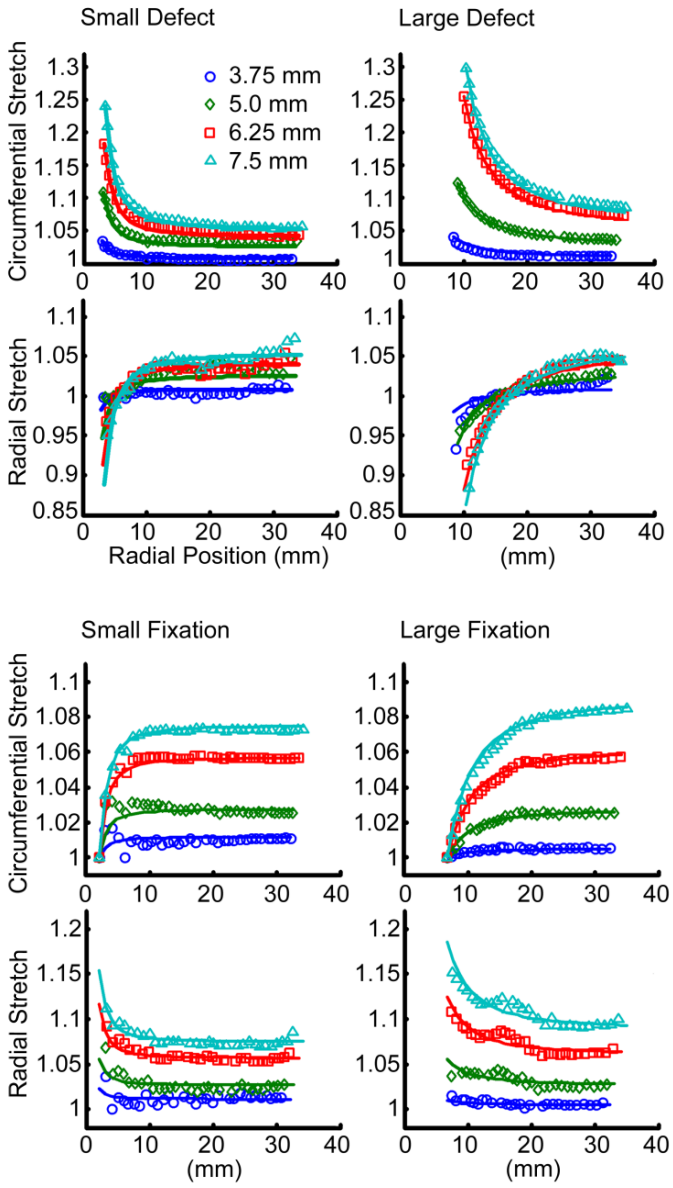

Fig. 2.3 Device stretching capabilities.
Deformation profiles for various central boundary conditions. Membranes were stretched via vertical displacement (3.75-7.5 mm) of the outer circumference. Stretch ratios were calculated from tracked positions of feduciary markers, and fit by iteratively solving the corresponding finite deformation problem using a Mooney-Rivlin strain energy function.

The stretch profiles were modulated by varying the size of the inner boundary or the load placed on the membrane's outer circumference. Increasing the vertical displacement of the clamp ring from 3.75 – 7.5mm expanded the ranges of stretch magnitude experienced across the membrane for all cases (Fig. 2.3). For a small defect at 3.75mm displacement, circumferential stretch varied from 3.4% at the inner boundary to 0.7% at the outer. At 7.5mm displacement, this range increased with circumferential stretch varying from 24.1% (inner) to 5.6% (outer). For a large defect, the same trends occur over greater ranges. For instance, circumferential stretch at 7.5mm displacement varies from 29.8% at the inner boundary to 8.6% at the outer. Importantly, this variation across the membrane for a large defect occurs more gradually than for a small defect, resulting in profiles with less-steep gradients. At the inner boundary, circ. stretch decreases 9.9% mm^{-1} with the small defect but only 6.1% mm^{-1} with the larger defect (both stretched with 7.5mm displacement). The effects of loading and boundary size on stretch ranges and gradients are generally the same for fixation cases as well, though circumferential and radial stretch components are reversed in magnitude.

2.3.2 Preliminary Cell Responses

To assess the feasibility of using the above stretches for cellular investigations, membranes with a large defect were seeded with either 3T3 fibroblasts or 10T1/2 cells and cyclically stretched for 24 hrs from 0 - 4% outer

circumferential stretch (5.0 mm vertical displacement) at a frequency of 1 Hz. Fluorescent images of both cell types after the stretching period showed healthy, viable cells still firmly attached to the substrate. There was a strong alignment tendency of fibroblasts in the radial direction as seen in Fig. 2.4, corresponding to the direction of lowest stretch.

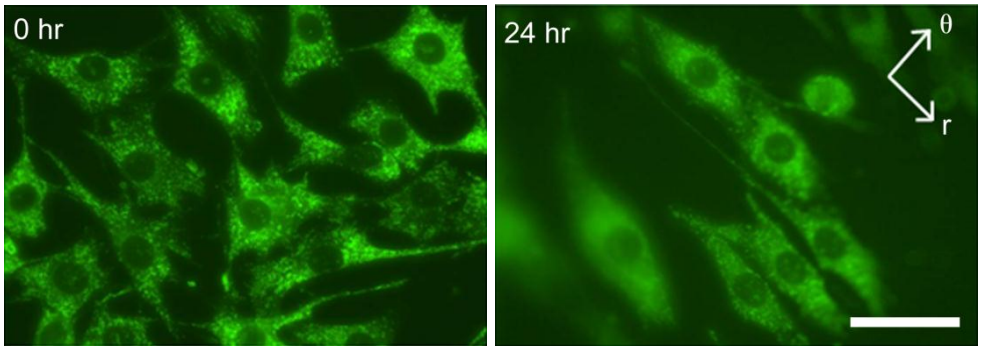

Fig. 2.4. 3T3 fibroblast alignment in response to 24 hrs of cyclic stretch.
Fibroblast cells oriented parallel to the minimal stretch component (radial stretch). These images are not taken at the same location but are representative of the overall cell population. Scale bar is 50 μm.

Gene expression of phenotype-related proteins quantified by RT-PCR revealed a mix of contractile and synthetic markers affected to various degrees (Table 2.2). Over repeated experiments (n=5), several mRNAs for genes associated with a mature contractile phenotype were downregulated including alpha-2-actin, gamma-2-actin, caldesmon, and alpha-V-integrin. However, other contractile phenotype markers were upregulated or unchanged (e.g., calponin, smoothelin, beta-3-integrin, and tropomyosin). Proteins associated with the de-

differentiated, synthetic phenotype also showed mixed responses. Collagen III and collagen I were significantly downregulated, while SKI-like oncogene, EGR-1, and c-Fos were upregulated and PDGF-beta remained unaffected by stretch. In most cases (except EGR-1 and c-Fos), there is little difference between expression in the inner and outer regions of the membrane.

Table 2.2. Gene expression of 10T1/2 cells quantified by RT-PCR.
After 24 hours of stretch, a cell-seeded membrane was separated into inner and outer concentric regions corresponding to high magnitude, 'simple uniaxial stretch; within the outer region, and a lower magnitude, near-equibiaxial stretch, respectively. Expression was quantified relative to GAPDH expression and normalized by static control.

Gene	Region	Stretch-to-Static Expression Ratio	P Value
Downregulated:			
Inhibitor of DNA binding 2	High, Uniaxial	0.11	0.002
	Low, Biaxial	0.11	0.001
Collagen III-α1	High, Uniaxial	0.20	0.040
	Low, Biaxial	0.20	0.064
Actin-α2	High, Uniaxial	0.23	0.001
	Low, Biaxial	0.21	0.001
Actin-γ2	High, Uniaxial	0.28	0.160
	Low, Biaxial	0.37	0.003
Collagen I-α2	High, Uniaxial	0.31	0.015
	Low, Biaxial	0.40	0.085
Caldesmon 1	High, Uniaxial	0.43	0.002
	Low, Biaxial	0.45	0.006
Inhibitor of DNA binding 1	High, Uniaxial	0.45	0.016
	Low, Biaxial	0.44	0.014
Integrin-αV	High, Uniaxial	0.61	0.063
	Low, Biaxial	0.73	0.043
Upregulated:			
Calponin 1	High, Uniaxial	17.06	0.015
	Low, Biaxial	19.66	0.005
Early growth response 1	High, Uniaxial	7.14	0.037
	Low, Biaxial	4.33	0.053
Serpin peptidase inhibitor 1	High, Uniaxial	3.70	0.010
	Low, Biaxial	2.79	0.048
c-Fos	High, Uniaxial	3.16	0.008
	Low, Biaxial	1.78	0.165
SKI-like oncogene	High, Uniaxial	2.08	0.028
	Low, Biaxial	1.89	0.002
Not significant (p> 0.05):			
Biglycan, Integrin-β3, MMP-2, PDGF-β, Smad1, Smad5, Smoothelin, Snail homolog 1, Transgelin, Tropomyosin 1			

2.4 DISCUSSION

The primary aim of this research is to add tunable, physiologic gradients to a biaxial cell stretching environment, thereby providing a better reproduction of *in vivo* conditions. By deforming a circular elastomeric membrane modified with either a defect or fixation central boundary condition, we are able to generate a variety of stretch gradients to which cells can be subjected. Historically, a variety of devices have been used to subject SMCs to solid mechanical stress. The first and simplest of these devices deformed rectangular elastic substrates (seeded with cells) by clamping on opposite ends and uniaxially stretching[13]. Additional complexity and *in vivo* relevance has been achieved with biaxial stretching devices such as the Flexercell apparatus, which became commercially available in the 1990s (Flexcell Int., Cary NC). This design uses vacuum pressure to pull on the bottom of circular substrates in culture dishes, resulting in a biaxial stretch environment. The stretch values generated with the Flexercell have been shown to vary tremendously depending on radial position[32]. However, the variation is a result of the device geometry and not a design feature. The majority of researchers using those and other devices seek to homogenize the stretch field as much as possible in an attempt to better relate cell response to mechanical signals[26; 30; 33].

Recently, a few studies have developed novel devices for studying gradient effects. Ohashi and colleagues subjected ECs to a gradient in strain

magnitude by uniaxially deforming a rectangular membrane with a circular cover glass embedded into its center[34]. They claim that stress fibers developed and nuclei localized at regions within a cell that were subjected to higher strain, but do not quantify these behaviors, nor state whether this was the case for the majority of cells or just a sporadic finding. Yung et al. used a similar setup for their “cellular strain assessment tool”, but after characterizing the mechanical environment of the uniaxial stretching device, they resumed a focus on homogeneous strain environments[35].

The most complete investigation of cell behavior in non-uniform stretching environments was conducted by Billiar and colleagues[36]. Fixing a circular glass coverslip to the center of a Flexercell substrate created gradients in radial and circumferential stretches across radial position. Human dermal fibroblasts subjected to this environment for two days showed alignment perpendicular to maximal stretch. The extent of orientation varied with the cell’s location on the substrate, effectively demonstrating the benefit of non-uniform environments to correlating cellular behavior responses to many particular levels of stretch magnitude. This can aid the generation of dose-response curves and improved mechanobiological models (a need that has been highlighted by recent reviews[3; 8]), as well as help identify potential signaling thresholds.

The device presented herein, though similar to Balestrini et al.’s, improves upon previous cell-stretching systems by generating a large variety of non-uniform stretching profiles. It is noteworthy that our device is capable of

deforming circular membranes with a central defect, which simulates the *in vivo* environment better than the fixation case by generating circumferential stretch greater than radial stretch as well as a region of compressive radial stretch near the center. Both of these conditions are true in the native artery. Importantly, the magnitudes and gradients achievable by our device cover much of the range predicted in healthy arteries[17; 37], during high-pressure angioplasty[20], and in atherosclerotic vessels[19], as listed in Table 2.3.

Table 2.3. Literature estimates of *in vivo* stretch gradients.

Reference	Condition	Residual Stress	Estimated $\nabla\lambda_{max}$
Delfino et al., 1997	Carotid bifurcation	Yes	13.4 (%/mm)
Younis et al., 2004	Carotid bifurcation	Yes	5.0
Holzapfel and Gasser, 2007	Balloon angioplasty during…		
	Inflation	Yes	2.3
	Peak Pressure	Yes	13.2
	Deflation	Yes	8.1
Hayashi and Imai, 1997	Atherosclerotic artery	No	53.6
Proposed Device	---	---	*≤ 22.0*

The usefulness of a stretching device is ultimately dependent on its ability to elicit cell responses to various loading conditions. 3T3 fibroblasts stretched for 24 hrs showed a strong orientation response to stretch, aligning in the radial direction upon a membrane, which corresponded to the direction of lowest stretch. This finding agrees with the vast amount of literature that has shown both fibroblasts and SMCs orient perpendicular to the direction of maximal stress or strain[38-41].

To demonstrate the feasibility of the device in studying effects of stretch on SMC phenotype, 10T1/2 cells were stretched for 24 hrs and RT-PCR was used to quantify gene expression. Fully differentiated vascular SMCs are characterized by a quiescent, strongly contractile state. However, they maintain a plasticity that allows them to respond to local environmental stimuli and undergo profound changes in phenotype. A shift in SMC phenotype from a differentiated contractile state to an undifferentiated synthetic state is a key process in the development and failed treatment of atherosclerosis, the deadliest disease in the US[11].

Due to differences in the stretching environment, cell type, stretch amplitude, stretch frequency and stretching duration, a number of groups over the past four decades have shown a “mixed bag” of results linking stretch to SMC phenotype[13; 42-45]. These studies demonstrated varied cell behaviors with some stretching regimens causing a shift toward the synthetic state, some causing a shift toward the contractile state, and many causing cells to enter a hybrid phenotype where both synthetic and contractile proteins are produced. It seems that 10T1/2 cells in our system indeed express a sort of hybrid phenotype, up- and down-regulating proteins related to both states of differentiation. In most cases, these changes in expression were significant over unstretched control cells. However, with the exceptions of EGR-1 and c-Fos, there was not much difference between cell expression in the inner and outer regions corresponding to high uniaxial stretch and lower biaxial stretch,

respectively. This could be directly due to a lack of cell-sensitivity to the difference in mechanical signals between those regions, or indirectly due to paracrine effects in the media. In either case, future studies can use more varied mechanical stimuli and employ controls which are treated with the same media in order to reveal more precisely the effects of stretch and stretch gradient on SMC gene expression and phenotype shift.

In summary, we have designed and tested a cell-stretching device for novel investigation of the effects of stretch gradients on cell behavior. By radially deforming an elastomeric, circular membrane with either a central defect or rigid fixation, gradients in biaxial stretch components are generated. These gradients can be fine-tuned by varying the type and size of the boundary condition as well as the load placed on the outer circumference of the membrane. Thus, experimental cases were identified which can separate the effects of stretch magnitude from the effects of stretch gradient. Both 3T3 fibroblasts and 10T1/2 cells were subjected to a sample stretching regimen and displayed good viability while altering their orientation and phenotype-related protein expression. Understanding these and other pathological processes can hopefully enable a more accurately targeted treatment to heal or inhibit disease, either through implantable device design or pharmaceutical delivery.

3. ORIENTATION RESPONSE OF 10T1/2 MESENCHYMAL CELLS

3.1 INTRODUCTION

It is widely known that cells of many types alter their behaviors in response to mechanical stimulation. One such behavior is the altered cellular orientation dependent upon the direction of substrate stretching. Numerous studies with endothelial cells (ECs), fibroblasts, and smooth muscle cells (SMCs) have demonstrated that, *in vitro*, cells will tend to align parallel to the direction of minimal stretch[38-41; 46; 47]. In true uniaxial environments, this direction is perpendicular to the direction of loading, but 'simple uniaxial' setups actually subject cells to a biaxial environment due to lateral compression, in which cases the direction of minimal stretch is slightly off-axis. The degree of alignment response typically correlates to the magnitude and duration of stretch imposed upon the matrix, or the relative ratio of principal stretch components in biaxial stretch cases[36; 47]. The mechanism for this orientation response is suspected to be mediated by the remodeling of the cytoskeleton via stretch-dependence of actin assembly and disassembly rate constants[48].

Understanding the orientation behavior of cells is important as it plays vital roles in numerous physiologic and pathologic conditions. For instance, SMCs in the artery wall are oriented primarily in the circumferential direction in a slightly helical fashion, which is important to function as it optimizes the cells'

ability to control lumen size via contraction and dilatation[49; 50]. Also, arterial EC alignment is indicative of vascular health as randomly orientated cell populations correlate to atherogenic behaviors[51]. Our ability to understand cell orientation behavior is important to understanding disease development as well as controlling this behavior to achieve better function with engineered tissue constructs.

Linking cell orientations to their local mechanical stimuli within the body, however, is made difficult by the complexity of stress and strain environments *in vivo*. For example, morphogenic structures have been shown to include large spatial variations in stress and strain. Taber and colleagues quantified the strain-environment of the chick head fold during embryological development revealing stark non-uniformities[52]. In computational models, these distributions have been predicted to play important roles in achieving final tissue form[53]. Similarly, Chen and colleagues have demonstrated how spatial variation in cell-generated traction forces can arise within cell populations cultured on micropatterned surfaces of various shapes, indicative of the diverse geometric forms taken by developing tissues[54].

In addition to the morphogenic environment, stretch in a mature artery wall can also be highly non-uniform, depending on location in the vasculature, presence of an atherosclerotic plaque, or implantation of a stent[17; 22; 23; 55]. In these cases, stretch at the inner wall is much greater than stretch at the outer wall, resulting in a dramatic stretch gradient through the artery thickness. After

stent implantation, there is also an introduction of stress concentrations at the ends of the implant. These stress concentrations result in gradients of stress along the axial direction of the artery, with high stresses at the edge of the stent and lower stresses farther from the stent. This stark non-uniformity is presumably pathogenic and therefore, as a result, stent designs that seek to smoothen the transition of stress from the stented region to the nearby non-stented region of the artery have been developed and tested. In particular, the "compliance matching stent" (CMS) of Berry et al. and Rolland et al. showed improved performance over a standard non-CMS stent, with inhibited local tissue restenotic processes after implantation in swine models[56; 57]. The detailed cellular mechanisms responsible for these beneficial effects, however, remain unclear, limiting our ability to optimize similar stent designs or develop pharmaceutical regimens to prevent end-stent restenosis. Thus, there remains a need to investigate the effects of *in vivo* loading conditions on particular cell behaviors related to disease.

Although the body's mechanical environments are highly non-uniform and spatially complex, the bulk history of cell stretching experiments has employed rather simple mechanical stimuli, most often uniaxial loading of cell-seeded constructs[33]. Such studies have provided crucial results to help develop our understanding of mechanobiological processes. Still, there remains a need to subject cells to more physiologic stretching environments, namely non-uniform stretch fields. We have previously designed and tested a cell-stretching device

capable of fine-tuning stretch gradients across 2-D elastomeric membranes[58]. Herein, we describe an additional device capable of subjecting cultured cells to a longitudinal stretch gradient upon a tubular substrate. We also analyze the orientation responses of mesenchymal mouse cells when stretched on both devices.

3.2 METHODS

3.2.1 Membrane Device Design

The device used to stretch cells cultured on elastomeric membranes has been previously described[58]. Briefly, a thin circular membrane is radially deformed in all directions via vertical displacement of its outer circumference over a stationary Teflon platen (Fig. 3.1). The deformation is driven by a computer-controlled stepper motor (Anaheim Automation) with a rack and pinion gear connected to the clamped membrane. The motor is controlled by manufacturer-provided software (SMC50WIN) allowing precise programming of cyclic stretch amplitude and frequency. Once the device is assembled, the membrane is suspended “upside-down” in an enclosed Lexan box containing culture medium, and the box is kept inside an incubator at 37°C and 5% CO_2. A glass coverslip is mounted in the bottom of the box to allow imaging of the cells with an inverted fluorescent microscope (Nikon TE-2000, Nikon Instruments).

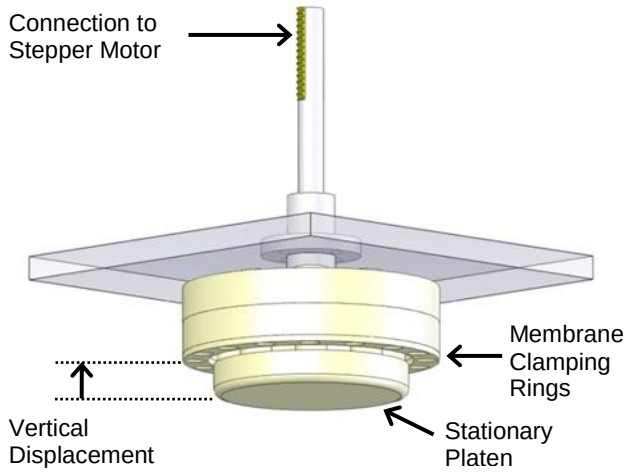

Fig. 3.1. Membrane device schematic.
A circular elastomeric membrane was radially deformed by stretching over a stationary platen driven by a computer-controlled stepper motor. Vertically displacing the clamped outer circumference of the membrane produces uniform radial loading of the membrane's edge.

Radial deformation of a circular elastomeric membrane generates both radial and circumferential stretches. By punching a defect (circular hole) in the center of the membrane, gradients in each of these stretch components are produced. The profiles of stretch gradients in such cases depend upon the magnitude of the displacement at the outer edge, as well as the outer and inner radius values. The solution for this finite-deformation problem has been previously solved by David and Humphrey, and the capabilities of this stretching device have been previously tested and reported[24; 58]. Importantly, with the inclusion of a central defect, circumferential stretch (λ_θ) ranges from high values at the inner edge to lower values at the outer edge, while radial stretch (λ_r) ranges from low values at the inner edge to higher values at the outer edge, but everywhere $\lambda_r < \lambda_\theta$. In this study, membranes with outer radius = 50mm and

inner radius = 7.5mm were stretched with stepper-motor displacement chosen to achieve ~11% circumferential stretch at the inner edge.

For cellular orientation and stretch direction comparison, the direction of minimal stretch is calculated for every point across the membrane. For this calculation, the equation for composite stretch, λ, is derived from the deformation gradient tensor **F**, yielding the following:

$$\lambda^2 = \lambda_r^2 cos^2(\phi) + \lambda_\theta^2 sin^2(\phi) \qquad \text{Eq. 3.1.}$$

where ϕ equals the angle measured off of the radial axis. Taking $\lambda = 1$ (minimal perturbation of cell cytoskeleton), the angle of least stretch can be calculated:

$$\phi = arcsin\left(\sqrt{\frac{1-\lambda_r^2}{\lambda_\theta^2-\lambda_r^2}}\right) \qquad \text{Eq. 3.2.}$$

Since λ_r and λ_θ vary with radial position, ϕ is a function of position as well. Also, note that Eq. 2 is only valid for $\lambda_r \leq 1$. Where $\lambda_r > 1$, of course $\phi = 0°$ since $\lambda_r < \lambda_\theta$ everywhere (i.e., direction of least stretch is in the radial direction).

3.2.2 Tube Device Design

To subject cells to longitudinal stretch gradients on tubular constructs, a tube-stretching device was built based upon tube inflation theory used by Mohammad et al. and Rachev et al.[59; 60]. Briefly, a thin elastomeric tube was

implanted with an oversized, cylindrical rigid insert (Fig. 3.2). When the tube is subsequently inflated by an intramural pressure wave, circumferential and longitudinal stretches are generated. The oversized insert introduces a boundary condition resulting in large variations of these stretch components depending on their location upon the tube.

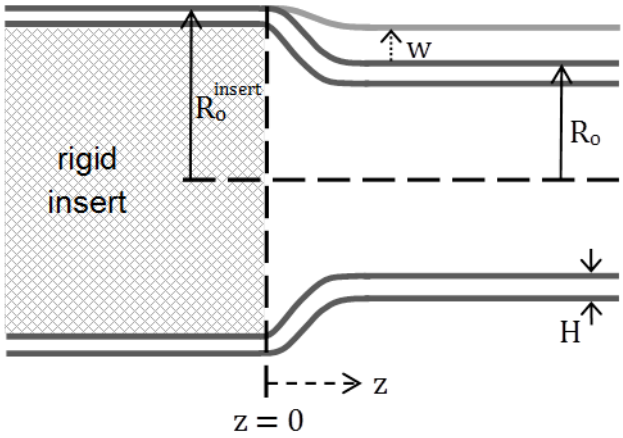

Fig. 3.2. Tube profile inflated over a rigid insert.
Thin-shell theory was used to calculate radial wall displacement, w, as a function of the longitudinal position, z, relative to the edge of the insert.

Tubes were manufactured using Sylguard 186 (Dow Corning, MI), a silicon based polymer solution. After mixing with a curing agent (10:1 ratio of polymer base:curing agent), the mixture was poured into a mold consisting of FEP shrink tubing (ID=5.25mm) mounted around a stainless steel inner mandrel (D=4.4mm). Once poured, the elastomer was cured by heating in an oven at 80°C overnight. After curing, the shrink tubing was removed, and the tube was slid off the inner mandrel using ethanol as a lubricant. Final dimensions of the

cylindrical tube were 50mm in length with 5.25mm outer diameter and 4.4mm inner diameter (0.425mm thickness). For the rigid insertion, a cylindrical glass segment (10mm in length, 6.0mm outer diameter,) was manually inserted and positioned at the center of the tube. Post manufacturing, tubes were autoclaved in deionized water, hydrophilized by soaking in 70% sulfuric acid for 60 seconds, autoclaved again, and stored in DI water.

For inflation, tubes were canulated and secured to metal tube attachments, and connected to a flow loop consisting of a gear pump (Ismatec BVP-Z; Ismatec SA, Switzerland) driven by a function generator (BK Precision 4016; BK Precision, CA), a glass compliance chamber, a resistance valve and a supply reservoir (Fig. 3.3). These elements allow for a wide variety of pulsatile pressure waveforms to be generated for tube inflation. The tube and its connections were housed inside a culture chamber to hold cell-culture medium. This box also contained a glass coverslip on the bottom surface to allow for imaging with a Nikon TE-2000 inverted fluorescent microscope (Nikon Instruments, Japan).

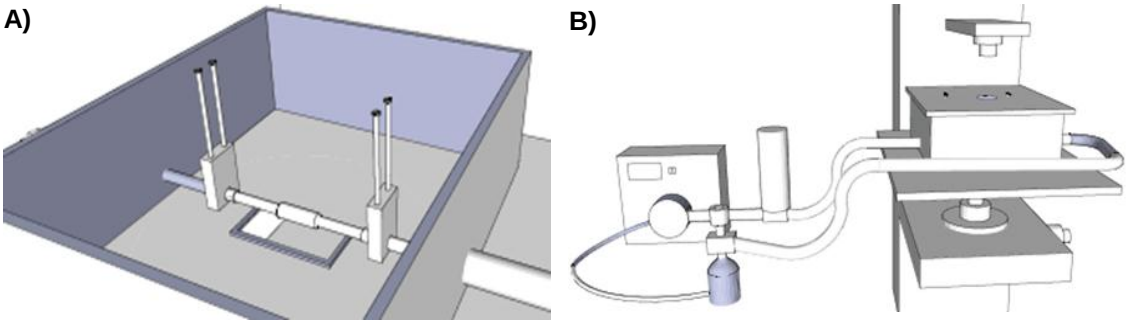

Fig. 3.3. Tube experimental setup.
A cell-seeded PDMS tube containing an oversized glass insert within a short segment of the tube was enclosed within a culture box (A) to contain cell-culture medium, with a glass coverslip in the bottom of the box to allow imaging via inverted microscopy. The connected flow loop (B) consisted of a gear pump driven by function generator, a capacitance reservoir, and a resistance valve over a supply reservoir.

3.2.3 Tube Device Deformation Field

As in Mohammad et al. and Rachev et al., thin-shell theory is applied to estimate deformations of a cylindrical tube stretched over a rigid insert[59; 60]. The 'thin tube' assumption requires the thickness:radius ratio to be negligibly small, allowing for simplification of the governing motion equation derived from equilibrium and displacement boundary conditions. By also assuming the tube is linearly elastic, isotropic ($E_\theta = E_r = E$), and incompressible ($\mu = 0.5$), the equilibrium equation for the case of tube deformation by a uniform radial pressure reduces to a 4th-order, linear ODE of radial displacement of the mid-wall surface, w (measured positive inward), as a function of axial position, z. The linear elasticity assumption is justified since the end-goal is to estimate stretches, which requires only the displacements rather than the calculation of stresses, and the displacements (rather than pressures) are calibrated

experimentally. For deformations caused by rigid insertion and pressurized inflation, boundary conditions were enforced for the edge behaviors in order to restrict the wall displacement at the insert to be exactly determined by the size of the insert, the wall displacement far from the insert to be exactly determined by the inflation due to intraluminal pressure change, and the wall displacement transitions to be smooth along the entire length of the tube (from 0<z<∞). These restrictions result in the following solution:

$$w(z) = \frac{PR_o}{EH} + \left(\frac{R_o^{insert} - R_o}{R_o} + \frac{PR_o}{EH}\right)\left(\sinh(kz) - \cosh(kz)\right)\left(\sin(kz) + \cos(kz)\right)$$

$$\text{with} \quad k = \sqrt{\frac{3R_o}{2H}} \qquad \text{Eq. 3.3.}$$

This displacement, w, is the dimensionless wall displacement (normalized by R_o) from a straight, undeformed tube to a pressurized tube with a rigid insert. Given the undeformed radius of the tube, R_o, undeformed tube thickness, H, and radius of the rigid insert, as well as intraluminal pressure, P, and linearized elastic modulus of the tube, E, the solution can be used to give the deformed tube wall position profile.

$$e_\theta = -\frac{\bar{w}}{R_o} \qquad e_z = -\frac{d^2\bar{w}}{d\bar{z}^2}(r^*) \qquad \text{Eq. 3.4, 3.5.}$$

where the overbar denotes actual (dimensional) values, and r* is the radial distance of the point of interest from the mid-wall surface (r* = -0.5 × thickness for the outer wall). In our experiments, the tube was cyclically inflated from a diastolic pressure to a systolic pressure, after the rigid insert had been implanted. To calculate stretches between these two conditions, w is used to find the tube wall positions at both diastolic and systolic time points. The circumferential and axial stretch values for deformation between diastolic and systolic inflation (and the respective stretch, λ) can then be calculated with the following:

$$e_{\theta,z} = \frac{e_{\theta,z}^{systolic} - e_{\theta,z}^{diastolic}}{e_{\theta,z}^{diastolic} + 1} \qquad \lambda_{\theta,z} = 1 + e_{\theta,z} \qquad \text{Eq. 3.6, 3.7.}$$

The deformation analysis accurately estimates the levels of stretch as they vary from the edge of the rigid insert to the end of the tube. This variation provides an experimental region to study the effects of stretch gradients on cell behavior.

3.2.4 Cell Culture and Stretching

For cell stretching experiments, 10T1/2 cells (ATCC CCL-226) were cultured in SMGM with 5% fetal bovine serum, and antibiotics (Lonza). The 10T1/2 cell line is a murine mesenchymal cell, used for its relevance to a variety of fully differentiated cell types, particularly SMCs[31]. Prior to cell-seeding, the surface of circular membranes (diameter = 100mm; cut from 0.5mm thick

silicone sheeting (Specialty Manufacturing Inc., MI) and tubes (described above) were coated in bovine fibronectin (Sigma-Aldrich) by submerging for 1.5 hours in a fibronectin-PBS suspension to yield a surface area concentration of 5μg/cm^2. Membranes and tubes were then washed with PBS, washed with medium, and then submerged in medium containing 10T1/2 cells (between passages 10-15) in suspension. Cell concentration in suspension was chosen to yield a seeding density of 10^4 cells cm^{-2}. The tube was slowly rotated for several hours post seeding to enable uniform seeding. Both constructs were subsequently incubated for 2 days prior to stretching to ensure adequate adhesion.

After 2 days incubation, membranes were attached to the stretching device and cyclically deformed at 1Hz for 24hours according to the stretch profile described above. Tubes were stretched via cyclic inflation at 1 Hz for 24 hours, with pressurization level selected to yield 10% circumferential stretch far from the rigid insert.

3.2.5 Orientation Analysis

After stretching, cells were imaged with bright field microscopy at 10x magnification. Across the membrane, images were captured at ~50 positions using a motorized stage to collect image coordinates. Radial position of each image was calculated by estimating the membrane's center based on a circular fit of the points around the inner edge. Within each image, the orientation of every cell was calculated using ImageJ software (NIH). Cell outlines were

manually traced and fit to ellipses using ImageJ's algorithm. This fit maintains the cell's total area and orientation direction. Each cell's orientation angle (measured from the horizontal axis of the image) was adjusted for the image's position on the membrane to give the angle measured off the radial direction. This angle was further adjusted for the direction of minimal stretch as a function of radial position, calculated by Eq. 2 above. The resulting angle for each cell describes that cell's angle away from the direction of minimal stretch, ranging from 0° (parallel to minimal stretch) to 90° (perpendicular to minimal stretch).

For the tube setup, images were captured above the rigid insert, far from the rigid insert, and within the transition region. Cell alignment was again quantified using ImageJ with orientation angle defined between a cell's major axis and the longitudinal direction of the tube.

Since it is suspected that subcellular cytoskeletal filament reorganization is the underlying mechanism for cellular re-orientation, actin filaments were stained and imaged subsequent to 24hrs of stretch. After stretch, membranes were removed from the device, and 10T1/2 cells fixed by covering in paraformaldehyde diluted to 4% in water for 10 minutes. Membranes were then washed 3 times with PBS before membrane permeabilization for 5 minutes using TritonX (Sigma-Aldrich) diluted to 0.5% in water. Again, membranes were washed 3 times with PBS, followed by actin staining with Alexa Fluor 488® phalloidin dye (Invitrogen) for 1 hour. Cells were then imaged at 40x magnification with the Nikon fluorescent microscope previously mentioned.

3.2.6 Statistical Analysis

Orientation histograms were generated for each microscope image, dividing cells into 10 orientation groups between 0° and 90° (0-9°, 9-18°… 81-90°). Images were grouped (n=2-6) according to their position upon the membrane or tube setups, and overall histograms for each position group were generated by averaging histogram values of individual images within the group. For average values of cell orientation at various positions, means were taken of all cells from all images within each group. Averaged data are reported as mean ± std. error.

3.3 RESULTS

3.3.1 Stretch Field Characterization

Radially deforming a circular elastomeric membrane with a central defect generates gradients in circumferential and radial stretch components (Fig. 3.4). With the selected membrane geometry and loading regimen, circumferential stretch decreased from 1.11 at the inner edge to 1.03 at the outer edge, while radial stretch increased from 0.95 to 1.02 (inner to outer). These gradients are steep near the center and shallower further from the center. Due to these non-uniformities, the resultant angle of minimal stretch varies with membrane position (Fig. 3.4b), decreasing from 33.8° off the radial axis at the inner edge to 0° (parallel) with the radial axis from r = 14.5mm and outward.

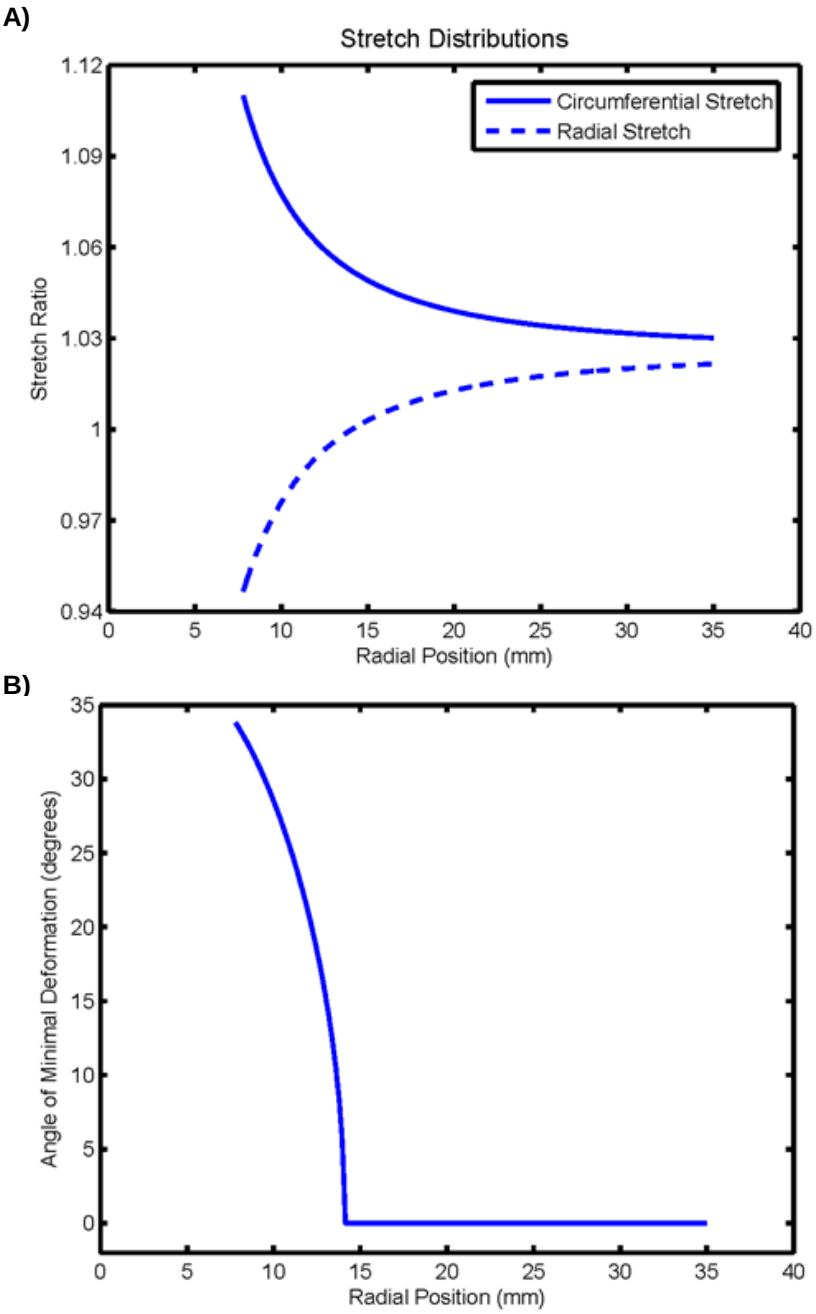

Fig. 3.4. Membrane stretch characterization.
Radially deforming a circular membrane with a central defect generated gradients in both circumferential and radial stretch components (A). The off-axis direction of minimal stretch varied with radial position due to circumferential: radial stretch ratio variation (B).

Tube deformation profiles were calculated using the governing displacement equation (Eq. 3.3) and the stretch relations (Eq. 3.7) for potential stretching cases yielding far-field circumferential strains of either 10% or 20% (Fig. 3.5). Above the rigid insert ($z \leq 0$mm), the tube wall does not move with inflation. Far from the glass insert ($z \geq 3$mm), the tube wall displacement is nearly uniform, and solely dependent upon the intraluminal pressure increase. When the tube is inflated from the baseline (diastolic) to either the 10% or 20% case (systolic), stretches are uniform above the glass insert and far from the glass insert, but with a highly non-uniform transition zone in between. For the nominal 10% case, circumferential stretch varies from 1.0 at the glass to 1.10 far field, while longitudinal stretch varies from 0.91 at the glass to 1.0 far field. Notably, the longitudinal stretch profile peaks at nearly 1.04 before falling back to 1.0. This biphasic behavior arises from the bending-inflation interactions within the transition zone. For the 20% case, the trends are identical with circumferential stretch varying from 1.0 to 1.20, and longitudinal stretch varying from 0.82 to 1.0 with a peak at 1.07.

3.3.2 Cellular Orientation Response

Prior to stretching, 10T1/2 cells seeded on both the membrane and tube constructs showed good viability and adequate adhesion to the substrate. After 24hours of cyclic stretch, cells remained adhered to both surfaces with healthy morphology and obvious orientation changes (Fig. 3.6-3.10). These changes

demonstrated a tendency for cells to orient parallel to the direction of least stretch (Fig. 3.7-3.9). On the membrane, the degree of this response varied greatly correlating to radial position (Fig.3.7, 3.8). At positions near the center, high alignment tendencies were evident, while lower alignment tendencies were seen far from the center. A smooth transition of orientation is demonstrated as radial position increases (Fig. 3.8). This transition is evident in mean alignment values across radial position varying from 1.75±1.21° at R=8mm to 45.1±3.65° at R=34mm (Fig. 3.8). Decreasing alignment tendency with increasing radial position is also evident in histograms of cellular alignment angles. At R=8mm, 62±4.5% of cells orient between 0-9° while that value is 31±5.6% at R=14mm, 17±4.2% at R = 23mm, and 14±5.5% at R =34mm. (Note that perfectly random alignment should yield a mean orientation of 45° with approximately 10% of cells between 0-9°.)

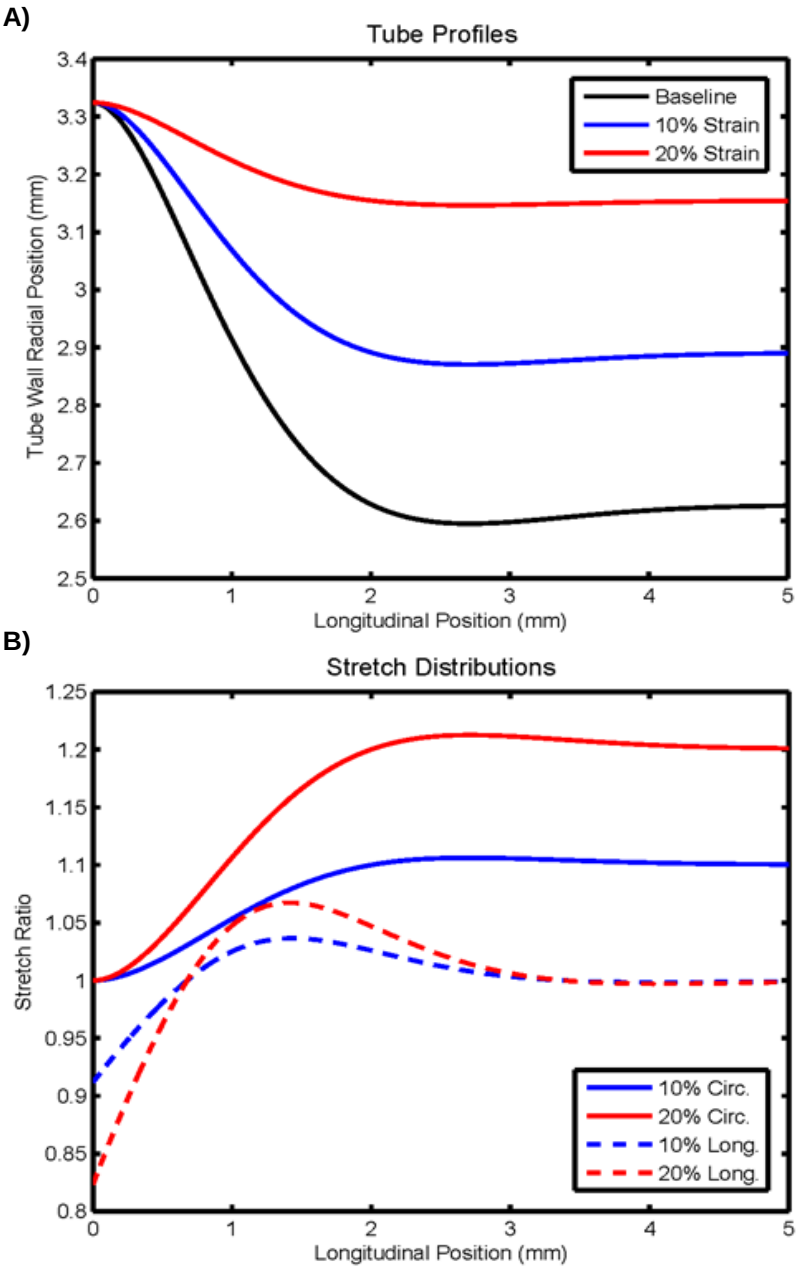

Fig. 3.5. Tube geometries and stretches.
A thin-walled tube was implanted with a rigid cylindrical insert and subsequently subjected to cyclic inflation. The tube geometric profile (A) and stretch ratios (B) were calculated for cases of 10% and 20% nominal stretched, defined by the circumferential stretch between systole and diastole, far from the rigid insert.

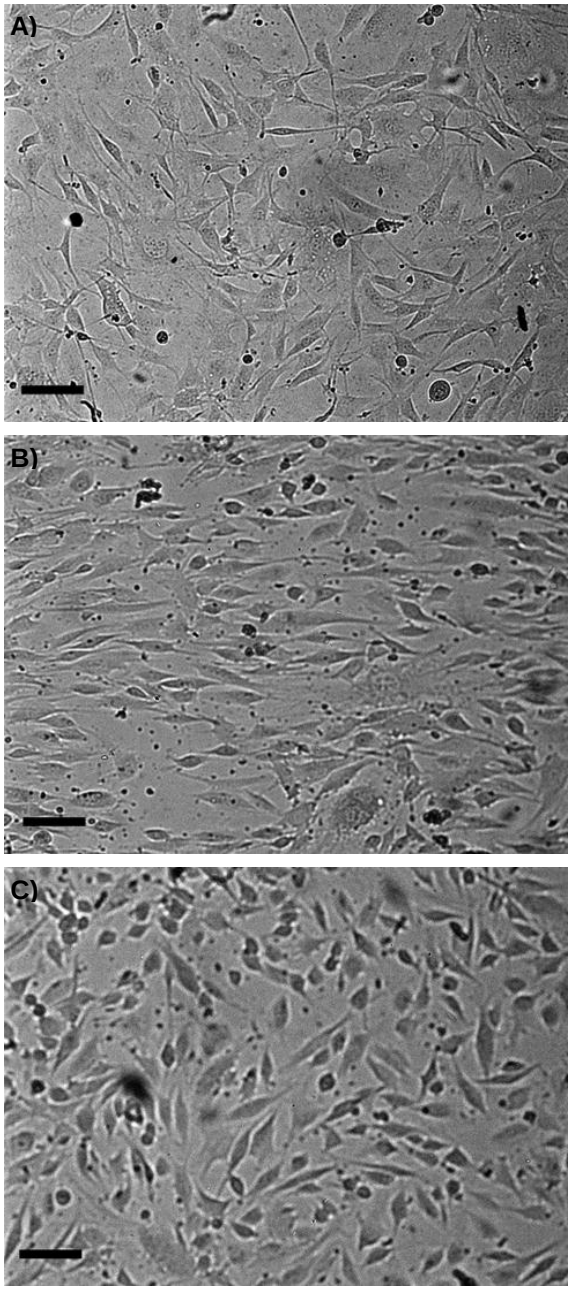

Fig. 3.6. 10T1/2 cell orientation on membranes.
Before stretch, 10T1/2 cells oriented randomly on elastomeric membranes (A). After 24hrs of cyclic stretch, cells aligned differentially according to radial position, with cells near the center demonstrating high alignment (B) and cells far from the center demonstrating low alignment (C). Scale bars equal 100 microns.

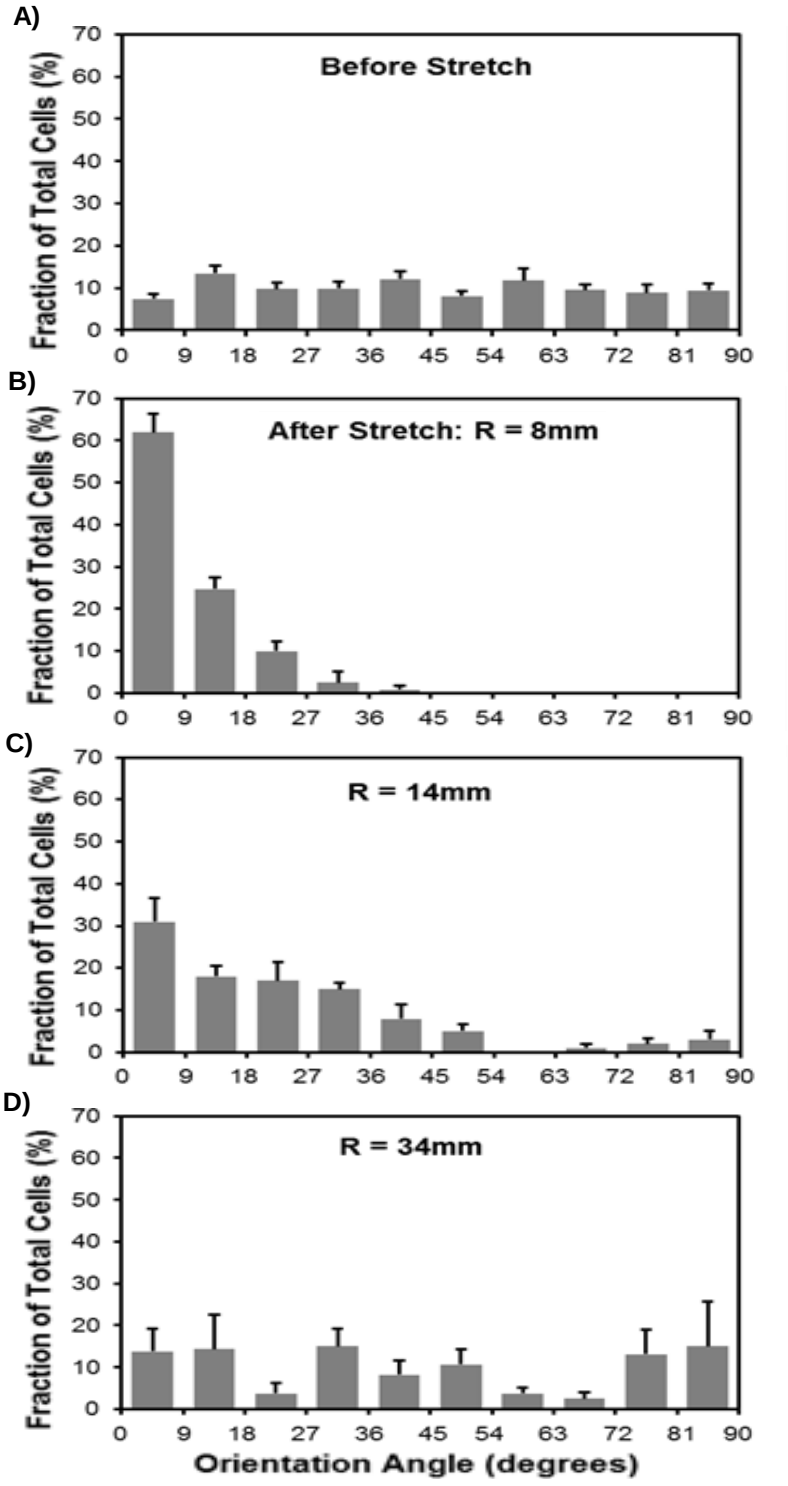

Fig. 3.7. Orientation histograms.
Prior to stretching, 10T1/2 cells showed random alignment (A). After 24 hrs of cyclic stretch, alignment varied from high near the center (B) to little far from the center (D).

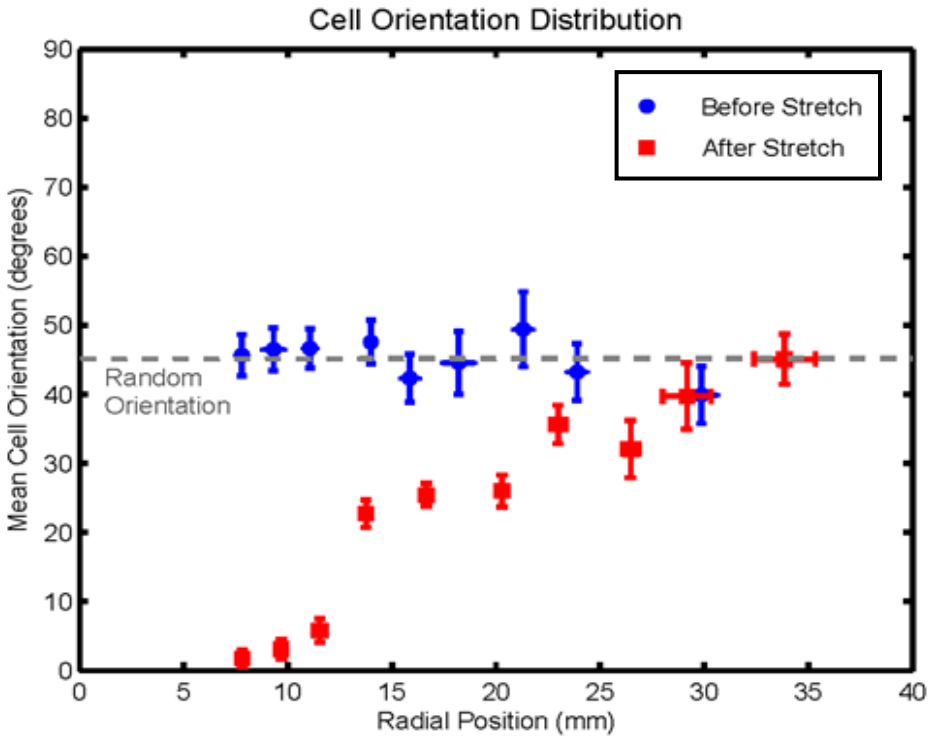

Fig. 3.8. 10T1/2 orientation across membrane.
Before stretch, 10T1/2 cells at all locations on the membrane showed random orientation. After 24 hrs cyclic stretch, cells demonstrated a gradual transition from high alignment near the membrane center to random alignment far from the center.

On the tube device, the degree of alignment varied with longitudinal position, presumably due to the longitudinal variation in stretch values (Fig. 3.9). Cells located above the rigid insert (where $\lambda_\theta = \lambda_z = 1$) showed no alignment tendencies (15±3.2% cells between 0-9°), while cells located far from the insert (where $\lambda_\theta > \lambda_z = 0$) showed a strong tendency to align axially (43±4.0% between 0-9°). Within the transition region, there is a slight tendency for longitudinal orientation (23±1.0% between 0-9°).

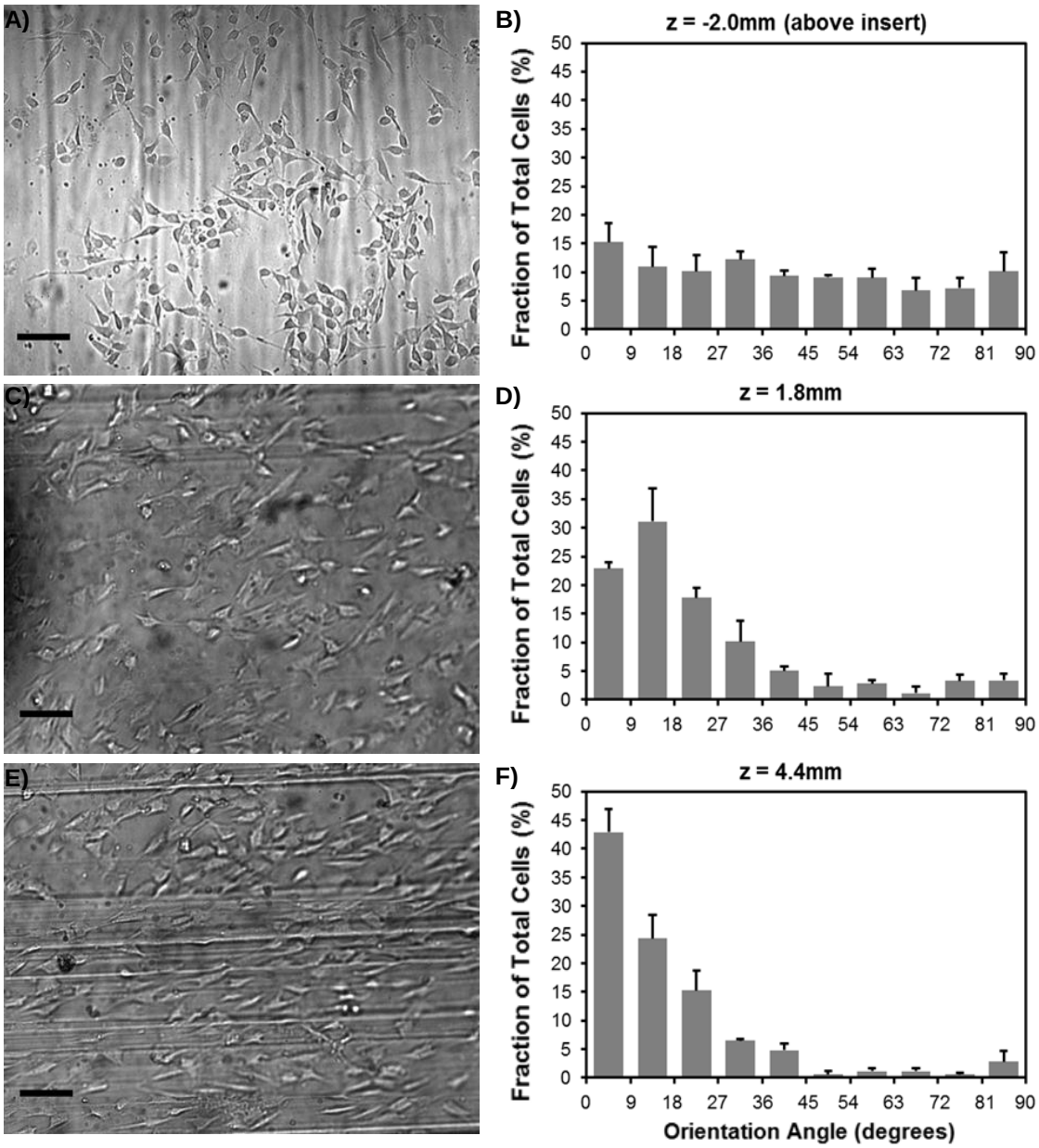

Fig. 3.9. 10T1/2 cell orientation along tube.
After 24 hours of cyclic stretch, 10T1/2 cell orientation varied with longitudinal position as evidenced qualitatively and quantitatively via histograms of orientation angles. Above the rigid insert, cells demonstrated no particular alignment (A and B). Within the transition zone, cells demonstrated moderate alignment in the longitudinal direction (C and D). Far from the glass insert, cells demonstrated drastic alignment in the longitudinal direction, which corresponds to the direction of minimal deformation (E and F). Scale bars equal 100 micrometers.

In addition to overall cell alignment, subcellular actin filaments also demonstrated orientation changes depending on cellular location (Fig. 3.10). Near the membrane center, actin filaments were highly aligned in the direction of least strain, with development of stress fibers (collected bundles of actin filaments) near the cell periphery, also highly aligned. Far from the membrane center, actin filaments were less aligned with distinct families of filaments oriented in more varied directions and stress fibers following the cell edge in no apparent alignment.

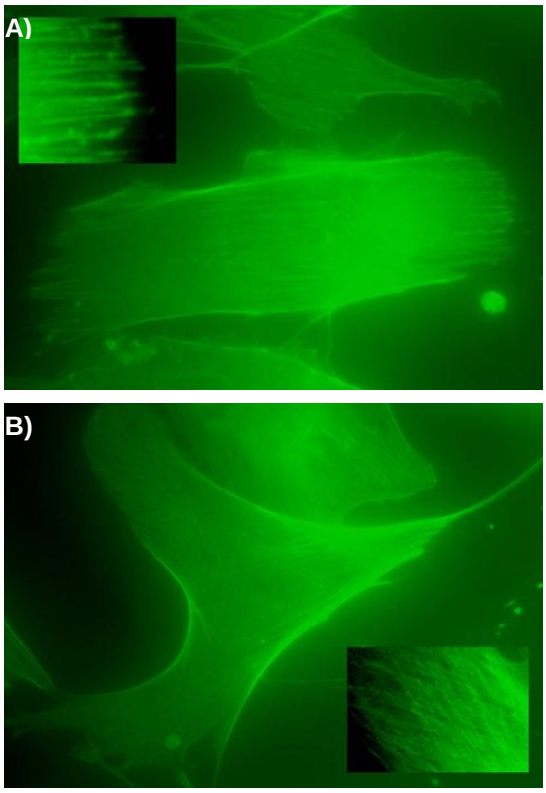

Fig. 3.10. Actin filament alignment.
Alexa Fluor® 488 phalloidin labeled cytoskeletons showed a single direction of highly aligned actin filaments in 10T1/2 cells near the membrane center (A), but multiple, non-aligned directions of actin filaments in cells far from the center (B). Scale bar equals 100 microns.

3.4 DISCUSSION

There is a pressing need for *in vitro* studies to subject cells to the realistic, spatially varying mechanical environments imposed in health and disease. Herein, we have demonstrated the feasibility of two cell-stretching devices designed to investigate cellular responses to non-uniform strain fields. By radially deforming a circular elastomeric membrane with a central defect, we can generate controllable gradients in radial and circumferential stretch components. Additionally, by inserting an over-sized rigid fixation into an elastomeric tube and subsequently inflating the tube, we can create a longitudinal gradient in circumferential and axial stretch components. 10T1/2 cells subjected to these stretching environments for 24 hours changed their alignment depending upon their location within the stretch gradients. As anticipated, cells adhered to regions of highest stretch demonstrated strong alignment tendency parallel to the direction of minimal stretch, while cells adhered to regions of low stretch or near equibiaxial stretch demonstrated random orientation. This behavior is consistent with numerous previous investigations that indicate cells of many types align in the direction of minimal deformation[38-41; 46; 47].

The vast majority of previous cell stretching devices subjected cultures to simplified mechanical stimuli. Several recent devices, however, have sought to represent more physiologic-like environments by incorporating non-uniform strain fields into culture substrates. For example, Ohashi et al. created a spatial

gradient in strain by uniaxially loading a rectangular elastomeric membrane with a circular glass disc embedded in the center[34]. ECs stretched with this device demonstrated marked changes in stress fiber organization depending on location along the gradient. In similar fashion, Yung et al. generated strain gradients by uniaxially loading PDMS wells with rectangular glass strips bonded to the bottom surface[35]. The non-uniform strain profile on this device was characterized but cell behaviors at different points along the gradient were not analyzed.

Balestrini et al. extended the rigid-fixation strategy to biaxial loading environments by employing the commercially available Flexcell system to stretch 2D membranes and 3D fibrin gels with a glass disc secured as a central fixation[36]. This setup generated radial gradients in both circumferential and radial stretch components, similar to the environment created by our device but with opposite relative magnitudes of the stretch components (i.e., radial stretch greater than circumferential stretch). When loaded with their device for several days, dermal fibroblasts showed varied alignment tendencies across different positions upon the membrane. In agreement with our results, fibroblast alignment was highest in a uniaxial stretch region and lowest in a near-equibiaxial stretch region.

Using an alternative approach, Tan et al. used topographical patterns (circumferential or radial grooves) to create nonuniform strain anisotropy upon circular membranes[61]. They found differential patterns of vascular SMC

proliferation and nuclear shape across these anisotropy gradients. However, their focus remained on the effects of strain anisotropy ratio rather than strain magnitude gradients, and their experiments restricted cell orientation to align with the imposed microgrooves regardless of local stretch components, thereby limiting their applicability to elucidating cell behavior when stretched on a 'free' surface without contact guidance cues. This recent handful of studies have revealed the great potential of non-uniform stretch environments within mechanobiological investigation for linking cell behavior to many levels of mechanical loading with single experiments. This capability is useful for efficiently collecting more complete data sets to build and test theoretical models of mechanobiological processes (e.g., alignment models such as those presented by Kaunas and Hsu, and De et al.)[48; 62].

With similar motivation, we have recently published a novel device employing platen displacement of a circular membrane with a central defect[58]. A unique feature of this design is that it generates a region of compressive radial strain in concert with a tensile circumferential strain. This combination is noteworthy as it represents what is seen in the *in vivo* arterial wall. Moreover, our device in fact generates three types of stretching environments including simple uniaxial ($\lambda_{e1}>1$, $\lambda_{e2}<1$), strip biaxial ($\lambda_{e1}>1$, $\lambda_{e2}=1$), and nearly equibiaxial ($\lambda_{e1}=\lambda_{e2}$). This allows the investigation of cellular behavior in diverse environments with individual experiments. The two devices used herein reflect a

move toward creating environments that attempt to directly mimic mechanical stimuli from particular implanted devices, in this case, a stented artery.

Admittedly, SMC alignment is not necessarily of greatest interest to the clinical problem of restenosis. Still, our findings demonstrate the devices' capability to successfully elicit differential cellular responses along a non-uniform stretch gradient. Since data collection and analysis for cell orientation is relatively straight-forward, we can quickly demonstrate feasibility of experimental protocols, confirm cell sensation of mechanical stimuli, and prove adequate cell viability. In addition, cellular alignment is a significant process in many other tissue behaviors, normal and diseased, such as morphogenesis wherein strain environments are highly non-uniform and potentially provide directional cues for tissue differentiation and development[54].

A principal limitation of this work is the use of 2D cell culture. Many studies have revealed differences in cell behavior when cultured on 2D vs 3D substrates[63]. Still, we believe 2D cell culture is a useful first step toward creating more physiologic mechanical environments, and both devices presented can be adapted to load 3D constructs in the same fashions. An additional limitation of this work is the ambiguity of primary vs interaction effects between stretch magnitude, "stretch anisotropy" ratio, and stretch gradients. All three of these mechanical parameters varied with spatial position upon our devices. Experiments remain to be conducted that test each of these parameters

independently in order to isolate the effects of each on biological responses of interest.

Future studies with these devices will focus on cell behaviors more closely related to arterial disease formation such as SMC migration, proliferation and phenotype modulation. 3D constructs will also be incorporated to subject cells to a mechanical environment even more representative of the physiologic conditions, thereby providing additional detail and investigative capability. A particular mechanical cue that remains to be adequately investigated is a gradient in stretch and its ability to act as a directional cue for cell behavior. Although one study noted cells' ability to potentially sense directionality via strain gradients, this data was qualitative and limited[34]. It would be interesting to know if stretch gradients are able to guide cell migration or division in a mechanism similar to durotactic motility. The non-uniform strain fields imposed by stenting and other conditions potentially play important roles in the development of disease as well as the success of possible treatment options. To that end, experimental devices recreating the mechanical stimuli as closely as possible can be used to help illuminate the cellular mechanisms involved in these conditions, a key step in designing adequate therapies and technologies to treat or prevent disease.

4. PHENOTYPE MODULATION OF 10T1/2 MESENCHYMAL CELLS

4.1 INTRODUCTION

It is widely known that mechanical loads can alter many cellular behaviors such as migration, orientation, proliferation, protein synthesis, phenotype modulation, and others. Knowing how mechanical signals are transduced into cell responses is therefore vital to our overall understanding of tissue and organ function, both in health and disease. For instance, numerous studies have demonstrated the role of biomechanics in atherosclerosis initiation, progression, and treatment success. Spatial distributions of both blood flow patterns and artery wall stress have been linked to early intimal thickening[6; 7], and biomechanical changes following stent implantation are thought to be involved in restenosis[8; 9].

Linking these loading conditions to particular *in vivo* cellular responses is made difficult by the complexity of physiologic mechanical environments, which can be non-uniform, anisotropic, and constantly remodeling. In by-pass grafts, concentrated zones of high stress are created at the suture line[64]. In stented arteries, intimal circumferential stresses are elevated well beyond physiologic norms, exacerbating transmural stress gradients[22; 23]. Also, in the carotid sinus, locations prone to atherogenesis exhibit a high ratio of inner wall to outer wall circumferential stress[7]. In all of these pathologic developments, SMC

proliferation and phenotype transformation are key events contributing to intimal hyperplasia[4; 5]. Additionally, in all of these pathologies, the mechanical environment is highly non-uniform, with greater levels of stress at the inner edge of the wall compared to the outer edge. Thus, there exists a need to investigate SMC phenotype modulation in the presence of non-uniform stretch environments.

SMCs in the normal adult vasculature undergo proliferation at a very slow rate and exhibit very low synthetic activity; however, they maintain a plasticity that allows them to respond to local environmental stimuli and undergo profound changes in phenotype, characterized by increased proliferation and synthesis and decreased expression of contractile proteins[65; 66]. While there is a short-term advantage to this response to injury, prolonged phenotypic changes in SMC phenotype lead to the pathogenic developments mentioned above. The specific molecular mechanisms regulating these responses remain unclear.

The literature contains reports of numerous devices that have been used to subject SMCs to cyclic stretch in order to reveal effects of stretch on SMC phenotype. These devices vary greatly in the types of mechanical stimuli employed, most of which do not invoke mechanical conditions representative of the *in vivo* environment. Similarly, there is much variety in the findings of these studies. This is not only due to differences in the stretching environment, but also cell type, nominal stretch amplitude, stretch frequency and total duration of the study. In a landmark early study, Leung et al. subjected rabbit aortic SMC to

10% uniaxial stretch at a frequency of 0.87 Hz for a total of 32 hours, and found enhanced synthesis of collagen I and III, indicating the presence of the synthetic phenotype[13]. Morawietz et al. employed the Flexcell system to subject rat aortic SMC to 25% nominal stretch at 1 Hz for a total of 4 hours[43]. Stretch increased early growth response factor 1 (egr-1) and c-jun mRNA, but not c-fos, which points toward a shift to the synthetic phenotype. Birukov et al. used the Flexcell system to subject rabbit aortic SMC to 15% nominal stretch at a frequency of 0.5 Hz for 8 days[42]. Stretch increased proliferation, but also increased expression of caldesmon (especially with laminin ECM), indicating perhaps a hybrid phenotype.

Butcher et al. subjected rat aortic SMC to 10% equibiaxial (circumferential and radial) stretch by deforming flexible substrates over a cylindrical post at 1 Hz over a 48 hour period[45]. The cells were cultured into collagen gels attached to silicone membranes. Compared to static controls, stretched cells exhibited less alpha actin and calponin, suggesting a shift toward the synthetic phenotype. Li et al. employed the Flexcell system with a post underneath that resulted in a more uniform, biaxial strain field[67]. They subjected mouse aortic SMC to 5%, 10%, and 15% strain at 1 Hz for a total of 3 hours. It was found that stretch at any level activated PKCδ translocation to the cytoskeleton, indicating maintenance of the contractile phenotype. Goldman et al. subjected segments of rat veins to pulsatile arterial pressure for 48 hours[44]. Stretch induced actin degradation, indicating transition to the synthetic phenotype.

There have also been some efforts to subject SMC to cyclic stress in a more physiologic 3D environment. Stegemann and Nerem suspended rat aortic SMC in a 3D collagen tubular matrix and subjected the constructs to 10% circumferential stretch at 1 Hz for 4 days[68]. Stretch increased compaction of the constructs and SMC proliferation, but had an insignificant effect on alpha-actin expression, indicating perhaps a hybrid phenotype. Kanda et al. subjected bovine aortic SMC to 10% cyclic uniaxial stretch in collagen rings at 1 Hz for 4 weeks[69]. The stretched cells showed higher levels of contractile apparatus compared to static controls, indicating a shift toward contractile phenotype. Other studies of SMC phenotype change in response to stretch include Zhao et al., Albinsson and Hellstrand, and Albinsson et al. who used static loading conditions for between 10 minutes and 72 hours[70-72]. Also, Cappadona et al. cultured SMC on the exterior surface of polypropylene tubes that were perfused in a pulsatile fashion at 2 Hz for 72 hours[73]. It was not indicated if the pressurization resulted in any stretch. While, each of these studies has contributed to our overall knowledge, the simplistic loading regimens do not adequately represent the *in vivo* mechanical environment.

In order to investigate SMC behavior on non-uniform stretch environments representative of *in vivo* conditions, we have designed an experimental stretching device capable of subjecting cells in 2D and 3D cultures to gradients in biaxial stretch[58]. A proper investigation of SMC phenotype change in response to mechanical stimuli should come as close as possible to

the fully 3D *in vivo* case. Herein, we initiate a progression toward this idealized situation by subjecting cell-seeded PEGDA hydrogels to gradients in stretch. To investigate the effects on cell phenotype modulation, quantitative real-time RT-PCR is employed to measure changes in mRNA expression of genes related to contractile and synthetic phenotypes. Proliferation is also assessed using BrdU immunostaining of cells stretched on an elastomeric membrane. A more complete understanding of the responses of SMC to stress gradients would add to our knowledge of atherosclerosis development and enhance our ability to design interventional devices and therapies.

4.2 METHODS

4.2.1 Cell Culture and PEGDA Hydrogel Construction

10T1/2 cells (ATCC CCL-226), a murine mesenchymal cell line, were purchased and maintained in a smooth muscle growth medium with 5% FBS and antibiotics (SmGM kit, Lonza), incubated at 37°C and 5% CO2, and passaged just prior to dishes reaching confluence. A smooth muscle precursor cell type, the 10T1/2 line is commonly used for *in vitro* SMC phenotype studies due to its ability to maintain a stable phenotype in culture[31]. For experiments, 10T1/2 cells at passages 8-12 were used.

Polyethylene glycol diacrylate (PEGDA) was synthesized by methodology adapted by Hahn and colleagues[74]. Briefly, 10kDa PEG (Sigma) was acrylated

by the addition of acryloyl chloride to a solution of PEG and triethylamine in anhydrous dichlromethane. The reaction was stirred for 24 hours, subsequently washed with potassium bicarbonate and dried with anhydrous sodium sulfate, at which point the product was precipitated in cold diethyl ether, dried under vacuum, and stored at -20C.

For hydrogel manufacturing, PEGDA was allowed to warm to room temperature, then dissolved in sterile cell culture medium (SmGM, Lonza) to yield a 20% PEGDA solution. To allow cell adhesion to the polymer network, acrylated-RGD peptide groups (Peptron, Inc.) were dissolved in sterile, ultra-pure water and added to the solution at a concentration of 1mM. 10T1/2 cells were collected from culture dishes via trypsinization (Invitrogen), centrifuged, and then resuspended into the medium-PEGDA-RGD solution at a density of 2million cells/mL. Irgacure 2959, a photoinitator curing agent, was dissolved in 70% ethanol and added to the bulk at 0.1%wt of total solution. The final solution was pipetted into a disc-shaped Lexan mold with a central post in order to produce gels with the following dimensions: Ro =35mm, Ri =6mm, and thickness =2mm. Another disc mold was used to produce gels for unstretched control samples (R=9mm, t=1mm; smaller in order to conserve construct material). Molds were covered by thin glass sheets, and the gels were cured by long wave UV exposure for 6 minutes (Ultraviolet Products High Performance UV Transilluminator, 365 nm). After removal from the molds, gels were moved to petri dishes, submerged in culture medium, and incubated for 48hours prior to

stretching experiments. This period allowed ample time for free-swelling of gels, and adequate cell adhesion to the RGD groups incorporated in the polymer network.

For elastomeric membrane experiments, circular membranes (Ri = 7.5mm, Ro = 50mm) were cut from 0.5mm thick silicon sheeting (Specialty Manufacturing Inc.), and sterilized by autoclave. Membranes were then coated for 1.5 hours with bovine fibronectin (Sigma-Aldrich) diluted in PBS in order to yield a surface area protein concentration of 5μg/cm^2. After coating, membranes were washed with successive changes of PBS and culture medium before finally being submerged with medium containing 10T1/2 cells. This process yielded adequate cell adhesion with a seeding density of 10^4 cells/cm^2. Like the hydrogels, cell-seeded membranes were also incubated for 48 hours prior to stretching.

4.2.2 Stretching Device Design and Characterization

The cell-stretching device employed herein is based on circular membrane deformation analysis[24], and has been previously described in detail[58]. Briefly, a computer-controlled stepper motor drives a rack-and-pinion mechanism that radially deforms circular constructs by vertically displacing the clamped outer circumference past a stationary circular platen (Teflon). The mechanism is housed within a culture chamber (Lexan) allowing the construct to remain submerged in medium during stretching.

The loading action generates uniform radial displacement of the outer circumference of the construct, resulting in unequal and non-uniform radial and circumferential stretch components. Stretching membranes or gels containing a circular central defect results in gradients in these stretch components, with low radial stretch (λ_r) at the center edge increasing to higher radial stretch near the outer edge, and conversely, high circumferential stretch (λ_θ) at the inner edge decreasing to lower circumferential stretch at the outer edge. This non-uniform stretch field yields a 'simple uniaxial' environment at the inner region, and a near-equibiaxial environment at the outer region.

Elastomeric membrane deformations on this device have previously been characterized[58]. PEGDA hydrogel deformation was characterized by tracking fiduciary markers before and after various levels of stretch. Radial positions were measured for markers arranged in 8 lines extending radially from the gel's inner edge. Stretch ratios were then calculated based on the changes in the radial positions of these markers: circumferential stretch = r/R, radial stretch = $\Delta r/\Delta R$, where r is deformed radial position and R is original radial position. Assuming incompressibility, the out-of-plane thinning of gels was calculated as $1/(\lambda_\theta * \lambda_r)$. Markers with similar original positions were grouped, and stretch components were averaged within each group. Deformation theory was then solved to fit the Mooney-Rivlin strain energy constitutive equation to the experimentally measured stretch data. Fitting this constitutive model allowed for the theoretical estimation of hydrogel deformation due to any prescribed loading,

so that selecting experimental regimens would not be restricted to the limited levels of loading at which measurements were taken.

4.2.3 Stretching Experiments

After 48 hours of incubation, cell-seeded hydrogels and membranes were mounted on the above stretching device. Sandpaper (180grit) was placed between the gels and outer circumference clamps to ensure adequate gripping. Based on the hydrogel constitutive modeling results, motor gear displacement was selected to achieve ~10% circumferential stretch at the inner edge of the hydrogels. Cell-seeded membrane stretches were preselected with circumferential stretch varying from $\lambda_\theta^{inner} = 1.11$ to $\lambda_\theta^{outer} = 1.03$, and radial stretch varying from $\lambda_r^{inner} = 0.95$, and $\lambda_r^{outer} = 1.02$ (Fig. 4.1). Both constructs were cyclically stretched for 24 hours at 1Hz. During this duration, the stretching device chamber was filled with culture medium and enclosed within an incubator at 37°C and 5%CO2.

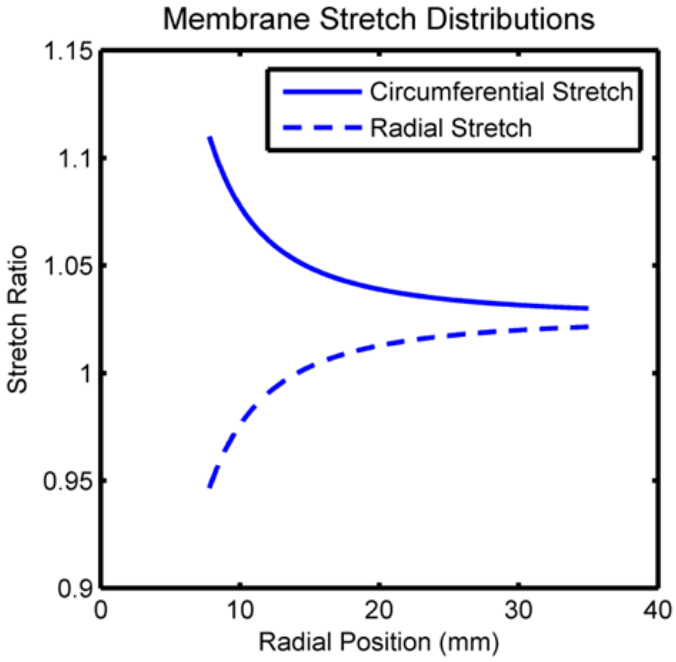

Fig. 4.1. Membrane experiment stretch distribution.
A circular elastomeric membrane with a central defect was radially deformed, producing gradients in circumferential and radial stretch components.

4.2.4 Real-time RT-PCR Analysis of mRNA Expression

To assess changes in phenotype-related gene expression due to stretch, real-time, reverse-transcription polymerase chain reaction (RT-PCR) was employed. After 24 hours of stretching, disc-shaped samples were taken from two regions of the gel: an inner ring ($7.5 < R < 11.5$mm) and outer ring ($28.6 < R < 30$mm) encompassing the locations of extreme mechanical conditions. Samples were also taken from a non-stretched control gel. For nucleic acid collection, samples were submerged in TRIzol® reagent and homogenized using a power tissue homogenizer (POLYTRON® PT2100, Kinematica). The PureLink® RNA Mini Kit was then used following manufacturer's instructions to

isolate mRNA, which was reverse transcribed into cDNA with the SuperScript™ First-Strand Synthesis System (Invitrogen).

To measure relative amounts of gene expression for various phenotype-related proteins, quantitative real-time RT-PCR was carried out with 2X SYBR® Green dye (ABI). Primers used for genes associated with the contractile and synthetic/proliferative phenotypes were previously generated using Primer Express Software (ABI), and have been published[58]. Expression levels were quantified using the ΔΔCT method, with GAPDH as a reference gene for normalization: $\Delta\Delta CT=(CT_{stretch}-CT_{nonstretch})^{gene} - (CT_{stretch}-CT_{nonstretch})^{GAPDH}$. CT represents the PCR cycle number at which the gene's fluorescent signal crosses a threshold value. The mRNA fold expression reported for each gene equals $2^{-\Delta\Delta CT}$ and represents the amount of that gene's mRNA collected within a sample relative to a non-stretched control sample, both normalized by GAPDH mRNA levels.

4.2.5 Cell Imaging

A limitation of PEGDA hydrogels is that cells are not able to alter morphology due to encapsulation within the small polymer mesh size. However, their intracellular structure could potentially be altered in response to mechanical loading. In order to examine overall cell morphology as well as intracellular changes in cytoskeletal organization, actin filaments were labeled and cells were imaged subsequent to stretching experiments. Following 24 hours of cyclic

stretching, a small wedge encompassing all radial positions was cut from the gel and washed with several changes of phosphate buffered saline (PBS). Cells were then fixed by submerging the gel with a 4% paraformaldehyde solution for 30minutes, washed 3 times with PBS for 5min each, and permeabilized for 15minutes with TritonX (Sigma-Aldrich) diluted in water to concentration of 0.5%. Following permeabilization, the gel was washed again (PBS, 3x 5minutes), then submerged in Alexa Fluor 488® phalloidin dye (Invitrogen) for 8 hours. The durations of these steps were longer than the prescribed protocol, extended to allow sufficient time for chemicals to diffuse through the hydrogel. Following staining, gels were briefly washed and imaged at 10x and 60x magnifications using a Nikon TE-2000 Inverted Fluorescent Microscope equipped with confocal capability and a Nikon C-FL FITC byHYQ filter set (Nikon Instruments, NY).

4.2.6 Proliferation Assessment

Cellular proliferation was quantified using the 5-bromo-2-deoxyuridine (BrdU) incorporation technique, a commonly used method for proliferation studies. A uridine group, BrdU can function as a thymidine substitute and is thereby incorporated into DNA during the synthesis-phase of the cell cycle. By subsequent immunostaining, a BrdU-positive reading preferentially indicates those cells that have undergone division while cultured in the presence of the molecule. The proliferation assay was conducted on cell monolayers stretched

on the membrane construct rather than the hydrogel setup to ensure uniform uptake of BrdU (i.e., not limited by diffusion through the gel thickness).

BrdU (Invitrogen) was diluted 1:100 in culture medium and used to replace plain culture medium in the stretching chamber after the membrane had been stretched for 16hours. After an additional 8 hours of stretching (total of 24hrs stretching), membranes were removed from the device. Cells were then washed with PBS several times, and fixed in 70% EtOH at 4°C for 30minutes. Following fixation, cells were washed with PBS 3 times for 2min each, then a BrdU immunostaining protocol (biotinylated monoclonal anti-BrdU antibody technique, Invitrogen) was carried out according to the manufacturer's instructions. After staining, cells that incorporated BrdU (i.e., proliferative cells) displayed darkened nuclei compared to those that did not (i.e., non-proliferative cells). Cells were then imaged with bright-field microscopy at 10x magnification using the microscope listed above. Between 6-10 images were taken within three different radial regions upon the membrane: Inner, $7.5 < R < 15$mm; Midway, $15 < R < 22.5$mm; and Outer, $22.5 < R < 30$mm. Cells from a non-stretched control membrane were also imaged at the same positions. Within all images, proliferation was quantified as the ratio of the number of darkened cells to non-darkened cells.

4.2.7 Statistical Analysis

For proliferation experiments, cell images were divided into six groups: three radial regions, either stretched or non-stretched. The non-stretched, control proliferation ratios were averaged for each of the 3 non-stretched groups, and proliferation ratios for all individual images were then normalized by the average control ratio for the corresponding radial region. The normalized proliferation ratios for all three stretched groups and unstretched controls were averaged and their distributions were compared with one-way ANOVA followed by post-hoc Tukey-Kramer multiple comparison test. Significance level was set at $p = 0.05$ and data are reported as mean ± st. error.

For RT-PCR data, four stretching experiments were conducted along with four non-stretched control gels. For each experiment, 3-4 real-time runs were performed on the collected mRNA samples, resulting in 13 total measurements for each gene's expression within each of the 3 experiment regions: no stretch, stretch inner, or stretch outer. Means and standard errors of ΔΔCT data were calculated for each and the expression levels are reported as $2^{-\text{mean}\Delta\Delta CT}$ with intervals ($2^{-(\Delta\Delta CT+\text{st. error})}$, $2^{-(\Delta\Delta CT-\text{st. error})}$). For statistical comparisons, one-way ANOVA followed by post-hoc Tukey-Kramer multiple comparison tests were performed with significance level set at $p = 0.05$.

4.3 RESULTS

4.3.1 Hydrogel Deformation Characterization

Radially deforming circular PEGDA hydrogels with a central defect generates non-uniform distributions of both circumferential and radial stretch components (Fig. 4.2). A Mooney-Rivlin strain-energy function fit the experimental data appropriately for both these stretch components as well as the out-of-plane thinning stretch. As predicted by finite-deformation theory, circumferential stretch is maximal at the inner edge and monotonically decreases toward the outer edge, while radial stretch is minimal at the inner edge and monotonically increases toward the outer edge. This produces a high magnitude 'simple uniaxial' stretching environment in the inner region that transitions to a lower magnitude near-equibiaxial environment toward the outer edge. Furthermore, by increasing the vertical displacement of the clamped outer-circumference of the gel, the degree of non-uniformity (i.e., steepness of the gradients) increases. For each case, the out-of-plane thinning remained relatively uniform across radial direction. Based on the stretching characterization, a moderate stretching regimen was selected for experimental cases (Fig. 4.3). The stretch distribution used for experiments subjected the hydrogels to $\lambda_\theta^{inner} = 1.10$, $\lambda_\theta^{outer} = 1.04$, $\lambda_r^{inner} = 0.98$, and $\lambda_r^{outer} = 1.037$. The out-of-plane thinning remained uniform at 0.93.

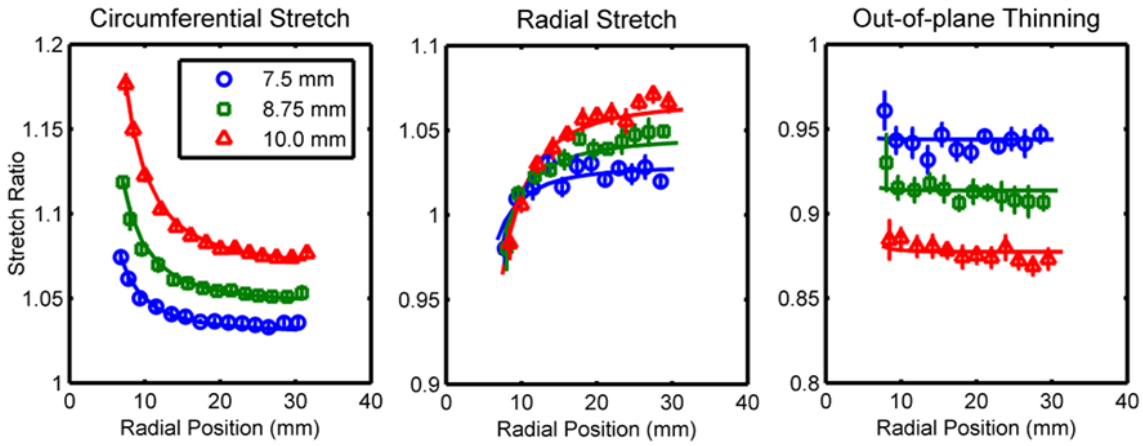

Fig. 4.2. Hydrogel stretching characterization.
A circular PEGDA hydrogel with a central defect was radially deformed by displacement over a stationary platen, generating non-uniform distributions within the three principal stretch components. Experimental data (shown as means ± st. error) were fit with a Mooney-Rivlin strain energy constitutive function.

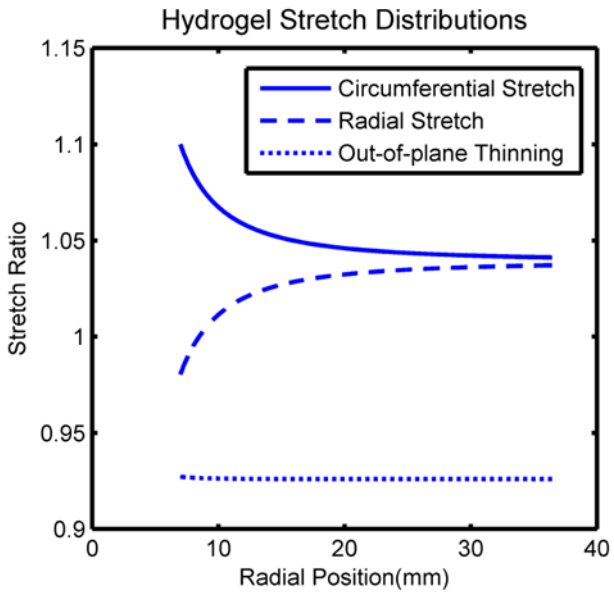

Fig. 4.3. Hydrogel experiment stretch distribution.
PEGDA hydrogels with central defects were radially deformed. The resulting circumferential and radial stretch components were highly non-uniform across radial position, while out-of-plane thinning remained relatively uniform.

4.3.2 mRNA Expression

Quantitative, real-time RT-PCR yielded expression values of phenotype-related genes for cells taken from inner and outer regions of hydrogels, corresponding to high magnitude 'simple uniaxial' stretch and lower magnitude near-equibiaxial stretch environments, respectively (henceforth referred to as high uniaxial and low biaxial, respectively). ANOVA with post-hoc comparisons identified significant differences in mRNA expression (relative to GAPDH reference gene) between stretched gels and unstretched gels, and in some instances between high uniaxial and low biaxial stretch regions (Fig. 4.4). However, of the 17 mRNA levels analyzed, the majority did not show statistically significant differences, though some tendencies were evident (Table 4.1).

Table 4.1. Insignificant mRNA expression levels.
Phenotype-related mRNA levels were analyzed using ΔΔCT method relative to a non-stretched control sample, both normalized by GAPDH. Fold expression data reported as $2^{-\text{mean}\Delta\Delta CT}$ with intervals ($2^{-(\Delta\Delta CT+\text{st. error})}$, $2^{-(\Delta\Delta CT-\text{st. error})}$).

Gene	Non-stretched mRNA expression	Low, biaxial stretch (28.6 < R < 30mm)	High, uniaxial stretch (7.5 < R < 11.5mm)
Actin- α2	1 (0.89, 1.13)	0.69 (0.53, 0.90)	0.95 (0.77, 1.18)
Biglycan	1 (0.78, 1.29)	1.16 (0.85, 1.58)	2.36 (1.52, 3.67)
Calponin	1 (0.83, 1.20)	0.68 (0.55, 0.85)	0.80 (0.56, 1.16)
Integrin αV	1 (0.83, 1.20)	1.04 (0.73, 1.47)	1.45 (1.09, 1.93)
Integrin β3	1 (0.79, 1.26)	1.09 (0.78, 1.52)	1.74 (1.26, 1.74)
Matrix metalloproteinase 2	1 (0.85, 1.18)	1.08 (0.90, 1.31)	1.17 (0.95, 1.44)
Platelet-derived growth factor β	1 (0.84, 1.18)	0.68 (0.59, 0.80)	1.05 (0.84, 1.31)
Smad1	1 (0.85, 1.18)	0.89 (0.74, 1.07)	1.11 (0.85, 1.44)
Smoothelin	1 (0.84, 1.19)	0.95 (0.73, 1.22)	1.24 (1.01, 1.51)
SKI-like oncogene	1 (0.72, 1.38)	0.49 (0.27, 0.87)	1.47 (0.73, 2.96)
Transgelin	1 (0.82, 1.22)	0.81 (0.66, 1.00)	1.37 (1.75, 1.08)

In the case of cFos, cells from the high uniaxial region showed significantly elevated expression of 1.82 (1.66, 2.00) fold compared to both non-stretched expression of 1 (0.84, 1.19) fold, and low biaxial expression of 1.05 (0.95, 1.16) fold (Fig. 4.4a). Similarly, expression of caldesmon was significantly highest in the high uniaxial region: 9.73 (5.64, 16.79) fold compared to 1 (0.56, 1.77) fold for non-stretched and 0.60 (0.40, 0.88) fold for low biaxial (Fig. 4.4b). Expression of smad5 was also significantly elevated in the high uniaxial region (3.84 (2.66, 5.55) fold) compared to the non-stretched (1 (0.85, 1.18) fold) (Fig. 4.4c). The expression of Smad5 in the low biaxial region was elevated at 2.05 (1.54, 2.72) fold, though not statistically different than the non-stretched expression.

Several mRNAs also showed significant downregulation compared to non-stretched controls. Early growth response factor 1 showed significance decrease in expression in both high uniaxial (0.22 (0.19, 0.26) fold) and low biaxial (0.18 (0.16, 0.21) fold) regions compared to non-stretched regions (1 (0.60, 1.68) fold) (Fig. 4.4d). Levels of Id2 were also decreased in high uniaxial (0.54 (0.41, 0.72) fold) and low biaxial (0.44 (0.39, 0.5) fold) regions compared to non-stretched (1 (0.92, 1.08) fold), though only the low biaxial region decrease was statistically significant (Fig. 4.4e). In similar fashion, PAI-1 levels were decreased for both high uniaxial (0.15 (0.06, 0.36) fold) and low biaxial (0.05 (0.02, 0.1) fold) regions, but again only the low biaxial was significantly different than the non-stretched (1 (0.73, 1.37) fold) (Fig. 4.4f).

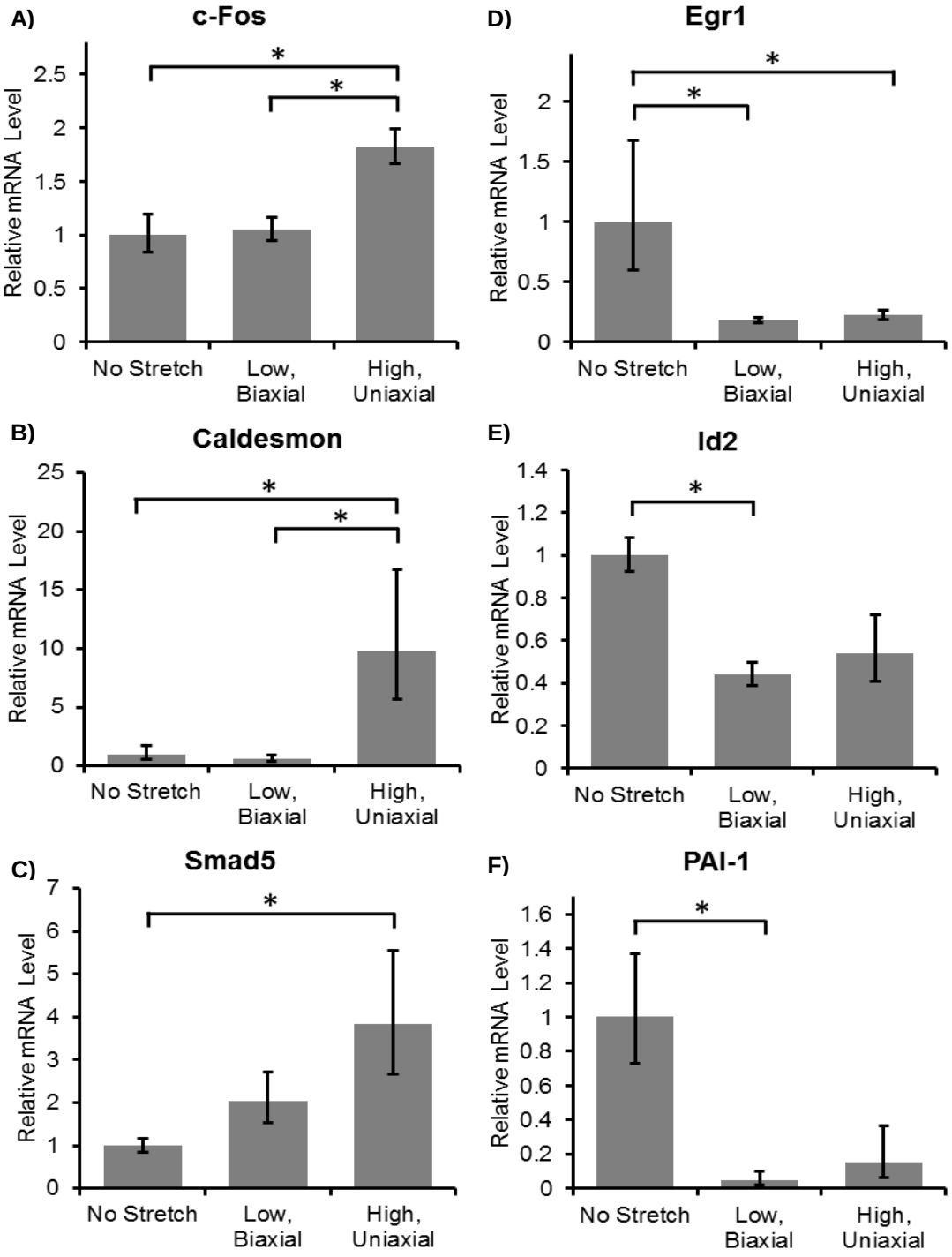

Fig. 4.4. Phenotype-related mRNA expression changes.
Quantitative, real-time RT-PCR was employed to measure phenotype-related mRNA levels. Data were analyzed using ΔΔCT method, relative to a non-stretched control and normalized by GAPDH. Expression reported as $2^{-\text{mean}\Delta\Delta CT}$ with intervals ($2^{-(\Delta\Delta CT+\text{st. error})}$, $2^{-(\Delta\Delta CT-\text{st. error})}$). Biaxial and Uniaxial regions refer to 7.5 < R < 11.5mm and 28.6 < R < 30mm, respectively.

4.3.3 Actin Cytoskeleton

After staining with Alexa Fluor® 488 phalloidin, actin filaments within 10T1/2 cells were clearly visible in samples from non-stretched gels and both inner and outer regions of stretched gels (Fig. 4.5). Low magnification revealed low cell distribution, most often in singles or small groupings (2-4 cells), and relatively uniform throughout gel regions. Cells also demonstrated a rounded, spherical morphology with no spreading or indications of filopodial extension. Higher magnification was able to capture cytoskeletal organization. In planar cross-section views, filaments appear punctate and not well connected. Taking a vertical stack of images, short fiber segments appear to run in the out-of-plane direction, i.e. through the gel thickness, though still not well developed nor well connected. In fact, it is possible these apparent fibers are image artifacts due to the z-resolution limit of the confocal microscopy setup. In any case, there appear to be no significant differences of actin organization between cells from non-stretched and stretched gel regions.

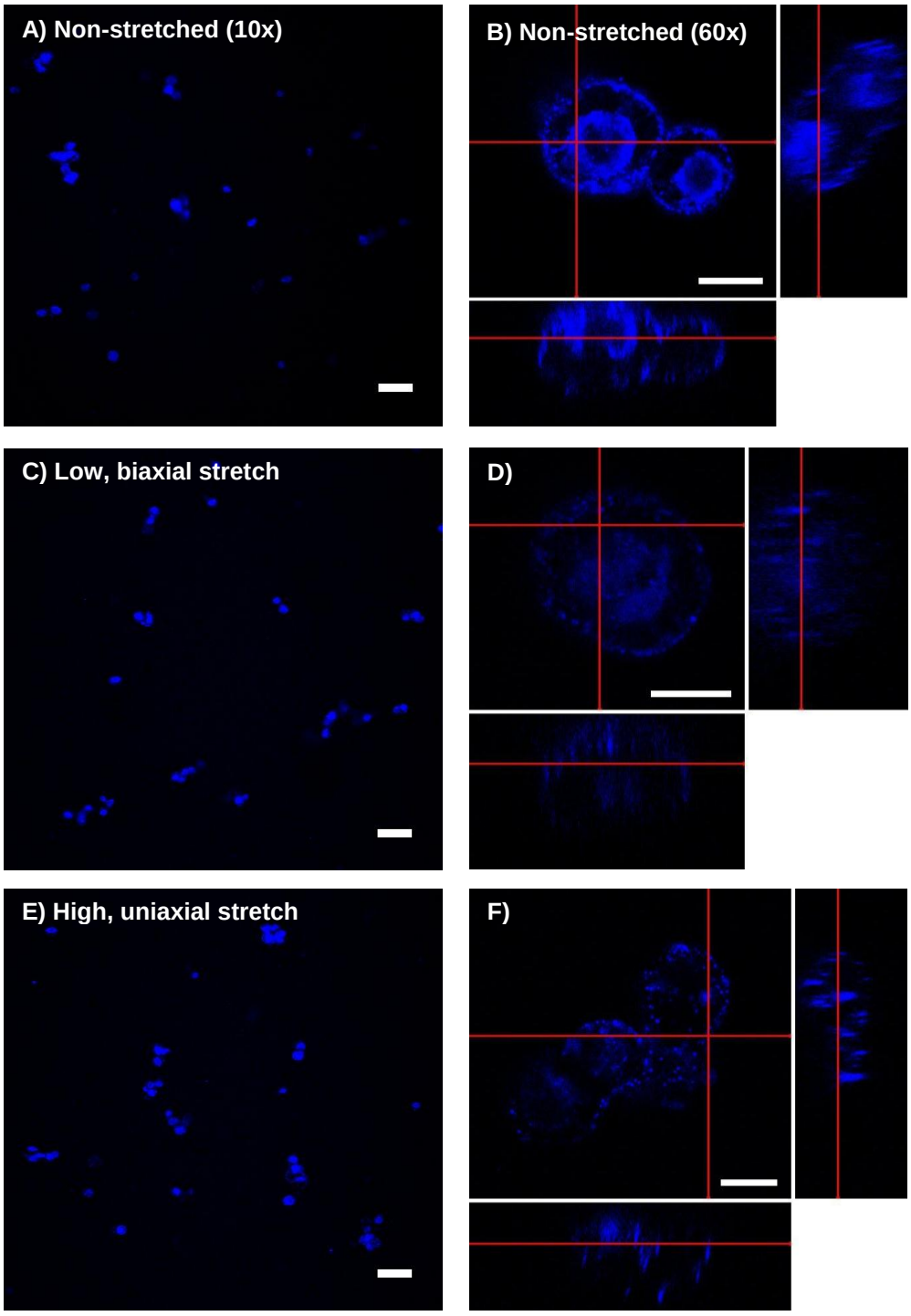

Fig. 4.5. Actin filament organization.
Alexa Fluor® 488 phalloidin dye was used to stain actin filaments within 10T1/2 cells cultured within PEGDA hydrogels. Cells were imaged within non-stretched gels (Panels A/B) and within the inner and outer regions of stretched gels (Panels C/D and E/F respectively). Scale bars equal 100 micrometers in 10x images, and 20 micrometers in 60x images.

4.3.4 Cellular Proliferation

After being cyclically stretched for 24hours, BrdU incorporation and staining demonstrated significantly different proliferation rates depending on cell location upon an elastomeric membrane, with a graded increase in the ratio of BrdU-positive cells to BrdU-negative cells from outer (low biaxial), to midway (transition), to inner (high uniaxial) regions of the membrane (Fig. 4.6.). Relative to a non-stretched control, cells subjected to high, 'simple uniaxial' stretch exhibited elevated proliferation of 2.65±0.34 fold. Interestingly, cells subjected to lower, near-equibiaxial stretch exhibited a decrease in proliferation (0.49±0.05 fold) compared to non-stretched control. The proliferation ratio within the midway transition region (0.83±0.07 fold) measured higher than that of the biaxial region and lower than that of the uniaxial region, but was not statistically different than the non-stretched control nor the low biaxial region.

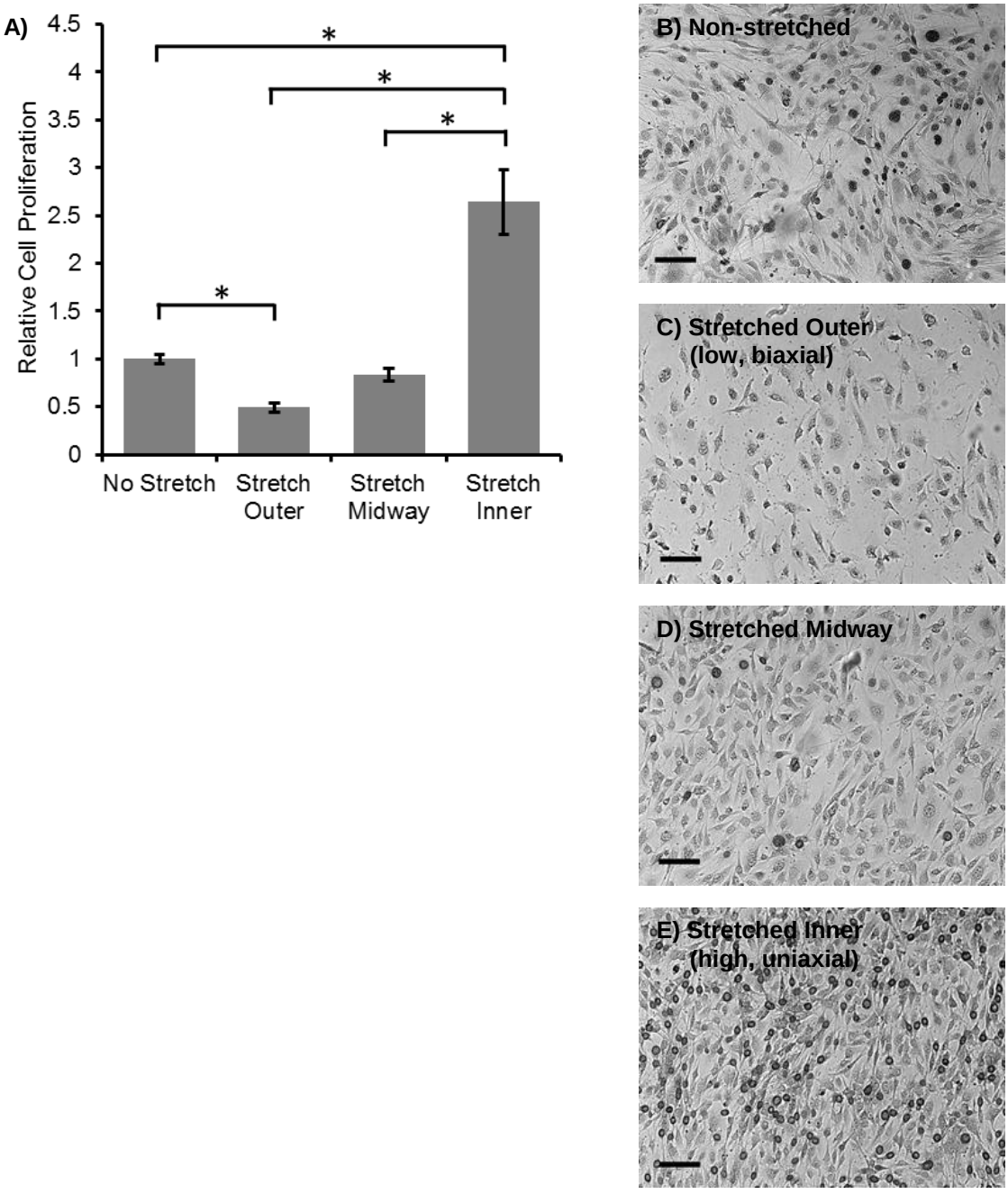

Fig. 4.6. BrdU staining for 10T1/2 cell proliferation.

After 24hrs of cyclic stretch on an elastomeric membrane, cells demonstrated significant changes in proliferation depending on their location upon the membrane (Panel A). Proliferation was quantified as the ratio of BrdU positive cells over BrdU negative cells, normalized by non-stretched control samples (shown in Panel B). This relative proliferation increased as radial position decreased from the low, biaxial stretch outer region of 22.5 < R < 30mm (Panel C), to midway region of 15 < R < 22.5mm (Panel D), to the high, uniaxial inner region of 7.5 < R < 15mm (Panel E). Scale bars equal 100 micrometers.

4.4 DISCUSSION

Numerous reviews have highlighted the seeming disparity among stretch-dependent SMC phenotype studies revealing a lack of complete understanding of the intricacies involved in this process[49; 75-77]. It appears that many stretch conditions induce cells to take on a 'hybrid' phenotype expressing both contractile and synthetic markers[49]. In the study herein, 10T1/2 cells are subjected to a complex, non-uniform stretching environment with an inner region of high magnitude, uniaxial stretch and an outer region of lower magnitude, biaxial stretch. Proliferation rates and mRNA expression values further demonstrate the complexity of phenotype modulation response with these parameters varying in cells taken from different positions upon elastomeric membranes or PEGDA hydrogels.

The actin cytoskeleton plays a large role in mediating many stretch-dependent responses of cells including differentiation and de-differentiation[77]. To assess changes in 10T1/2 cytoskeleton due to stretch, actin filaments were fluorescently labeled and imaged with confocal microscopy. Although stretch conditions typically result in marked reorganization of actin fibers, there were no apparent differences between cytoskeletons of stretched and nonstretched 10T1/2 cells within PEGDA hydrogels. In fact, actin was mostly punctate with short fiber segments running in the out-of-plane direction. This lack of actin organization and stress fiber formation is potentially attributable to the tight

encapsulation of cells within PEGDA hydrogels which restricts cells to a spherical morphology.

Quantified by BrdU incorporation, 10T1/2 proliferation was graded across the radial position of cells stretched upon a circular membrane, with increased proliferation (relative to non-stretch membrane) within the region of high uniaxial stretch, decreased proliferation within the region of low equibiaxial stretch, and statistically unchanged within the midway transition region. Many studies have shown cells of several types (including mesenchymal cells) tend to upregulate proliferation in the presence of stretch[42; 61; 68; 78; 79]. Also, fibroblasts have been shown to proliferate more rapidly in uniaxial stretch rather than biaxial, supporting the graded response result found herein[78]. However, it is unclear why proliferation rate is presently decreased in the biaxial stretch region. Such a disparate result between stretch conditions is seen in other mechanobiological responses such as the α-actin expression of bone marrow mesenchymal cells, which was increased in response to uniaxial stretch but decreased by equibiaxial stretch[80]. Potentially, such a disparity is due to the ability of cells to reorient themselves to a mechanically-preferred position by aligning perpendicular to the direction of stretch in uniaxial environments, whereas they are unable to 'escape' the stretch components of a biaxial environment.

In addition to a differential proliferation response, real-time RT-PCR quantified phenotype-related mRNA expression levels were varied between the uniaxial and equibiaxial stretch environments within a PEGDA hydrogel.

Although most of the genes analyzed yielded insignificant results, several mRNAs were significantly upregulated or downregulated. cFos expression was significantly elevated in the uniaxial region but not significantly changed in the biaxial region. An intermediate early gene, cFos is known to mediate cell growth and has been shown to increase expression in as little as 0.5-1hr in rat mesenchymal cells and SMCs exposed to equibiaxial stretch[81; 82]. However, in one study, this heightened expression reduced back to normal levels after ~2 hours[82].

Similarly, the mRNA coding for caldesmon was significantly upregulated within the uniaxial region but insignificantly changed in the biaxial region. Caldesmon is a calmodulin- and actin-binding protein that is involved in the regulation of acto-myosin contraction within SMCs, and thereby associated to their more contractile phenotype[83]. Birukov et al. also reported increased expression of caldesmon by rabbit aortic SMCs subjected to stretch, though their study subjected cells to 8 days of 15% biaxial stretch[42]. Smad5, a receptor regulated SMAD involved in TGFβ signaling and cell proliferation showed slightly (but non-significant) elevated expression in biaxial stretching region, and significantly increased expression in the uniaxial stretching region. To our knowledge, no other study has examined Smad5 mRNA expression in response to stretch, though another member of the Smad family (Smad2) was shown to be increasingly phosphorylated when human umbilical cord perivascular cells were stretched equibiaxially in the presence of an adipogenic medium[84].

Early growth response factor 1 (egr-1) is a DNA binding cofactor involved in transcription regulation and related to cell proliferation[85]. Several studies have shown egr-1 levels increase with stretch but with a very quick response of 1-4hrs, after which, levels begin to decrease[43; 85]. Interestingly, our measured egr-1 levels showed reduced expression in both stretch regions compared to the non-stretch control. It is possible that the stretching duration employed herein (24hrs) was long enough for egr1 to quickly increase but then decrease over time, even past the initial control level. ID2 (inhibitor of DNA binding) is a transcription regulator that contributes to SMC proliferation after vascular injury[86]. Levels of ID2 mRNA were marginally decreased in both stretch regions. Finally, Plasminogen Activator Inhibitor 1, an inhibitor of fibrinolysis and thrombin activity, showed reduced mRNA levels as well. PAI1 has been shown to play a significant role in intimal hyperplasia with PAI1 deficient mice producing greater neo-intimal formation, and treatments of recombinant PAI1 inhibiting neo-intimal formation in rat carotid injuries[87; 88]. The sum of our gene expression results reveal that indeed stretch induces a sort of ‘hybrid’ phenotype with the up- and down-regulation of both synthetic and contractile proteins.

We have previously measured mRNA expression of these same genes from 2D monolayers of 10T1/2 cells stretched upon elastomeric membranes with the same device used herein[58]. Interestingly, when stretched in 2D, caldesmon and Id2 mRNA levels were decreased, while egr1, cFos, and pai1 mRNA levels were increased (SMAD5 mRNA levels were insignificantly changed). The

disparity between the 2D and 3D cases can potentially be attributable to several factors. Most simply, cells of most types are known to exhibit different adhesion behaviors and morphologies (e.g., spread and rounded vs. stellate) when cultured on any 2D vs 3D environments[63]. These fundamental cell behaviors can drastically impact how stretch stimuli are transduced, and subsequently affect many different biological responses such as gene expression. In addition, it should be noted that 10T1/2 2D monolayers were near confluent when mRNA was collected, whereas cells within PEGDA gels were sparse and isolated (as shown above). Cell-cell contacts have been shown to play a significant role in several phenotype-related behaviors[49]. Furthermore, cells in PEGDA hydrogels are encapsulated within the polymer matrix. As mentioned above, this encapsulation potentially interferes with actin cytoskeletal remodeling and thereby potentially interferes with intracellular force transduction into phenotype-related expression changes. It is important to keep all of these factors in mind when comparing expression data from 2D and 3D cases, and therefore great care should be taken to isolate and verify all such factors for thorough understanding of specific genes and proteins.

The primary limitations of this study are related to the use of PEGDA hydrogels as 3D constructs. Besides the issue of encapsulation, isolating quality mRNA from hydrogels after stretching experiments is made difficult due to the abundance of polymer chains[89]. Low yields of nucleic acids greatly increase the amount of error in RT-PCR measurement and analysis. Also, the use of PEGDA

requires the addition of an adhesion molecule (RGD in our case) in order to allow cell attachment to the polymer network. Due to the large size of our gels (volume ~ 8mL), economically feasible amounts of acrylated-RGD and cell seeding numbers resulted in relatively low RGD concentration and cell density. Still, PEGDA gels offer experimental benefit due to their high degree of mechanical tunability, as well as their bioinertness. Future experiments should seek to increase RGD and cell density, as well as incorporate degradable segments into gels as several groups have done to allow for remodeling of the polymer network and enable changes in cell morphology and potential migration[90].

A concern with cell-stretching devices is ensuring that the deformations applied to the bulk polymer+cell aggregate translate directly to deformations on the cellular level. It is possible that fiber slippage, bending, and non-affine motion can result in potentially ambiguously heterogeneous deformations applied to cells. It is also possible that cell groupings scattered within the gel introduce focal points of heterogeneity, altering the local stretch distributions. Though there is a general lack of investigation into deformation coupling across scales, it has been shown that these heterogeneities can be significant at the micro-scale of 3D polymer constructs[63; 91; 92].

It was beyond the scope of this work to fully characterize the cell-construct deformation coupling. Even so, concerns for the above possibilities are attenuated by several factors. First, the fiber network is effectively ‘pre-loaded’

by allowing free swelling prior to experiments, thereby engaging fibers and enhancing deformation affinity. Secondly, it is important to note the very small mesh size of the PEGDA hydrogels (roughly 1/1000 of 10T1/2 cell size). Studies have shown that the heterogeneity of micro-deformations in some constructs became homogeneous with an approximately 200x increase in length scale, suggesting that any non-affine deformation of our PEGDA polymer network is potentially negligible at the cell level[91; 92].

With regards to scattered cell groupings altering local stretch distributions, Caille et al. have shown high correlation of cellular and substrate deformations across 2D polymer constructs[93]. In the case of 3D environments, very little work has been done to study this effect, though focal inclusions of very stiff calcifications have shown to alter the stress distributions in atherosclerotic plaques[94; 95]. However, in that case the stiffness mismatch of materials was a factor of 10 (i.e., mechanical stiffness properties of calcifications were 10 times greater than those of the surrounding fibrin cap). Within our gels, the mismatch of cell and hydrogel stiffnesses is probably not as drastic, as evidenced by previous mechanical characterizations[96-98]. Browning *et al.* uniaxially strained PEGDA hydrogel rings and calculated a secant modulus of stress-strain data, which yielded a value of 19kPa for 20% concentration, 10kDa molecular weight gels as used herein[96]. The apparent elastic moduli of rat aortic smooth muscle cells and murine embryonic cells have been measured by AFM indentation in the respective ranges of 10-25kPa and 0.5-16kPa, depending on level of serum

deprivation or differentiation state[97; 98]. Thus, in our case, though the stiffnesses of 10T1/2 cells and PEGDA hydrogels are certainly not identical, they are probably within the same order of magnitude. These findings, taken with the very low cell density in our gels, lead us to suspect that the inclusion of cells had minimal perturbation on neighboring substrate deformations.

In summary, a novel cell-stretching device has been employed to stretch cell-seeded membranes and PEGDA hydrogels in order to subject cultures to non-uniform stretch environments and investigate SMC phenotype modulation therein. Proliferation measured by BrdU, and mRNA expression measured by quantitative, real-time RT-PCR revealed differential responses of 10T1/2 cells depending on their location within the stretching environment, which ranged from a high magnitude uniaxial stretch to a lower magnitude near-equibiaxial stretch. These results reveal the complexity of phenotype modulation, while establishing the capability of this device to study this process in the presence of physiologic stretch conditions representative of that *in vivo*.

5. CONCLUSIONS

5.1 SUMMARY OF FINDINGS

By subjecting 10T1/2 mesenchymal cells to cyclic biaxial stretching for 24hrs upon the non-uniform environments described herein, biological responses were elicited at various levels depending upon cell location on the constructs. On 2D elastomeric membranes and PDMS tube surfaces, cells tended to orient parallel to the direction of least stretch, with the greatest alignment exhibited in regions of uniaxial stretch. Regions of near equibiaxial stretch exhibited random alignment, and a graded response was found in the transition region between uniaxial and equibiaxial stretch locations. In addition to alignment, 10T1/2 proliferation (assessed by BrdU incorporation) was modulated by cyclic stretching. Within the uniaxial stretching region, cells demonstrated increased proliferation rates compared to a non-stretched control. This response was reduced in the (outer) equibiaxial region, where cell proliferation was lower than that of a non-stretched control.

Gene expression for phenotype-related proteins was measured using quantitative real-time RT-PCR. These results demonstrated varied mRNA expression levels of 10T1/2 cells subjected to non-uniform stretch environments within 3D PEGDA hydrogels. Interestingly, a variety of contractile and synthetic markers were both upregulated and downregulated compared to a non-stretched

control, indicating that stretch induces a type of hybrid phenotype. Moreover, expression differences were evident between uniaxial and equibiaxial stretching regions, agreeing with many previous studies that mechanosensitivity of these genes is more complicated than binary ‘stretch’ or ‘no stretch’ responses. Instead, the altered expression due to stretch is a variable response that can result in quite different levels depending upon a cell’s stretching environment parameters.

5.2 GENERAL CONCLUSIONS AND SIGNIFICANCE OF WORK

To our knowledge, the present work is the most extensive investigation to date of the behavior of any type of cell on non-uniform stretch environments. These results reveal particular attributes of cellular orientation and phenotypic responses of mesenchymal cells stimulated by heterogeneous stretch distributions, while more generally demonstrating the capabilities of non-uniform stretches to improve mechanobiological studies. Such improvements include 1) the ability of a single experiment to probe biological responses at many levels of stretch, thereby aiding in the generation of dose-response curves; 2) the potential identification of mechanical input threshold values for various responses; 3) the anatomical localization of particular maladaptive cellular responses to enable accurate targeting of therapies; and others.

The historical approach for elucidating cell mechanobiological behavior has been a sort of ‘bottom up’ methodology, wherein mechanical stimuli have been simplified and isolated to generate 1:1 relationships between a single stimuli input and a single response output. This approach has been vital to developing our fundamental understanding of the types and patterns of mechanical cues that elicit biological responses. However, this approach is limited in its ability to predict cell behaviors in the more complex mechanical loadings present in the body. *In vivo* mechanical environments are a multi-faceted combination of loading type (uni- vs multi-axial), magnitude, frequency, duration, substrate stiffness, etc. Moreover, these parameters can be highly non-uniform in both space and time. Thus, accurate predictions of cell behavior *in vivo* requires an understanding of the roles each of these factors play, as well as an understanding of their interaction effects. This understanding clearly requires a massive amount of experimentation, further compounded by the fact that cells of different types and in the presence of different chemical stimuli (growth factors etc.) respond in various ways. With such a large amount of possible mechanobiological relationships, it is important to judiciously select and run investigations that are of the most significance. To that end, our stretching devices subjected cells to the non-uniform hoop stretch gradients characteristic of the disease-prone artery wall.

It is important to note that while the cell-seeded membranes and gels herein were subjected to a physiologic stretching environment, biological

measurements of cell behavior were only compared to non-stretched controls, and not uniform uniaxial or uniform biaxial controls at various magnitudes. Therefore it may be difficult to distinguish between the particular effects of different stretch parameters within these experiments. However, tissues *in vivo* respond to many stretch stimuli working in concert, and our motivation for these cell-stretching devices is to seek to replicate that combination of stimuli *in vitro*. Proper conclusions of this work should be that the particular combination of stretch conditions used herein generated the responses evident herein.

To make ultimate conclusions about the response particulars (e.g., proliferation or a specific gene expression level), thorough investigation should be conducted with controls for the various stretch parameters and potential interactions. These yield information on the detailed molecular pathways involved, which are necessary for designing pharmaceutical treatment options. The present work presents devices which may serve ‘first-pass’ type of studies to yield indications of what overall behaviors may be contributing to disease progression and therefore warrant further and more thorough study.

Herein, we show that proliferation and cell phenotype are altered by the loading conditions present in disease-prone arteries. Interestingly, increased proliferation only occurs in the uniaxial stretching region near the inner radius. This finding suggests that the cell populations contributing to intimal hyperplasia might be localized to the inner arterial wall, perhaps allowing for more targeted therapy delivery to this region only. Regarding cellular phenotype modulation,

we show that cells undertake a hybrid phenotype when exposed to these physiologic stretch regimens. Again, this response is not uniform across all stretched regions, potentially supporting a localized contribution to atherogenic development. It is clear that SMC phenotype remains a convoluted process balanced by many various signaling pathways. Our results identify several mRNAs that might be involved, but further study is required to elucidate each of their precise roles.

5.3 LIMITATIONS

While a number of limitations have been mentioned in previous sections, the primary limitation related to adequate controls is admitted above. For example, consider the varied expression levels between the inner and outer regions of the construct. These differences were potentially due to the difference in type of stretching environment (i.e., simple uniaxial vs near equibiaxial), or due to a gene sensitivity to the overall magnitude of stretching since the uniaxial region was subjected to greater principal deformation than the equibiaxial region. Proper controls of uniform uni- and equibiaxial at various levels of magnitude would delineate those possibilities.

On the topic of gene expression, it is important to note that the measure of expression employed herein (quantification of steady-state mRNA levels as assessed by RT-PCR) does not necessarily correlate to DNA transcription

changes, nor altered translation into protein, nor ultimate changes in protein concentrations. Though connected, each of these steps is independently regulated by cofactors and enzymes that are able to degrade, protect, or stimulate their respective targets. Furthermore, many of these regulating factors are also mechanosensitive. Therefore, it is possible that while stretch upregulates the mRNA expression of a protein, the overall secreted level of that protein remains unchanged. The benefit of using RT-PCR to measure expression changes lies in the ability to analyze total RNA yields and quantify expression for dozens of mRNAs at one time. These results then give credence to further blotting techniques for quantification of particular protein levels.

Another primary limitation that should be mentioned is the general use of *in vitro* cell culture models. It is widely known that cellular behavior *in vitro* does not always correlate to behavior *in vivo* due to the drastic increase in complicating factors. However, cell culture is a well-established method to simplify physiological behaviors and elucidate fundamental biological relationships. Ideally, arterial cell mechanobiological should seek to replicate the *in vivo* conditions as realistically as possible. Many features of the native environment (e.g., extracellular matrix structure, neighboring cell types, chemical signals, etc.) remain to be replicated in our experiments, and these differences limit the interpretation of our findings. Yet the current work makes a step in the realistic direction by applying a more physiologic mechanical environment to 2D and 3D cell cultures.

5.4 FUTURE DIRECTIONS AND APPLICATIONS

The ultimate goal of this project is to add physiologic relevance to cell stretching environments in order to gain improved understanding of disease-related cell responses in non-uniform stretch distributions. The majority of the current discussion has focused on results that elucidate variable cell behavior dependent upon their location within the constructs. These devices are also well-suited to investigate cellular behaviors in response to stretch gradients themselves. A major mechanical parameter, stretch gradients (to our knowledge) have yet to be decisively shown to modulate cell behavior. Yet, they hold the potential to act as directional cues to guide cell polarization, directed mitosis, or persistent migration, much like substrate stiffness gradients direct some of these behaviors[28; 99].

In order to test the effect of stretch gradients on these behaviors, experimental cases can be selected in order to isolate the effects of point-wise stretch magnitude vs. stretch gradient. For example, Fig. 5.1 shows the computed stretch profiles for defects and fixations of different radii (small or large). Regions have been identified (highlighted rectangles) which cover an identical range of circumferential and radial stretch magnitudes as well as the anisotropy ratio between them, but with drastically different gradients across that range (high for small defect and low for large defect; high for small fixation and

low for large fixation). Thus, by comparing the cellular responses within each of these regions, the effects of stretch gradient can be revealed.

Various cellular behaviors could be analyzed to reveal cell polarization such as subcellular cytoskeletal reorganization (e.g., stress fiber formation on one side vs the other), nuclei localization, or microtubule organizing center localization. Cell motility (a key behavior involved in intimal thickening) can also be assessed upon these devices to reveal whether or not cells tend to migrate toward higher or lower regions of stretch in an adaptive remodeling mechanism. These studies can easily be conducted with cells on the surface of membranes, or within 3D hydrogels with the addition of degradable linking groups into the polymer network[90]. Incorporating degradable sections into hydrogels allows cells to remodel their local surroundings and subsequently alter morphology and even migrate. If stretch gradients were shown to induce and direct SMC migration toward the inner edge, this would reveal a major process potentially contributing to atherogenesis and in-stent restenosis. Furthermore, the stretching device could serve as a model for elucidating the underlying mechanisms of this behavior as well as testing potential therapeutic regimens to control SMC motility.

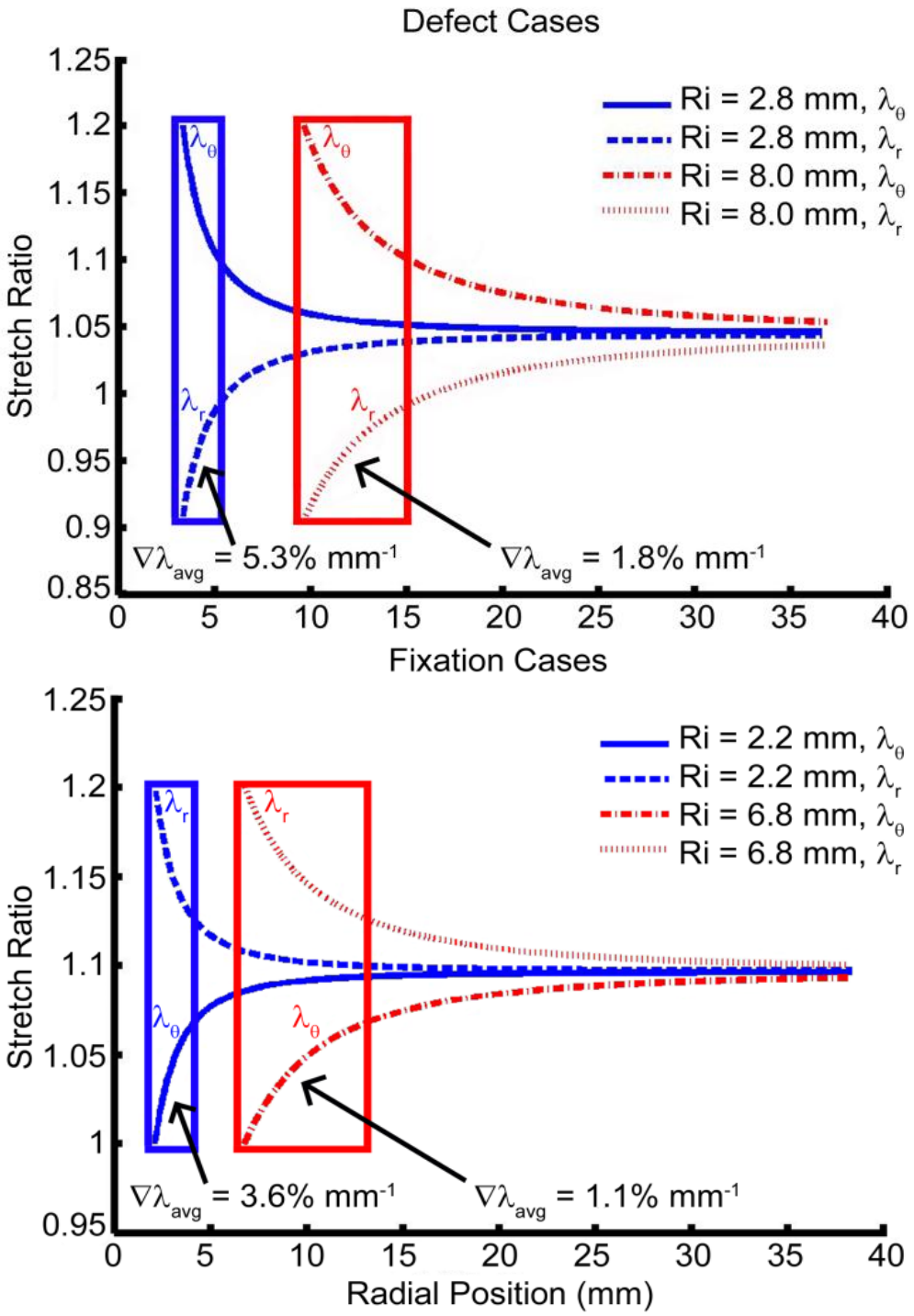

Fig. 5.1. Potential experimental stretching cases.
Boxes highlight regions that span identical stretch magnitude ranges and anisotropy ratios, but different stretch gradients.

For improved anatomic representation of the arterial wall, the tube-stretching device could be employed with the construction of 3D PEGDA hydrogel tubes. Such a setup would be capable of nearly exactly replicating the tri-axial stretching environment with non-uniform distributions as seen *in vivo* while allowing for all the biological assessments employed herein.

It is also important to note the applications of non-uniform stretch environments beyond arterial disease. Many tissues experience heterogeneous load distributions such as musculoskeletal and connective tissues, as well as morphologic structures[52; 54; 100]. Although vascular disease is the largest focus of this work, the general methods and findings are potentially applicable to many cell types and disease conditions of these various tissues. In addition, the application of non-uniform loads is potentially useful in the engineering of replacement constructs for many complex tissues that are spatially non-uniform in their makeup. Such tissues include myocardium where myocyte orientation varies from the epi- to endocardial surfaces, osteotendinous junctions where the chondrocyte- and collagen-encompassed tendon seemingly transitions to the osteoblastic bone, or articular cartilage thickness where chondrocyte morphology changes from an elongated, flattened shape near the surface to a more rounded shape far from the surface[101-103]. Using similar cell stretching devices that heterogeneously apply mechanical forces and deformations, tissue engineers can potentially develop these complicated structures more predictably. With an improved understanding of cell behavior in non-uniform

stretches and an improved ability to selectively manipulate cellular responses depending on their anatomical location, stretching devices like the ones presented herein offer much potential to vastly improve our ability to prevent and treat disease conditions of many types via enhanced device designs and accurately targeted pharmaceutical therapies.

REFERENCES

1. Wang, J.H., and B.P. Thampatty. An introductory review of cell mechanobiology. Biomech Model Mechanobiol. 5:1-16, 2006.

2. Haga, J.H., Y.S. Li, and S. Chien. Molecular basis of the effects of mechanical stretch on vascular smooth muscle cells. J Biomech. 40:947-960, 2007.

3. Humphrey, J.D. Vascular adaptation and mechanical homeostasis at tissue, cellular, and sub-cellular levels. Cell Biochem Biophys. 50:53-78, 2008.

4. Rudijanto, A. The role of vascular smooth muscle cells on the pathogenesis of atherosclerosis. Acta Med Indones. 39:86-93, 2007.

5. Schwartz, S.M. Smooth muscle migration in atherosclerosis and restenosis. J Clin Invest. 100:S87-89, 1997.

6. Ku, D.N., D.P. Giddens, C.K. Zarins, and S. Glagov. Pulsatile flow and atherosclerosis in the human carotid bifurcation. Positive correlation between plaque location and low oscillating shear stress. Arteriosclerosis. 5:293-302, 1985.

7. Delfino, A., J.E. Moore, Jr., N. Stergiopulos, V. Vaclavik, C.Y. Genton, and J.J. Meister. Wall stresses in the carotid bifurcation: effects of wall non-homogeneity and correlation with intimal thickness. J Vasc Inv. 4:11, 1998.

8. Moore, J.E., Jr. Biomechanical issues in endovascular device design. J Endovasc Ther. 16 Suppl 1:I1-11, 2009.

9. Moore, J., Jr., and J.L. Berry. Fluid and solid mechanical implications of vascular stenting. Ann Biomed Eng. 30:498-508, 2002.

10. World Health Organization. Cardiovascular diseases, fact sheet number 317. Geneva, Switzerland: WHO. September 2011.

11. Lloyd-Jones, D., R.J. Adams, T.M. Brown, M. Carnethon, S. Dai, G. De Simone, T.B. Ferguson, E. Ford, K. Furie, C. Gillespie*, et al.* Executive summary: heart disease and stroke statistics--2010 update: a report from the American Heart Association. Circulation. 121:948-954, 2010.

12. Levesque, M.J., and R.M. Nerem. The elongation and orientation of cultured endothelial cells in response to shear stress. J Biomech Eng. 107:341-347, 1985.

13. Leung, D.Y., S. Glagov, and M.B. Mathews. Cyclic stretching stimulates synthesis of matrix components by arterial smooth muscle cells in vitro. Science. 191:475-477, 1976.

14. Cheng, G.C., W.H. Briggs, D.S. Gerson, P. Libby, A.J. Grodzinsky, M.L. Gray, and R.T. Lee. Mechanical strain tightly controls fibroblast growth factor-2 release from cultured human vascular smooth muscle cells. Circ Res. 80:28-36, 1997.

15. Chuong, C.J., and Y.C. Fung. Three-dimensional stress distribution in arteries. J Biomech Eng. 105:268-274, 1983.

16. Chuong, C.J., and Y.C. Fung. On residual stresses in arteries. J Biomech Eng. 108:189-192, 1986.

17. Delfino, A., N. Stergiopulos, J.E. Moore, Jr., and J.J. Meister. Residual strain effects on the stress field in a thick wall finite element model of the human carotid bifurcation. J Biomech. 30:777-786, 1997.

18. Matsumoto, T., and K. Hayashi. Stress and strain distribution in hypertensive and normotensive rat aorta considering residual strain. J Biomech Eng. 118:62-73, 1996.

19. Hayashi, K., and Y. Imai. Tensile property of atheromatous plaque and an analysis of stress in atherosclerotic wall. J Biomech. 30:573-579, 1997.

20. Holzapfel, G.A., and T.C. Gasser. Computational stress-deformation analysis of arterial walls including high-pressure response. Int J Cardiol. 116:78-85, 2007.

21. Kiousis, D.E., T.C. Gasser, and G.A. Holzapfel. A numerical model to study the interaction of vascular stents with human atherosclerotic lesions. Ann Biomed Eng. 35:1857-1869, 2007.

22. Bedoya, J., C.A. Meyer, L.H. Timmins, M.R. Moreno, and J.E. Moore. Effects of stent design parameters on normal artery wall mechanics. J Biomech Eng. 128:757-765, 2006.

23. Lally, C., F. Dolan, and P.J. Prendergast. Cardiovascular stent design and vessel stresses: a finite element analysis. J Biomech. 38:1574-1581, 2005.

24. David, G., and J.D. Humphrey. Redistribution of stress due to a circular hole in a nonlinear anisotropic membrane. J Biomech. 37:1197-1203, 2004.

25. Mori, D., G. David, J.D. Humphrey, and J.E. Moore, Jr. Stress distribution in a circular membrane with a central fixation. J Biomech Eng. 127:549-553, 2005.

26. Lee, A.A., T. Delhaas, L.K. Waldman, D.A. MacKenna, F.J. Villarreal, and A.D. McCulloch. An equibiaxial strain system for cultured cells. Am J Physiol. 271:C1400-1408, 1996.

27. Mitra, A.K., and D.K. Agrawal. In stent restenosis: bane of the stent era. J Clin Pathol. 59:232-239, 2006.

28. Lo, C.M., H.B. Wang, M. Dembo, and Y.L. Wang. Cell movement is guided by the rigidity of the substrate. Biophys J. 79:144-152, 2000.

29. Raeber, G.P., M.P. Lutolf, and J.A. Hubbell. Part II: Fibroblasts preferentially migrate in the direction of principal strain. Biomech Model Mechanobiol. 7:215-225, 2008.

30. Huang, L., P.S. Mathieu, and B.P. Helmke. A stretching device for high-resolution live-cell imaging. Ann Biomed Eng. 38:1728-1740, 2010.

31. Hirschi, K.K., L. Lai, N.S. Belaguli, D.A. Dean, R.J. Schwartz, and W.E. Zimmer. Transforming growth factor-beta induction of smooth muscle cell phenotpye requires transcriptional and post-transcriptional control of serum response factor. J Biol Chem. 277:6287-6295, 2002.

32. Vande Geest, J.P., E.S. Di Martino, and D.A. Vorp. An analysis of the complete strain field within Flexercell membranes. J Biomech. 37:1923-1928, 2004.

33. Brown, T.D. Techniques for mechanical stimulation of cells in vitro: a review. J Biomech. 33:3-14, 2000.

34. Ohashi, T., M. Masuda, T. Matsumoto, and M. Sato. Nonuniform strain of substrate induces local development of stress fibers in endothelial cells under uniaxial cyclic stretching. Clin Hemorheol Microcirc. 37:37-46, 2007.

35. Yung, Y.C., H. Vandenburgh, and D.J. Mooney. Cellular strain assessment tool (CSAT): precision-controlled cyclic uniaxial tensile loading. J Biomech. 42:178-182, 2009.

36. Balestrini, J.L., J.K. Skorinko, A. Hera, G.R. Gaudette, and K.L. Billiar. Applying controlled non-uniform deformation for in vitro studies of cell mechanobiology. Biomech Model Mechanobiol. 9:329-344, 2010.

37. Younis, H.F., M.R. Kaazempur-Mofrad, R.C. Chan, A.G. Isasi, D.P. Hinton, A.H. Chau, L.A. Kim, and R.D. Kamm. Hemodynamics and wall mechanics in human carotid bifurcation and its consequences for atherogenesis: investigation of inter-individual variation. Biomech Model Mechanobiol. 3:17-32, 2004.

38. Buck, R.C. Reorientation response of cells to repeated stretch and recoil of the substratum. Exp Cell Res. 127:470-474, 1980.

39. Dartsch, P.C., H. Hammerle, and E. Betz. Orientation of cultured arterial smooth muscle cells growing on cyclically stretched substrates. Acta Anat (Basel). 125:108-113, 1986.

40. Kanda, K., T. Matsuda, and T. Oka. Two-dimensional orientational response of smooth muscle cells to cyclic stretching. ASAIO J. 38:M382-385, 1992.

41. Houtchens, G.R., M.D. Foster, T.A. Desai, E.F. Morgan, and J.Y. Wong. Combined effects of microtopography and cyclic strain on vascular smooth muscle cell orientation. J Biomech. 41:762-769, 2008.

42. Birukov, K.G., V.P. Shirinsky, O.V. Stepanova, V.A. Tkachuk, A.W. Hahn, T.J. Resink, and V.N. Smirnov. Stretch affects phenotype and proliferation of vascular smooth muscle cells. Mol Cell Biochem. 144:131-139, 1995.

43. Morawietz, H., Y.H. Ma, F. Vives, E. Wilson, V.P. Sukhatme, J. Holtz, and H.E. Ives. Rapid induction and translocation of Egr-1 in response to mechanical strain in vascular smooth muscle cells. Circ Res. 84:678-687, 1999.

44. Goldman, J., L. Zhong, and S.Q. Liu. Degradation of alpha-actin filaments in venous smooth muscle cells in response to mechanical stretch. Am J Physiol Heart Circ Physiol. 284:H1839-1847, 2003.

45. Butcher, J.T., B.C. Barrett, and R.M. Nerem. Equibiaxial strain stimulates fibroblastic phenotype shift in smooth muscle cells in an engineered tissue model of the aortic wall. Biomaterials. 27:5252-5258, 2006.

46. Mudera, V.C., R. Pleass, M. Eastwood, R. Tarnuzzer, G. Schultz, P. Khaw, D.A. McGrouther, and R.A. Brown. Molecular responses of human dermal fibroblasts to dual cues: contact guidance and mechanical load. Cell Motil Cytoskeleton. 45:1-9, 2000.

47. Kanda, K., and T. Matsuda. Behavior of arterial wall cells cultured on periodically stretched substrates. Cell Transplant. 2:475-484, 1993.

48. Kaunas, R., and H.J. Hsu. A kinematic model of stretch-induced stress fiber turnover and reorientation. J Theor Biol. 257:320-330, 2009.

49. Williams, B. Mechanical influences on vascular smooth muscle cell function. J Hypertens. 16:1921-1929, 1998.

50. Wolinsky, H., and S. Glagov. A lamellar unit of aortic medial structure and function in mammals. Circ Res. 20:99-111, 1967.

51. Nerem, R.M., M.J. Levesque, and J.F. Cornhill. Vascular endothelial morphology as an indicator of the pattern of blood flow. J Biomech Eng. 103:172-176, 1981.

52. Filas, B.A., V.D. Varner, D.A. Voronov, and L.A. Taber. Tracking morphogenetic tissue deformations in the early chick embryo. J Vis Exp. e3129, 2011.

53. Varner, V.D., D.A. Voronov, and L.A. Taber. Mechanics of head fold formation: investigating tissue-level forces during early development. Development. 137:3801-3811, 2010.

54. Nelson, C.M., R.P. Jean, J.L. Tan, W.F. Liu, N.J. Sniadecki, A.A. Spector, and C.S. Chen. Emergent patterns of growth controlled by multicellular form and mechanics. Proc Natl Acad Sci U S A. 102:11594-11599, 2005.

55. Li, Z.Y., T. Tang, U.K.-I. J, M. Graves, M. Sutcliffe, and J.H. Gillard. Assessment of carotid plaque vulnerability using structural and geometrical determinants. Circ J. 72:1092-1099, 2008.

56. Rolland, P.H., C. Mekkaoui, V. Vidal, J.L. Berry, J.E. Moore, M. Moreno, P. Amabile, and J.M. Bartoli. Compliance matching stent placement in the carotid artery of the swine promotes optimal blood flow and attenuates restenosis. Eur J Vasc Endovasc Surg. 28:431-438, 2004.

57. Berry, J.L., E. Manoach, C. Mekkaoui, P.H. Rolland, J.E. Moore, Jr., and A. Rachev. Hemodynamics and wall mechanics of a compliance matching stent: in vitro and in vivo analysis. J Vasc Interv Radiol. 13:97-105, 2002.

58. Richardson, W.J., R.P. Metz, M.R. Moreno, E. Wilson, and J.E. Moore, Jr. A device to study the effects of stretch gradients on cell behavior. J Biomech Eng. 133:101008, 2011.

59. Mohammad, Z., J.E. Moore, Jr., A. Rachev, J.L. Berry, and E. Manoach. Stress concentration reduction in stented arteries using compliance transitioning. Int J Cardio Med Science. 3:1-7, 2000.

60. Rachev, A., E. Manoach, J. Berry, and J.E. Moore, Jr. A model of stress-induced geometrical remodeling of vessel segments adjacent to stents and artery/graft anastomoses. J Theor Biol. 206:429-443, 2000.

61. Tan, W., D. Scott, D. Belchenko, H.J. Qi, and L. Xiao. Development and evaluation of microdevices for studying anisotropic biaxial cyclic stretch on cells. Biomed Microdevices. 10:869-882, 2008.

62. De, R., A. Zemel, and S.A. Safrani. Dynamics of cell orientation. Nature Physics. 3:655-659, 2007.

63. Pedersen, J.A., and M.A. Swartz. Mechanobiology in the third dimension. Ann Biomed Eng. 33:1469-1490, 2005.

64. Ballyk, P.D., C. Walsh, J. Butany, and M. Ojha. Compliance mismatch may promote graft-artery intimal hyperplasia by altering suture-line stresses. J Biomech. 31:229-237, 1998.

65. Owens, G.K. Regulation of differentiation of vascular smooth muscle cells. Physiol Rev. 75:487-517, 1995.

66. Owens, G.K., M.S. Kumar, and B.R. Wamhoff. Molecular regulation of vascular smooth muscle cell differentiation in development and disease. Physiol Rev. 84:767-801, 2004.

67. Li, C., F. Wernig, M. Leitges, Y. Hu, and Q. Xu. Mechanical stress-activated PKCdelta regulates smooth muscle cell migration. FASEB J. 17:2106-2108, 2003.

68. Stegemann, J.P., and R.M. Nerem. Altered response of vascular smooth muscle cells to exogenous biochemical stimulation in two- and three-dimensional culture. Exp Cell Res. 283:146-155, 2003.

69. Kanda, K., T. Matsuda, and T. Oka. Mechanical stress induced cellular orientation and phenotypic modulation of 3-D cultured smooth muscle cells. ASAIO J. 39:M686-690, 1993.

70. Albinsson, S., and P. Hellstrand. Integration of signal pathways for stretch-dependent growth and differentiation in vascular smooth muscle. Am J Physiol Cell Physiol. 293:C772-782, 2007.

71. Zhao, X.H., C. Laschinger, P. Arora, K. Szaszi, A. Kapus, and C.A. McCulloch. Force activates smooth muscle alpha-actin promoter activity through the Rho signaling pathway. J Cell Sci. 120:1801-1809, 2007.

72. Albinsson, S., I. Nordstrom, and P. Hellstrand. Stretch of the vascular wall induces smooth muscle differentiation by promoting actin polymerization. J Biol Chem. 279:34849-34855, 2004.

73. Cappadona, C., E.M. Redmond, N.G. Theodorakis, I.H. McKillop, R. Hendrickson, A. Chhabra, J.V. Sitzmann, and P.A. Cahill. Phenotype dictates the growth response of vascular smooth muscle cells to pulse pressure in vitro. Exp Cell Res. 250:174-186, 1999.

74. Hahn, M.S., L.J. Taite, J.J. Moon, M.C. Rowland, K.A. Ruffino, and J.L. West. Photolithographic patterning of polyethylene glycol hydrogels. Biomaterials. 27:2519-2524, 2006.

75. Stegemann, J.P., H. Hong, and R.M. Nerem. Mechanical, biochemical, and extracellular matrix effects on vascular smooth muscle cell phenotype. J Appl Physiol. 98:2321-2327, 2005.

76. Halka, A.T., N.J. Turner, A. Carter, J. Ghosh, M.O. Murphy, J.P. Kirton, C.M. Kielty, and M.G. Walker. The effects of stretch on vascular smooth muscle cell phenotype in vitro. Cardiovasc Pathol. 17:98-102, 2008.

77. Hellstrand, P., and S. Albinsson. Stretch-dependent growth and differentiation in vascular smooth muscle: role of the actin cytoskeleton. Can J Physiol Pharmacol. 83:869-875, 2005.

78. Gould, R.A., K. Chin, T.P. Santisakultarm, A. Dropkin, J.M. Richards, C.B. Schaffer, and J.T. Butcher. Cyclic strain anisotropy regulates valvular interstitial cell phenotype and tissue remodeling in three-dimensional culture. Acta Biomater. 8:1710-1719, 2012.

79. Ghazanfari, S., M. Tafazzoli-Shadpour, and M.A. Shokrgozar. Effects of cyclic stretch on proliferation of mesenchymal stem cells and their differentiation to smooth muscle cells. Biochem Biophys Res Commun. 388:601-605, 2009.

80. Park, J.S., J.S. Chu, C. Cheng, F. Chen, D. Chen, and S. Li. Differential effects of equiaxial and uniaxial strain on mesenchymal stem cells. Biotechnol Bioeng. 88:359-368, 2004.

81. Song, G., Y. Ju, X. Shen, Q. Luo, Y. Shi, and J. Qin. Mechanical stretch promotes proliferation of rat bone marrow mesenchymal stem cells. Colloids Surf B Biointerfaces. 58:271-277, 2007.

82. Shynlova, O.P., A.D. Oldenhof, M. Liu, L. Langille, and S.J. Lye. Regulation of c-fos expression by static stretch in rat myometrial smooth muscle cells. Am J Obstet Gynecol. 186:1358-1365, 2002.

83. Sobue, K., K. Hayashi, and W. Nishida. Expressional regulation of smooth muscle cell-specific genes in association with phenotypic modulation. Mol Cell Biochem. 190:105-118, 1999.

84. Turner, N.J., H.S. Jones, J.E. Davies, and A.E. Canfield. Cyclic stretch-induced TGFbeta1/Smad signaling inhibits adipogenesis in umbilical cord progenitor cells. Biochem Biophys Res Commun. 377:1147-1151, 2008.

85. Wu, X., J. Cheng, P. Li, M. Yang, S. Qiu, P. Liu, and J. Du. Mechano-sensitive transcriptional factor Egr-1 regulates insulin-like growth factor-1 receptor expression and contributes to neointima formation in vein grafts. Arterioscler Thromb Vasc Biol. 30:471-476, 2010.

86. Matsumura, M.E., D.R. Lobe, and C.A. McNamara. Contribution of the helix-loop-helix factor Id2 to regulation of vascular smooth muscle cell proliferation. J Biol Chem. 277:7293-7297, 2002.

87. Ji, Y., T.L. Strawn, E.A. Grunz, M.J. Stevenson, A.W. Lohman, D.A. Lawrence, and W.P. Fay. Multifaceted role of plasminogen activator inhibitor-1 in regulating early remodeling of vein bypass grafts. Arterioscler Thromb Vasc Biol. 31:1781-1787, 2011.

88. Wu, J., L. Peng, G.A. McMahon, D.A. Lawrence, and W.P. Fay. Recombinant plasminogen activator inhibitor-1 inhibits intimal hyperplasia. Arterioscler Thromb Vasc Biol. 29:1565-1570, 2009.

89. Wang, C., J. Hao, F. Zhang, K. Su, and D.A. Wang. RNA extraction from polysaccharide-based cell-laden hydrogel scaffolds. Anal Biochem. 380:333-334, 2008.

90. Lee, S.H., J.S. Miller, J.J. Moon, and J.L. West. Proteolytically degradable hydrogels with a fluorogenic substrate for studies of cellular proteolytic activity and migration. Biotechnol Prog. 21:1736-1741, 2005.

91. Stella, J.A., J. Liao, Y. Hong, W. David Merryman, W.R. Wagner, and M.S. Sacks. Tissue-to-cellular level deformation coupling in cell micro-integrated elastomeric scaffolds. Biomaterials. 29:3228-3236, 2008.

92. Stella, J.A., W.R. Wagner, and M.S. Sacks. Scale-dependent fiber kinematics of elastomeric electrospun scaffolds for soft tissue engineering. J Biomed Mater Res A. 93:1032-1042, 2010.

93. Caille, N., Y. Tardy, and J.J. Meister. Assessment of strain field in endothelial cells subjected to uniaxial deformation of their substrate. Ann Biomed Eng. 26:409-416, 1998.

94. Bluestein, D., Y. Alemu, I. Avrahami, M. Gharib, K. Dumont, J.J. Ricotta, and S. Einav. Influence of microcalcifications on vulnerable plaque mechanics using FSI modeling. J Biomech. 41:1111-1118, 2008.

95. Rambhia, S.H., X. Liang, M. Xenos, Y. Alemu, N. Maldonado, A. Kelly, S. Chakraborti, S. Weinbaum, L. Cardoso, S. Einav*, et al.* Microcalcifications Increase Coronary Vulnerable Plaque Rupture Potential: A Patient-Based Micro-CT Fluid-Structure Interaction Study. Ann Biomed Eng. 40:1443-1454, 2012.

96. Browning, M.B., T. Wilems, M. Hahn, and E. Cosgriff-Hernandez. Compositional control of poly(ethylene glycol) hydrogel modulus independent of mesh size. J Biomed Mater Res A. 98:268-273, 2011.

97. Hemmer, J.D., D. Dean, A. Vertegel, E. Langan, 3rd, and M. LaBerge. Effects of serum deprivation on the mechanical properties of adherent vascular smooth muscle cells. Proc Inst Mech Eng H. 222:761-772, 2008.

98. Pillarisetti, A., J.P. Desai, H. Ladjal, A. Schiffmacher, A. Ferreira, and C.L. Keefer. Mechanical phenotyping of mouse embryonic stem cells: increase in stiffness with differentiation. Cell Reprogram. 13:371-380, 2011.

99. Isenberg, B.C., P.A. Dimilla, M. Walker, S. Kim, and J.Y. Wong. Vascular smooth muscle cell durotaxis depends on substrate stiffness gradient strength. Biophys J. 97:1313-1322, 2009.

100. Neu, C.P., M.L. Hull, and J.H. Walton. Heterogeneous three-dimensional strain fields during unconfined cyclic compression in bovine articular cartilage explants. J Orthop Res. 23:1390-1398, 2005.

101. Kock, L., C.C. van Donkelaar, and K. Ito. Tissue engineering of functional articular cartilage: the current status. Cell Tissue Res. 347:613-627, 2012.

102. Smith, L., Y. Xia, L.M. Galatz, G.M. Genin, and S. Thomopoulos. Tissue-engineering strategies for the tendon/ligament-to-bone insertion. Connect Tissue Res. 53:95-105, 2012.

103. Anderson, R.H., M. Smerup, D. Sanchez-Quintana, M. Loukas, and P.P. Lunkenheimer. The three-dimensional arrangement of the myocytes in the ventricular walls. Clin Anat. 22:64-76, 2009.

104. Doyle, J.F. Nonlinear analysis of thin-walled structures: statics, dynamics, and stability. New York: Springer, 2001.

105. Gibson, J.E. Linear elastic theory of thin shells. Oxford, New York: Pergamon Press, 1965.

APPENDIX A: ELASTOMERIC MEMBRANE DEFORMATION THEORY

Briefly in cylindrical coordinates, we map an original position (R, Θ) to a deformed position (r, θ) with motion equations r = r(R), and θ = Θ. This results in the following deformation gradient tensor:

$$\tilde{F} \equiv \begin{bmatrix} \lambda_r & 0 \\ 0 & \lambda_\theta \end{bmatrix} = \begin{bmatrix} r' & 0 \\ 0 & r/R \end{bmatrix} \qquad \text{Eq. A.1}$$

and Green strain tensor:

$$\tilde{E} \equiv \begin{bmatrix} E_{rr} & 0 \\ 0 & E_{\theta\theta} \end{bmatrix} = \frac{1}{2}\begin{bmatrix} \lambda_r^2 - 1 & 0 \\ 0 & \lambda_\theta^2 - 1 \end{bmatrix} \qquad \text{Eq. A.2}$$

where λ_i are principal stretch ratios, and the prime symbol represents differentiation with respect to R. Given a particular strain energy function W(Ẽ), the radial and circumferential components of the Cauchy stress tensor can be found using these stretch ratios and strain components as follows:

$$t_{rr} = \lambda_r^2 \frac{\partial W}{\partial E_{rr}} \qquad t_{\theta\theta} = \lambda_\theta^2 \frac{\partial W}{\partial E_{\theta\theta}} \qquad \text{Eq. A.3, A.4}$$

The stress equilibrium equations for our particular case (radial deformation of a circular membrane) reduces to only the following non-zero equation:

$$\frac{\partial t_{rr}}{\partial r} + \frac{1}{r}(t_{rr} - t_{\theta\theta}) = 0 \qquad \text{Eq. A.5}$$

Using the chain rule, Eq.'s A.1 – A.4 can be combined with Eq. A.5 to yield a 2nd-order ODE for the deformed radial position r(R):

$$r'' = \frac{(t_{\theta\theta} - t_{rr})\lambda_r / r + (\partial t_{rr}/\partial \lambda_\theta)(\lambda_\theta - \lambda_r)/R}{\partial t_{rr}/\partial \lambda_r} \qquad \text{Eq. A.6}$$

This governing equation can be solved according to the following boundary conditions for a central defect (Eq. A.7, A.8) or a central fixation (Eq. A.9, A.10), respectively:

$$t_{rr}(R_o) = t_o = \lambda_r^2(R_o)\left.\frac{\partial W}{\partial E_{rr}}\right|_{R=R_o} \qquad \text{Eq. A.7}$$

$$t_{rr}(R_i) = 0 = \lambda_r^2(R_i)\left.\frac{\partial W}{\partial E_{rr}}\right|_{R=R_i} \qquad \text{Eq. A.8}$$

$$t_{rr}(R_o) = t_o = \lambda_r^2(R_o)\left.\frac{\partial W}{\partial E_{rr}}\right|_{R=R_o} \qquad \lambda_\theta(R_i) = 1 \qquad \text{Eq. A.9, A.10}$$

Thus, given the size of the defect or fixation and the extent of deformation at the outer edge of the membrane, the stretch field over the entire membrane can be calculated. In the case of a central defect, the resulting circumferential stretch component varies from its maximal value at the inner edge to its minimal value

at the outer edge with monotonic decrease in between (Fig. A1.1). Conversely, radial stretch is minimal at the inner edge and maximal at the outer edge, and everywhere less than the value of circumferential stretch. In fact, radial stretch is compressive for the region nearest the inner edge. This represents a 'simple uniaxial' stretch environment ($\lambda_{e1} > 1$, $\lambda_{e2} < 1$) near the inner edge, which transitions to a near equibiaxial stretch environment ($\lambda_{e1} \approx \lambda_{e2}$) toward the outer edge.

In the case of a central fixation, the shapes of the non-uniform curves are similar, though their relative magnitudes are reversed (Fig. A1.1). Radial stretch is greater than circumferential stretch everywhere, and varies from its maximal value at the inner edge to its minimal value at the outer. Circumferential stretch varies from its minimal value at the inner edge to its maximal value at the outer. It is interesting to note that the fixation boundary condition restricts the inner circumference to no deformation, thus inner circumferential stretch equals 1. Since there is no compressive region, this scenario represents a 'strip-biaxial' condition ($\lambda_{e1} > 1$, $\lambda_{e2} = 1$) at the inner edge that transitions to a near equibiaxial condition toward the outer.

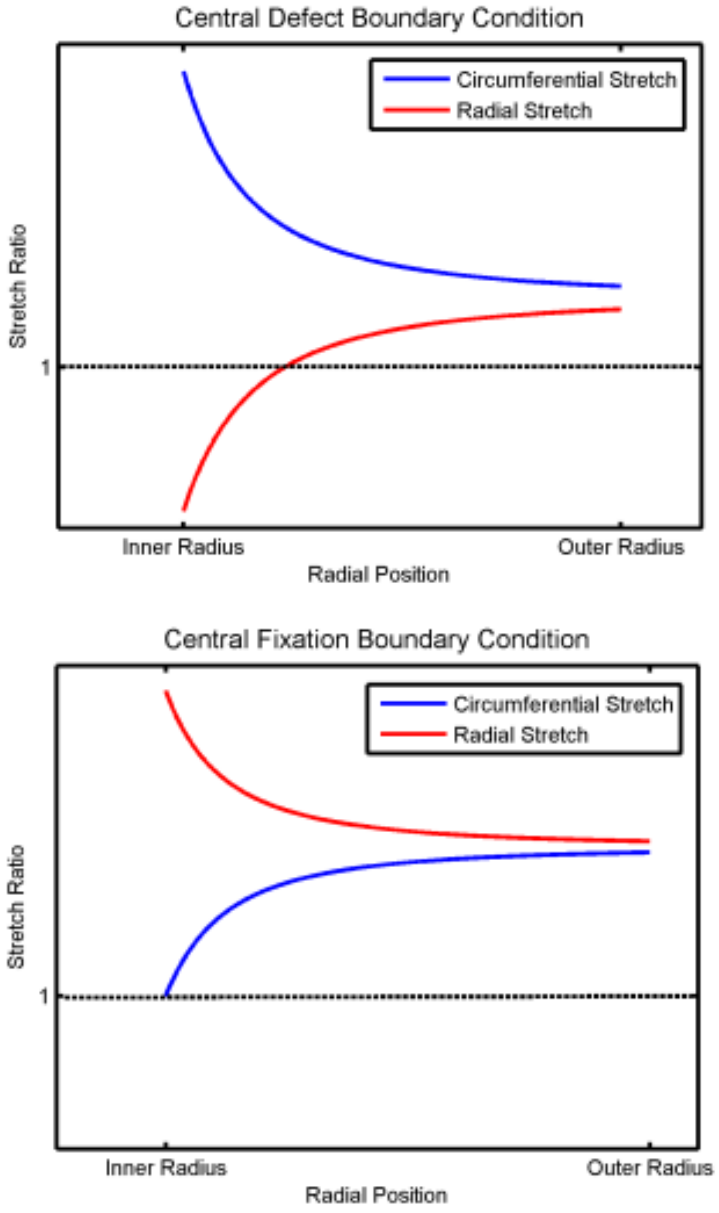

Fig. A.1. Non-uniform stretch distributions.
Gradients in circumferential and radial stretch components are generated when circular elastomeric membranes with a central defect or fixation are radially deformed.

APPENDIX B: THIN-WALLED TUBE DEFORMATION THEORY

B.1 THIN-SHELL THEORY AND ASSUMPTIONS

A shell is a structure composed by material between two closely spaced curved surfaces [Gibson, Linear elastic theory of thin shells]. In cases where the space between the surfaces (i.e., thickness) is much smaller than the object's other dimensions, the structure is termed a thin shell. This simplification is made for cylindrical shells based upon the ratio of radius (R) to wall thickness (H). When R/h = 5, the difference between exact and thin-walled approximated hoop stresses is ~1%[104]. The PDMS tubes employed in the work herein had an R/H value of 5.7, thus justifying the thin wall assumption.

In analysis of shell stresses and strains, two types of motion are distinguished: membrane and bending. Membrane action refers to motion as if the shell is incapable of supporting bending loads, and therefore stresses are induced only in the shell surfaces (related to extensions without rotations). Bending action refers to motion wherein loads induce stresses within the shell, which are supported by internal moments and forces (related to changes in curvature)[105].

For a cylindrical shell, stress resultants (M_{ij}, N_{ij}, Q_{ij}) are derived using geometries and equilibriums (force, moment, and displacement) for both membrane and bending actions. The 'thin'-shell assumption allows us to ignore

several terms in the equilibrium equations, and assume the radial stress component to be 0, thereby simplifying Hooke's Law relating stress resultants to shell strains.

In the case of deformation by uniform intraluminal radial pressure P, the governing equilibrium equation reduces to a 4th-order ODE of radial displacement of the mid-wall surface, w (measured positive inward), as a function of axial position, z:

$$\frac{E_z H^3}{12R_o^3(1-\mu_z\mu_\theta)}\frac{d^4w}{dz^4}+\frac{E_\theta H}{R_o}w=P \qquad \text{Eq. B.1.}$$

with w and z equal to w_{actual} and z_{actual}, respectively (both normalized by the initial undeformed radius, R_o), H equal to undeformed tube thickness, E_z and E_θ equal to axial and circumferential elastic moduli, respectively, μ_z and μ_θ equal to axial and circumferential Poisson's ratios, respectively. Assuming the material is isotropic ($E_z = E_\theta = E$) and incompressible ($\mu_z = \mu_\theta = 0.5$) further simplifies the governing equation:

$$\frac{d^4w}{dz^4}+\frac{9R_o^2}{H^2}w=\frac{9R_o^3P}{EH^3} \qquad \text{Eq. B.2.}$$

Once radial displacement w(z) is known, circumferential and axial strains can be calculated for a particular location anywhere on the tube:

$$e_\theta = -\frac{\bar{w}}{R_o} \qquad e_z = \frac{d\bar{u}}{d\bar{z}} - \frac{d^2\bar{w}}{d\bar{z}^2}(r^*) \qquad \text{Eq. B.3, B.4.}$$

where the overbar denotes actual (dimensional) values, u is displacement in the axial direction, and r* is the radial distance of the point of interest from the mid-wall surface (measured positive inward; thus, r* = -0.5*thickness for the outer wall). It is important to note that du/dz accounts for strain due to membrane action, while d^2w/dz^2 accounts for strain due to bending. Herein, we assume there is no axial displacement (du/dz = 0), which further simplifies Eq. B.4.

B.2 GOVERNING EQUATION AND SOLUTION

Again, we have the governing equation:

$$\frac{d^4w}{dz^4} + \frac{9R_o^2}{H^2}w = \frac{9R_o^3(P)}{EH^3}$$

For the problem of a tube deformed by an over-sized, rigid, cylindrical insert, we restrict the wall displacement at the insert to be exactly determined by the size of the insert, the wall displacement far from the insert to be exactly determined by the inflation due to intraluminal pressure, and the wall displacement transitions to be smooth along the entire length of the tube (from $0 < z < \infty$). The following

boundary conditions are thus enforced with z=0 corresponding to the edge of the insert:

$$w(z=0) = -\left(\frac{R_o^{insert} - R_o}{R_o}\right) \qquad \left.\frac{dw}{dz}\right|_{z=0} = 0$$

$$w(z \to \infty) = -\frac{PR_o}{EH} \qquad \left.\frac{dw}{dz}\right|_{z\to\infty} = 0$$

Particular Solution:

$$w_p(z) = \frac{PR_o}{EH}$$

Homogeneous Solution:

$$w_h(z) = c_1\, cosh(kz)\, cos(kz) + c_2\, cosh(kz)\, sin(kz) + c_3\, sinh(kz)\, cos(kz) + c_4\, sinh(kz)\, sin(kz)$$

with $k = \sqrt{\frac{3R_o}{2H}}$

Use boundary conditions to find constants 1-4:

$$\left.\frac{dw}{dz}\right|_{z=0} = k[(c_4 - c_1)(0) + (c_2 + c_3)(1)] = 0$$

$$\therefore c_2 = -c_3$$

$$\left.\frac{dw}{dz}\right|_{z\to\infty} = k[\cos(\infty)\sinh(\infty)(c_1 + c_4) + \sin(\infty)(\sinh(\infty)(c_2 - c_3) + \cosh(\infty)(c_4 - c_1))] = 0$$

$$\therefore c_1 = -c_4$$

$$\& -2\sinh(\infty)\, c_3 + 2\cosh(\infty)\, c_4 = 0 \quad \rightarrow \quad \frac{c_4}{c_3} = \frac{\sinh(\infty)}{\cosh(\infty)} = \tanh(\infty) = 1$$

$$\therefore c_4 = c_3 \quad \& \quad c_1 = c_2$$

$$w(z=0) =$$

$$c_1(\cosh(0)\cos(0) + \cosh(0)\sin(0) - \sinh(0)\cos(0) - \sinh(0)\sin(0)) + \frac{PR_o}{EH}$$

$$= -\left(\frac{R_o^{insert} - R_o}{R_o}\right)$$

$$\therefore c_1 = c_2 = -\frac{R_o^{insert} - R_o}{R_o} - \frac{PR_o}{EH} \quad \& c_3 = c_4 = \frac{R_o^{insert} - R_o}{R_o} + \frac{PR_o}{EH}$$

Final Solution:

$$w(z) = w_p(z) + w_h(z)$$

$$\mathrm{w(z)} = \frac{\mathrm{PR_o}}{\mathrm{EH}} + \left(\frac{\mathrm{R_o^{insert} - R_o}}{\mathrm{R_o}} + \frac{\mathrm{PR_o}}{\mathrm{EH}}\right)(\sinh(\mathrm{kz}) - \cosh(\mathrm{kz}))(\sin(\mathrm{kz}) + \cos(\mathrm{kz}))$$

with $k = \sqrt{\frac{3R_o}{2H}}$

This equation can be used to solve for the deformed tube wall position profile given a particular value for undeformed radius, R_0, and undeformed thickness, H, as well as intraluminal pressure and linearized elastic modulus of the tube. In our case, we desire to find stretch due to inflation from diastolic to systolic pressure, subsequent to rigid insert implantation. Wall displacement, w, and corresponding strains are calculated for the deformation cases from an

undeformed, straight tube to both diastolic and systolic inflated positions. The circumferential and axial strain values for deformation between diastolic and systolic inflation (and the respective stretch, λ) can then be calculated with the following:

$$e_{\theta,z} = \frac{e_{\theta,z}^{systolic} - e_{\theta,z}^{diastolic}}{e_{\theta,z}^{diastolic} + 1} \qquad \lambda_{\theta,z} = 1 + e_{\theta,z}$$

APPENDIX C: MATLAB SOLVER CODE FILES

C.1 CIRCLE FIT FOR MEMBRANE AND GEL DEFECT GEOMETRY

```
%Finding Circle with data points.
%Circle centered at (a,b); r is radius;
%Eq: (x-a)^2 + (y-b)^2 = r^2
%Uses Sum of the Least Squares
%Must give 'data' in command window.
%(It helps to transpose graph so xdata is positive.)
function [Geometry] = circlesolver(data)
start = [15000 -5000 2200];
regress = @sumfctn;
Geometry = fminsearch(regress, start);
   function [Summation] = sumfctn(par)
      a = par(1);
      b = par(2);
      r = par(3);
           Summation = sum(((sqrt((a-data(:,1)).^2+(b-data(:,2)).^2)) –
                   r).^2);
   end
end
```

C.2 MEMBRANE DEFORMATION DATA FIT (DEFECT CASE)

```
%%%This m-file will fit constitutive parameters for various strain-%%%energy functions
to the experimental gradient data measured on an %%%elastomeric membrane with
central defect.
function [neohook, moonriv, fung, delfino, rivsaw] = gradientfit_defect()
clear all
%%%%%%%%%%%%%%%%%%%GIVEN%%%%%%%%%%%%%%%%%%%%
%%
%%Small defect
% sdR = xlsread('membrane stretch analysis for publication.xlsx','small defect','D3:D40');
% sd3r_a = xlsread('membrane stretch analysis for publication.xlsx','small
defect','I3:I40');
% sd3lambda_circ = xlsread('membrane stretch analysis for publication.xlsx','small
defect','J3:J40');
%   sd3r_b = xlsread('membrane stretch analysis for publication.xlsx','small
defect','K7:K39');
%   sd3lambda_r = xlsread('membrane stretch analysis for publication.xlsx','small
defect','L7:L39');
```

```
% sd6r_a = xlsread('membrane stretch analysis for publication.xlsx','small
defect','O3:O40');
% sd6lambda_circ = xlsread('membrane stretch analysis for publication.xlsx','small
defect','P3:P40');
%    sd6r_b = xlsread('membrane stretch analysis for publication.xlsx','small
defect','Q7:Q39');
%   sd6lambda_r = xlsread('membrane stretch analysis for publication.xlsx','small
defect','R7:R39');
% sd9r_a = xlsread('membrane stretch analysis for publication.xlsx','small
defect','U3:U40');
% sd9lambda_circ = xlsread('membrane stretch analysis for publication.xlsx','small
defect','V3:V40');
%   sd9r_b = xlsread('membrane stretch analysis for publication.xlsx','small
defect','W7:W39');
%   sd9lambda_r = xlsread('membrane stretch analysis for publication.xlsx','small
defect','X7:X39');
% sd12r_a = xlsread('membrane stretch analysis for publication.xlsx','small
defect','AA3:AA40');
% sd12lambda_circ = xlsread('membrane stretch analysis for publication.xlsx','small
defect','AB3:AB40');
%   sd12r_b = xlsread('membrane stretch analysis for publication.xlsx','small
defect','AC7:AC39');
%   sd12lambda_r = xlsread('membrane stretch analysis for publication.xlsx','small
defect','AD7:AD39');
%%Large defect
ldR = xlsread('membrane stretch analysis for publication.xlsx','data for matlab','R3:R33');
ld3r_a = xlsread('membrane stretch analysis for publication.xlsx','data for
matlab','S3:S33');
ld3lambda_circ = xlsread('membrane stretch analysis for publication.xlsx','data for
matlab','T3:T33');
ld3r_b = xlsread('membrane stretch analysis for publication.xlsx','data for
matlab','U3:U30');
ld3lambda_r = xlsread('membrane stretch analysis for publication.xlsx','data for
matlab','V3:V30');
ld6r_a = xlsread('membrane stretch analysis for publication.xlsx','data for
matlab','W3:W33');
ld6lambda_circ = xlsread('membrane stretch analysis for publication.xlsx','data for
matlab','X3:X33');
ld6r_b = xlsread('membrane stretch analysis for publication.xlsx','data for
matlab','Y3:Y30');
ld6lambda_r = xlsread('membrane stretch analysis for publication.xlsx','data for
matlab','Z3:Z30');
ld9r_a = xlsread('membrane stretch analysis for publication.xlsx','data for
matlab','AA3:AA33');
ld9lambda_circ = xlsread('membrane stretch analysis for publication.xlsx','data for
matlab','AB3:AB33');
ld9r_b = xlsread('membrane stretch analysis for publication.xlsx','data for
matlab','AC3:AC30');
ld9lambda_r = xlsread('membrane stretch analysis for publication.xlsx','data for
matlab','AD3:AD30');
ld12r_a = xlsread('membrane stretch analysis for publication.xlsx','data for
matlab','AE3:AE33');
```

```
ld12lambda_circ = xlsread('membrane stretch analysis for publication.xlsx','data for
matlab','AF3:AF33');
ld12r_b = xlsread('membrane stretch analysis for publication.xlsx','data for
matlab','AG3:AG30');
ld12lambda_r = xlsread('membrane stretch analysis for publication.xlsx','data for
matlab','AH3:AH30');
Ri = ldR(1); %microns
N = length(ldR);
Ro = ldR(N);
%%%%%%%%%%%%%%%%%%%%%%%%%%SOLVER%%%%%%%%%%%%%%%%%%
%%%%%%%%%%%%%%%%%%%%%
%%%NEOHOOKEAN FIT
startn = [1];
% results =[];
[neohook, Errorsumn] = fminsearch(@sumfctnn, startn)
   function [Summationn] = sumfctnn(c)
      c1 = c(1);
      function dy = neohookeq12(x,y)
         trr = 2*c1*(y(2)^2 - 1);
         ttheta = 2*c1*((y(1)/x)^2 - 1);
         dtrr_dlambdatheta = 0;
         dtrr_dlambdar = 4*c1*y(2);
         dy = zeros(2,1);
         dy(1) = y(2); % = r' = dr/dR
         dy(2) = ((y(2)/y(1))*(ttheta - trr) + dtrr_dlambdatheta*((y(1)/x) -
y(2))*(1/x))/dtrr_dlambdar ;
            % = r'' = d2r/dR2
            %Eq. 12, David&Humphrey, 2004
      end
      ri9 = ld9r_a(1);
      dr_dRi = 1;
      [Rn Yn]=ode45(@neohookeq12,ldR,[ri9 dr_dRi]);

      R9n = Rn;
      r9n = Yn(:,1);
      lambda_theta_9n = r9n./R9n;
      lambda_r_9n = Yn(:,2);

      Summationn = sum((lambda_theta_9n - ld9lambda_circ).^2) +
sum((lambda_r_9n(2:N-2) - ld9lambda_r).^2);
   end
%%%MOONEY-RIVLIN FIT
startm = [1 1]; %[1 0.82]
% resultsm = [];
[moonriv,Errorsumm] = fminsearch(@sumfctnm, startm)
  function [Summationm] = sumfctnm(c)
     c1 = c(1);
     c2 = c(2);
     function dy = moonriveq12(x,y)
         trr = 2*c1*(y(2)^2 - 1) + 2*c2*((y(2)*y(1)/x)^2 - 1);
         ttheta = 2*c1*((y(1)/x)^2 - 1) + 2*c2*((y(2)*y(1)/x)^2 - 1);
         dtrr_dlambdatheta = 4*c2*(y(2)^2)*y(1)/x;
```

```
        dtrr_dlambdar = 4*c1*y(2) + 4*c2*y(2)*(y(1)/x)^2;
        dy = zeros(2,1);
        dy(1) = y(2); % = r' = dr/dR
        dy(2) = ((y(2)/y(1))*(ttheta - trr) + dtrr_dlambdatheta*((y(1)/x) -
y(2))*(1/x))/dtrr_dlambdar ;
            % = r'' = d2r/dR2
            %Eq. 12, D&H 2004
    end
%       ri3 = ld3r_a(1);
%       dr_dRi = abs(sqrt((c1+c2)/(c1 + c2*(ri3/Ri)^2)));
%       [Rm Ym]=ode45(@moonriveq12,ldR,[ri3 dr_dRi]);
%       resultsm = [resultsm Rm Ym];
%
%       ri6 = ld6r_a(1);
%       dr_dRi = abs(sqrt((c1+c2)/(c1 + c2*(ri6/Ri)^2)));
%       [Rm Ym]=ode45(@moonriveq12,ldR,[ri6 dr_dRi]);
%       resultsm = [resultsm Rm Ym];
    ri9 = ld9r_a(1);
    dr_dRi = abs(sqrt((c1+c2)/(c1 + c2*(ri9/Ri)^2)));
    [Rm Ym]=ode45(@moonriveq12,ldR,[ri9 dr_dRi]);
%       resultsm = [resultsm Rm Ym];
    R9m = Rm;
    r9m = Ym(:,1);
    lambda_theta_9m = r9m./R9m;
    lambda_r_9m = Ym(:,2);
%       ri12 = ld12r_a(1);
%       dr_dRi = abs(sqrt((c1+c2)/(c1 + c2*(ri12/Ri)^2)));
%       [Rm Ym]=ode45(@moonriveq12,ldR,[ri12 dr_dRi]);
%       resultsm = [resultsm Rm Ym]
%       R3 = resultsm(:,1);
%       r3 = resultsm(:,2);
%       lambda_theta_3 = r3./R3;
%       lambda_r_3 = resultsm(:,3);
%       R6 = resultsm(:,4);
%       r6 = resultsm(:,5);
%       lambda_theta_6 = r6./R6;
%       lambda_r_6 = resultsm(:,6);
%       R9 = resultsm(:,7);
%       r9 = resultsm(:,8);
%       lambda_theta_9 = r9./R9;
%       lambda_r_9 = resultsm(:,9);
%       R12 = resultsm(:,10);
%       r12 = resultsm(:,11);
%       lambda_theta_12 = r12./R12;
%       lambda_r_12 = resultsm(:,12);
    Summationm = sum((lambda_theta_9m - ld9lambda_circ).^2) +
sum((lambda_r_9m(2:N-2) - ld9lambda_r).^2);
  end
% R9 = R9;
% r3=r3;
% lambda_theta_3 = lambda_theta_3;
% lambda_r_3= lambda_r_3;
% r6=r6;
```

```
% lambda_theta_6 = lambda_theta_6;
% lambda_r_6= lambda_r_6;
% r9=r9;
% lambda_theta_9 = lambda_theta_9;
% lambda_r_9= lambda_r_9;
% r12=r12;
% lambda_theta_12 = lambda_theta_12;
% lambda_r_12= lambda_r_12;
%%%FUNG FIT
startf = [1 1 1];
[fung,Errorsum] = fminsearch(@sumfctnf, startf)
   function [Summationf] = sumfctnf(cs)
       c = cs(1);
       c1 = cs(2);
       c2 = cs(2); %This forces isotropy.
       c3 = cs(3);
       function dy = fungeq12(x,y)
           Q = (c1/4)*(y(2)^2 - 1)^2 + (c2/4)*((y(1)/x)^2 - 1)^2 + (c3/4)*(y(2)^2 -
1)*((y(1)/x)^2 - 1);
           trr = (y(2)^2)*(c/2)*exp(Q)*(c1*(y(2)^2 - 1) + c3*((y(1)/x)^2 - 1));
           ttheta = ((y(1)/x)^2)*(c/2)*exp(Q)*(c3*(y(2)^2 - 1) + c2*((y(1)/x)^2 - 1));
           dtrr_dlambdatheta = (y(2)^2)*(c/2)*exp(Q)*[(2*c3*y(1)/x) + (c2*((y(1)/x)^2 -
1)*(y(1)/x) + c3*(y(2)^2 - 1)*(y(1)/x))*(c1*(y(2)^2 - 1) + c3*((y(1)/x)^2 - 1))];
           dtrr_dlambdar = (y(2)^2)*(c/2)*exp(Q)*[(2*c1*y(2)) + (c3*((y(1)/x)^2 - 1)*y(2) +
c1*(y(2)^2 - 1)*y(2))*(c1*(y(2)^2 - 1) + c3*((y(1)/x)^2 - 1))] + y(2)*c*exp(Q)*(c1*(y(2)^2 -
1) + c3*((y(1)/x)^2 - 1));
           dy = zeros(2,1);
           dy(1) = y(2); % = r' = dr/dR
           dy(2) = ((y(2)/y(1))*(ttheta - trr) + dtrr_dlambdatheta*((y(1)/x) -
y(2))*(1/x))/dtrr_dlambdar ;
               % = r'' = d2r/dR2
               %Eq. 12, D&H 2004
       end
       ri9 = ld9r_a(1);
       dr_dRi = abs(sqrt(1-(c3/c1)*((ri9/Ri)^2-1)));
       [Rf Yf]=ode45(@fungeq12,ldR,[ri9 dr_dRi]);
       R9f = Rf;
       r9f = Yf(:,1);
       lambda_theta_9f = r9f./R9f;
       lambda_r_9f = Yf(:,2);
       Summationf = sum((lambda_theta_9f - ld9lambda_circ).^2) +
sum((lambda_r_9f(2:N-2) - ld9lambda_r).^2);
   end
%%%DELFINO FIT
startd = [1 1];
[delfino,Errorsumd] = fminsearch(@sumfctnd, startd)
  function [Summationd] = sumfctnd(cs)
      a = cs(1);
      b = cs(2);
      function dy = delfinoeq12(x,y)
          expterm = (b/2)*(y(2)^2 + (y(1)/x)^2 - 2);
          trr = a*y(2)^2*exp(expterm) - a;
          ttheta = a*(y(1)/x)^2*exp(expterm) - a;
```

```
        dtrr_dlamdatheta = a*(y(1)/x)^2*exp(expterm)*b*y(1)/x;
        dtrr_dlamdar = 2*a*y(2)*exp(expterm) + a*y(2)^2*exp(expterm)*b*y(2);
        dy = zeros(2,1);
        dy(1) = y(2); % = r' = dr/dR
        dy(2) = ((y(2)/y(1))*(ttheta - trr) + dtrr_dlamdatheta*((y(1)/x) -
y(2))*(1/x))/dtrr_dlamdar ;
            % = r'' = d2r/dR2
            %Eq. 12, D&H 2004
    end
    ri9 = ld9r_a(1);
        function [zero] = delfinoBC(lamdar)
        zero = (lamdar^2)*exp((b/2)*(lamdar^2 + (ri9/Ri)^2 - 2)) - 1;
        end
    range = [0 1.5];
    dr_dRi = fzero(@delfinoBC,range);
    [Rd Yd]=ode45(@delfinoeq12,ldR,[ri9 dr_dRi]);
    R9d = Rd;
    r9d = Yd(:,1);
    lambda_theta_9d = r9d./R9d;
    lambda_r_9d = Yd(:,2);
    Summationd = sum((lambda_theta_9d - ld9lambda_circ).^2) +
sum((lambda_r_9d(2:N-2) - ld9lambda_r).^2);
  end
%%%RIVLIN-SAWYERS FIT
startrv = [1 1 1];
[rivsaw,Errorsumrv] = fminsearch(@sumfctnrv, startrv)
  function [Summationrv] = sumfctnrv(cs)
    c1 = cs(1);
    c2 = cs(2);
    c3 = cs(3);
    function dy = rivsaweq12(x,y)
        trr = 2*c1*(y(2)^2 - 1) + 2*c2*((y(2)*y(1)/x)^2 - 1) + 4*c3*((y(2)*y(1)/x)^4 -
(y(2)*y(1)/x)^2);
        ttheta = 2*c1*((y(1)/x)^2 - 1) + 2*c2*((y(2)*y(1)/x)^2 - 1) + 4*c3*((y(2)*y(1)/x)^4 -
(y(2)*y(1)/x)^2);
        dtrr_dlambdatheta = 4*c2*(y(2)^2)*y(1)/x + 4*c3*(4*(y(2)^4)*(y(1)/x)^3 -
2*(y(2)^2)*y(1)/x);
        dtrr_dlambdar = 4*c1*y(2) + 4*c2*y(2)*(y(1)/x)^2 + 4*c3*(4*(y(2)^3)*(y(1)/x)^4 -
2*y(2)*(y(1)/x)^2);
        dy = zeros(2,1);
        dy(1) = y(2); % = r' = dr/dR
        dy(2) = ((y(2)/y(1))*(ttheta - trr) + dtrr_dlambdatheta*((y(1)/x) -
y(2))*(1/x))/dtrr_dlambdar ;
            % = r'' = d2r/dR2
            %Eq. 12, D&H 2004
    end
     ri9 = ld9r_a(1);
     bc = [2*c3*(ri9./Ri)^4 0 c1+(c2-2*c3)*(ri9./Ri)^2 0 -c1-c2];
     rts = roots(bc);
     rt_location = 0.1 < rts & rts < 1.1;
     rt = rts(rt_location);
     dr_dRi = max(rt);
     [Rrv Yrv]=ode45(@rivsaweq12,ldR,[ri9 dr_dRi]);
```

```
        R9rv = Rrv;
        r9rv = Yrv(:,1);
        lambda_theta_9rv = r9rv./R9rv;
        lambda_r_9rv = Yrv(:,2);
        Summationrv = sum((lambda_theta_9rv - ld9lambda_circ).^2) +
sum((lambda_r_9rv(2:N-2) - ld9lambda_r).^2);
  end
%%%%%%%%%%%%%%%%%%FIGURES%%%%%%%%%%%%%%%%%%%%
figure
subplot(2,1,1)
plot(r9n,lambda_theta_9n,r9m,lambda_theta_9m,r9f,lambda_theta_9f,r9d,lambda_theta
_9d,r9rv,lambda_theta_9rv,ld9r_a,ld9lambda_circ,'o')
    ylabel('Circ. Stretch'), xlabel('Radial Position (mm)'), legend('Neo-Hook','Mooney-
Rivlin','Fung','Delfino','Rivlin-Sawyers','Data')
subplot(2,1,2)
plot(r9n,lambda_r_9n,r9m,lambda_r_9m,r9f,lambda_r_9f,r9d,lambda_r_9d,r9rv,lambda_
r_9rv,ld9r_b,ld9lambda_r,'o')
    ylabel('Radial Stretch'), xlabel('Radial Position (mm)'), legend('Neo-Hook','Mooney-
Rivlin','Fung','Delfino','Rivlin-Sawyers','Data')
% figure
% subplot(2,1,1)
%
plot(r3,lambda_theta_3,ld3r_a,ld3lambda_circ,'o',r6,lambda_theta_6,ld6r_a,ld6lambda_c
irc,'o',r9,lambda_theta_9,ld9r_a,ld9lambda_circ,'o',r12,lambda_theta_12,ld12r_a,ld12la
mbda_circ,'o')
%     ylabel('Circ. Stretch')
% subplot(2,1,2)
%
plot(r3,lambda_r_3,ld3r_b,ld3lambda_r,'o',r6,lambda_r_6,ld6r_b,ld6lambda_r,'o',r9,lamb
da_r_9,ld9r_b,ld9lambda_r,'o',r12,lambda_r_12,ld12r_b,ld12lambda_r,'o')
%     ylabel('Radial Stretch')
End
```

C.3 MEMBRANE DEFORMATION DATA FIT (FIXATION CASE)

```
%%%This m-file will fit constitutive parameters for various strain-%%%energy functions
to the experimental gradient data measured on an %%%elastomeric membrane with
central fixation.
function [moonriv] = gradientfit_fixation()
%%%%%%%%%%%%%%%%%%%%%GIVEN%%%%%%%%%%%%%%%%%%%%%%%%
%%Small fixation
sfR = xlsread('membrane stretch analysis for publication.xlsx','small fixation','D3:D40');
sf3r_a = xlsread('membrane stretch analysis for publication.xlsx','small
fixation','G3:G40');
sf3lamda_circ = xlsread('membrane stretch analysis for publication.xlsx','small
fixation','H3:H40');
```

```
sf3r_b = xlsread('membrane stretch analysis for publication.xlsx','small fixation','I3:I40');
sf3lamda_r = xlsread('membrane stretch analysis for publication.xlsx','small
fixation','J3:J40');
sf6r_a = xlsread('membrane stretch analysis for publication.xlsx','small
fixation','M3:M40');
sf6lamda_circ = xlsread('membrane stretch analysis for publication.xlsx','small
fixation','N3:N40');
sf6r_b = xlsread('membrane stretch analysis for publication.xlsx','small
fixation','O3:O40');
sf6lamda_r = xlsread('membrane stretch analysis for publication.xlsx','small
fixation','P3:P40');
sf9r_a = xlsread('membrane stretch analysis for publication.xlsx','small
fixation','S3:S40');
sf9lamda_circ = xlsread('membrane stretch analysis for publication.xlsx','small
fixation','T3:T40');
sf9r_b = xlsread('membrane stretch analysis for publication.xlsx','small
fixation','U3:U40');
sf9lamda_r = xlsread('membrane stretch analysis for publication.xlsx','small
fixation','V3:V40');
sf12r_a = xlsread('membrane stretch analysis for publication.xlsx','small
fixation','Y3:Y40');
sf12lamda_circ = xlsread('membrane stretch analysis for publication.xlsx','small
fixation','Z3:Z40');
sf12r_b = xlsread('membrane stretch analysis for publication.xlsx','small
fixation','AA3:AA40');
sf12lamda_r = xlsread('membrane stretch analysis for publication.xlsx','small
fixation','AB3:AB40');
%%Large fixation
% lfR = xlsread('membrane stretch analysis for publication.xlsx','big fixation','D3:D40');
% lf3r_a = xlsread('membrane stretch analysis for publication.xlsx','big
fixation','G3:G40');
% lf3lamda_circ = xlsread('membrane stretch analysis for publication.xlsx','big
fixation','H3:H40');
% lf3r_b = xlsread('membrane stretch analysis for publication.xlsx','big fixation','I3:I40');
% lf3lamda_r = xlsread('membrane stretch analysis for publication.xlsx','big
fixation','J3:J40');
% lf6r_a = xlsread('membrane stretch analysis for publication.xlsx','big
fixation','M3:M40');
% lf6lamda_circ = xlsread('membrane stretch analysis for publication.xlsx','big
fixation','N3:N40');
% lf6r_b = xlsread('membrane stretch analysis for publication.xlsx','big
fixation','O3:O40');
% lf6lamda_r = xlsread('membrane stretch analysis for publication.xlsx','big
fixation','P3:P40');
% lf9r_a = xlsread('membrane stretch analysis for publication.xlsx','big fixation','S3:S40');
% lf9lamda_circ = xlsread('membrane stretch analysis for publication.xlsx','big
fixation','T3:T40');
% lf9r_b = xlsread('membrane stretch analysis for publication.xlsx','big
fixation','U3:U40');
% lf9lamda_r = xlsread('membrane stretch analysis for publication.xlsx','big
fixation','V3:V40');
% lf12r_a = xlsread('membrane stretch analysis for publication.xlsx','big
fixation','Y3:Y40');
```

```
% lf12lamda_circ = xlsread('membrane stretch analysis for publication.xlsx','big
fixation','Z3:Z40');
% lf12r_b = xlsread('membrane stretch analysis for publication.xlsx','big
fixation','AA3:AA40');
% lf12lamda_r = xlsread('membrane stretch analysis for publication.xlsx','big
fixation','AB3:AB40');
Ri = sfR(1); %microns
N = length(sfR);
Ro = sfR(N);
ri = Ri;
n = 40;
%%%%%%%%%%%%%%%%%%%%%%%%%SOLVER%%%%%%%%%%%%%%%%%%%%%%%%%%%%%%%%%%%%%%%%%%
%MOONEY-RIVLIN FIT
results = [];
c1 = 1;
c2 = 1;
function dy = moonriveq12(x,y)
        trr = 2*c1*(y(2)^2 - 1) + 2*c2*((y(2)*y(1)/x)^2 - 1);
        ttheta = 2*c1*((y(1)/x)^2 - 1) + 2*c2*((y(2)*y(1)/x)^2 - 1);
        dtrr_dlamdatheta = 4*c2*(y(2)^2)*y(1)/x;
        dtrr_dlamdar = 4*c1*y(2) + 4*c2*y(2)*(y(1)/x)^2;
        dy = zeros(2,1);
        dy(1) = y(2); % = r' = dr/dR
        dy(2) = ((y(2)/y(1))*(ttheta - trr) + dtrr_dlamdatheta*((y(1)/x) -
y(2))*(1/x))/dtrr_dlamdar ;
            % = r'' = d2r/dR2
            %Eq. 12, D&H 2004
end
for dr_dRi = [1.023 1.055 1.116 1.154]; %small fixation
%for dr_dRi = [1.01 1.055 1.125 1.185]; %large fixation
        [Rm Ym]=ode45(@moonriveq12,[Ri:(Ro-Ri)/(N-1):Ro],[ri dr_dRi]);
        results = [results Rm Ym];
end
R3 = results(:,1);
r3 = results(:,2);
lamda_theta_3 = r3./R3;
lamda_r_3 = results(:,3);
R6 = results(:,4);
r6 = results(:,5);
lamda_theta_6 = r6./R6;
lamda_r_6 = results(:,6);
R9 = results(:,7);
r9 = results(:,8);
lamda_theta_9 = r9./R9;
lamda_r_9 = results(:,9);
R12 = results(:,10);
r12 = results(:,11);
lamda_theta_12 = r12./R12;
lamda_r_12 = results(:,12);
%%%%%%%%%%%%%%%%%%FIGURES%%%%%%%%%%%%%%%%%%%%%%%%%%%%%%%%%%%%%%%%%%%%%%%%
figure
subplot(2,1,1)
```

```
plot(r3,lamda_theta_3,sf3r_a,sf3lamda_circ,'o',r6,lamda_theta_6,sf6r_a,sf6lamda_circ,'o'
,r9,lamda_theta_9,sf9r_a,sf9lamda_circ,'o',r12,lamda_theta_12,sf12r_a,sf12lamda_circ,'
o')
    ylabel('Circ. Stretch')
subplot(2,1,2)
plot(r3,lamda_r_3,sf3r_b,sf3lamda_r,'o',r6,lamda_r_6,sf6r_b,sf6lamda_r,'o',r9,lamda_r_9
,sf9r_b,sf9lamda_r,'o',r12,lamda_r_12,sf12r_b,sf12lamda_r,'o')
    ylabel('Radial Stretch')
end
```

C.4 STRETCH PROFILES FOR EXPERIMENTAL CASES (DEFECT CASE)

```
%%% This file will plot experimental case deformation profiles %%% for a membrane
with central defect.
function [moonriv] = defect_cases()
%%%%%%%%%%%%%%%%%%%%GIVEN%%%%%%%%%%%%%%%%%%%%%%
%%
%%Small defect
sdR = xlsread('membrane stretch analysis for publication.xlsx','small defect','D3:D40');
% sd3r_a = xlsread('membrane stretch analysis for publication.xlsx','small
defect','I3:I40');
% sd3lamda_circ = xlsread('membrane stretch analysis for publication.xlsx','small
defect','J3:J40');
% sd3r_b = xlsread('membrane stretch analysis for publication.xlsx','small
defect','K3:K40');
% sd3lamda_r = xlsread('membrane stretch analysis for publication.xlsx','small
defect','L3:L40');
% sd6r_a = xlsread('membrane stretch analysis for publication.xlsx','small
defect','O3:O40');
% sd6lamda_circ = xlsread('membrane stretch analysis for publication.xlsx','small
defect','P3:P40');
% sd6r_b = xlsread('membrane stretch analysis for publication.xlsx','small
defect','Q3:Q40');
% sd6lamda_r = xlsread('membrane stretch analysis for publication.xlsx','small
defect','R3:R40');
% sd9r_a = xlsread('membrane stretch analysis for publication.xlsx','small
defect','U3:U40');
% sd9lamda_circ = xlsread('membrane stretch analysis for publication.xlsx','small
defect','V3:V40');
% sd9r_b = xlsread('membrane stretch analysis for publication.xlsx','small
defect','W3:W40');
% sd9lamda_r = xlsread('membrane stretch analysis for publication.xlsx','small
defect','X3:X40');
% sd12r_a = xlsread('membrane stretch analysis for publication.xlsx','small
defect','AA3:AA40');
% sd12lamda_circ = xlsread('membrane stretch analysis for publication.xlsx','small
defect','AB3:AB40');
```

```
% sd12r_b = xlsread('membrane stretch analysis for publication.xlsx','small
defect','AC3:AC40');
% sd12lamda_r = xlsread('membrane stretch analysis for publication.xlsx','small
defect','AD3:AD40');
%%Large defect
ldR = xlsread('membrane stretch analysis for publication.xlsx','big defect','D3:D40');
% ld3r_a = xlsread('membrane stretch analysis for publication.xlsx','big
defect','G3:G40');
% ld3lamda_circ = xlsread('membrane stretch analysis for publication.xlsx','big
defect','H3:H40');
% ld3r_b = xlsread('membrane stretch analysis for publication.xlsx','big defect','I3:I40');
% ld3lamda_r = xlsread('membrane stretch analysis for publication.xlsx','big
defect','J3:J40');
% ld6r_a = xlsread('membrane stretch analysis for publication.xlsx','big
defect','M3:M40');
% ld6lamda_circ = xlsread('membrane stretch analysis for publication.xlsx','big
defect','N3:N40');
% ld6r_b = xlsread('membrane stretch analysis for publication.xlsx','big
defect','O3:O40');
% ld6lamda_r = xlsread('membrane stretch analysis for publication.xlsx','big
defect','P3:P40');
% ld9r_a = xlsread('membrane stretch analysis for publication.xlsx','big defect','S3:S40');
% ld9lamda_circ = xlsread('membrane stretch analysis for publication.xlsx','big
defect','T3:T40');
% ld9r_b = xlsread('membrane stretch analysis for publication.xlsx','big defect','U3:U40');
% ld9lamda_r = xlsread('membrane stretch analysis for publication.xlsx','big
defect','V3:V40');
% ld12r_a = xlsread('membrane stretch analysis for publication.xlsx','big
defect','Y3:Y40');
% ld12lamda_circ = xlsread('membrane stretch analysis for publication.xlsx','big
defect','Z3:Z40');
% ld12r_b = xlsread('membrane stretch analysis for publication.xlsx','big
defect','AA3:AA40');
% ld12lamda_r = xlsread('membrane stretch analysis for publication.xlsx','big
defect','AB3:AB40');
Ris = sdR(1); %microns
Ril = 7800; ldR(1);
Ro = 35000;
N = 400;
%%%%%%%%%%%%%%%%%%%%%%%%SOLVER%%%%%%%%%%%%%%%%%%%%%%%%%%%%%%%%%%%%%%%%%%
%MOONEY-RIVLIN FIT
c1 = 1;
c2 = 1;
function dy = moonriveq12(x,y)
    trr = 2*c1*(y(2)^2 - 1) + 2*c2*((y(2)*y(1)/x)^2 - 1);
    ttheta = 2*c1*((y(1)/x)^2 - 1) + 2*c2*((y(2)*y(1)/x)^2 - 1);
    dtrr_dlamdatheta = 4*c2*(y(2)^2)*y(1)/x;
    dtrr_dlamdar = 4*c1*y(2) + 4*c2*y(2)*(y(1)/x)^2;
    dy = zeros(2,1);
    dy(1) = y(2); % = r' = dr/dR
    dy(2) = ((y(2)/y(1))*(ttheta - trr) + dtrr_dlamdatheta*((y(1)/x) - y(2))*(1/x))/dtrr_dlamdar
;
```

```
        % = r'' = d2r/dR2
        %Eq. 12, D&H 2004
end
ris = 1.10994*Ris;
dr_dRis = abs(sqrt((c1+c2)/(c1 + c2*(ris/Ris)^2)));
[Rs Ys]=ode45(@moonriveq12,[Ris:(Ro-Ris)/(N-1):Ro],[ris dr_dRis]);
    Rs = Rs(:,1);
    rs = Ys(:,1);
    lamda_theta_s = rs./Rs;
    lamda_r_s = Ys(:,2);
ril = 1.10994*Ril;
dr_dRil = abs(sqrt((c1+c2)/(c1 + c2*(ril/Ril)^2)));
[Rl Yl]=ode45(@moonriveq12,[Ril:(Ro-Ril)/(N-1):Ro],[ril dr_dRil]);
    Rl = Rl(:,1)
    rl = Yl(:,1);
    lamda_theta_l = rl./Rl
    lamda_r_l = Yl(:,2)
    min_strain_angle = asind(real(sqrt((1-lamda_r_l.^2)./(lamda_theta_l.^2 -
lamda_r_l.^2))));
    strain_anisotropy_ratio_stretch = (lamda_theta_l)./(lamda_r_l);
    strain_anisotropy_ratio_stretch_b = (lamda_r_l)./(lamda_theta_l);
    strain_anisotropy_ratio_engineering = (lamda_r_l - 1)./(lamda_theta_l - 1);
    strain_anisotropy_ratio_psuedoengineering = (abs(lamda_r_l -
1))./(abs(lamda_theta_l - 1));
    strain_anisotropy_ratio_green = (lamda_r_l.^2 - 1)./(lamda_theta_l.^2 - 1);
    strain_anisotropy_ratio_log = log(lamda_r_l)./log(lamda_theta_l);
%%%%%%%%%%%%%%%%%%FIGURES%%%%%%%%%%%%%%%%%%%%
figure
plot(Rl,lamda_theta_l,Rl,lamda_r_l)
figure
plot(Rl, min_strain_angle)
figure
plot(Rl, strain_anisotropy_ratio_stretch, Rl, strain_anisotropy_ratio_stretch_b, Rl,
strain_anisotropy_ratio_engineering, Rl, strain_anisotropy_ratio_psuedoengineering, Rl,
strain_anisotropy_ratio_green, Rl, strain_anisotropy_ratio_log)
end
```

C.5 STRETCH PROFILES FOR EXPERIMENTAL CASES (FIXATION CASE)

```
%%% This file will plot experimental case deformation profiles %%% for a membrane
with central fixation.
function [moonriv] = fixation_cases()
%%%%%%%%%%%%%%%%%%%%%%GIVEN%%%%%%%%%%%%%%%%%%%%%%%%
%%Small fixation
sfR = xlsread('membrane stretch analysis for publication.xlsx','small fixation','D3:D40');
```

```
% sf3r_a = xlsread('membrane stretch analysis for publication.xlsx','small
fixation','G3:G40');
% sf3lamda_circ = xlsread('membrane stretch analysis for publication.xlsx','small
fixation','H3:H40');
% sf3r_b = xlsread('membrane stretch analysis for publication.xlsx','small
fixation','I3:I40');
% sf3lamda_r = xlsread('membrane stretch analysis for publication.xlsx','small
fixation','J3:J40');
% sf6r_a = xlsread('membrane stretch analysis for publication.xlsx','small
fixation','M3:M40');
% sf6lamda_circ = xlsread('membrane stretch analysis for publication.xlsx','small
fixation','N3:N40');
% sf6r_b = xlsread('membrane stretch analysis for publication.xlsx','small
fixation','O3:O40');
% sf6lamda_r = xlsread('membrane stretch analysis for publication.xlsx','small
fixation','P3:P40');
% sf9r_a = xlsread('membrane stretch analysis for publication.xlsx','small
fixation','S3:S40');
% sf9lamda_circ = xlsread('membrane stretch analysis for publication.xlsx','small
fixation','T3:T40');
% sf9r_b = xlsread('membrane stretch analysis for publication.xlsx','small
fixation','U3:U40');
% sf9lamda_r = xlsread('membrane stretch analysis for publication.xlsx','small
fixation','V3:V40');
% sf12r_a = xlsread('membrane stretch analysis for publication.xlsx','small
fixation','Y3:Y40');
% sf12lamda_circ = xlsread('membrane stretch analysis for publication.xlsx','small
fixation','Z3:Z40');
% sf12r_b = xlsread('membrane stretch analysis for publication.xlsx','small
fixation','AA3:AA40');
% sf12lamda_r = xlsread('membrane stretch analysis for publication.xlsx','small
fixation','AB3:AB40');
%%Large fixation
lfR = xlsread('membrane stretch analysis for publication.xlsx','big fixation','D3:D40');
% lf3r_a = xlsread('membrane stretch analysis for publication.xlsx','big
fixation','G3:G40');
% lf3lamda_circ = xlsread('membrane stretch analysis for publication.xlsx','big
fixation','H3:H40');
% lf3r_b = xlsread('membrane stretch analysis for publication.xlsx','big fixation','I3:I40');
% lf3lamda_r = xlsread('membrane stretch analysis for publication.xlsx','big
fixation','J3:J40');
% lf6r_a = xlsread('membrane stretch analysis for publication.xlsx','big
fixation','M3:M40');
% lf6lamda_circ = xlsread('membrane stretch analysis for publication.xlsx','big
fixation','N3:N40');
% lf6r_b = xlsread('membrane stretch analysis for publication.xlsx','big
fixation','O3:O40');
% lf6lamda_r = xlsread('membrane stretch analysis for publication.xlsx','big
fixation','P3:P40');
% lf9r_a = xlsread('membrane stretch analysis for publication.xlsx','big fixation','S3:S40');
% lf9lamda_circ = xlsread('membrane stretch analysis for publication.xlsx','big
fixation','T3:T40');
```

```
% lf9r_b = xlsread('membrane stretch analysis for publication.xlsx','big
fixation','U3:U40');
% lf9lamda_r = xlsread('membrane stretch analysis for publication.xlsx','big
fixation','V3:V40');
% lf12r_a = xlsread('membrane stretch analysis for publication.xlsx','big
fixation','Y3:Y40');
% lf12lamda_circ = xlsread('membrane stretch analysis for publication.xlsx','big
fixation','Z3:Z40');
% lf12r_b = xlsread('membrane stretch analysis for publication.xlsx','big
fixation','AA3:AA40');
% lf12lamda_r = xlsread('membrane stretch analysis for publication.xlsx','big
fixation','AB3:AB40');
Ris = sfR(1); %microns
Ril = lfR(1);
Ro = 35000;
N = 1000;
%%%%%%%%%%%%%%%%%%%%%%%%%SOLVER%%%%%%%%%%%%%%%%%%
%%%%%%%%%%%%%%%%%%%%
%MOONEY-RIVLIN FIT
c1 = 1;
c2 = 1;
function dy = moonriveq12(x,y)
    trr = 2*c1*(y(2)^2 - 1) + 2*c2*((y(2)*y(1)/x)^2 - 1);
    ttheta = 2*c1*((y(1)/x)^2 - 1) + 2*c2*((y(2)*y(1)/x)^2 - 1);
    dtrr_dlamdatheta = 4*c2*(y(2)^2)*y(1)/x;
    dtrr_dlamdar = 4*c1*y(2) + 4*c2*y(2)*(y(1)/x)^2;
    dy = zeros(2,1);
    dy(1) = y(2); % = r' = dr/dR
    dy(2) = ((y(2)/y(1))*(ttheta - trr) + dtrr_dlamdatheta*((y(1)/x) - y(2))*(1/x))/dtrr_dlamdar
;
      % = r'' = d2r/dR2
      %Eq. 12, D&H 2004
end
ris = Ris;
dr_dRis = 1.2;
[Rs Ys]=ode45(@moonriveq12,[Ris:(Ro-Ris)/(N-1):Ro],[ris dr_dRis]);
   Rs = Rs(:,1);
   rs = Ys(:,1);
   lamda_theta_s = rs./Rs;
   lamda_r_s = Ys(:,2);
ril = Ril;
dr_dRil = 1.12;
[Rl Yl]=ode45(@moonriveq12,[Ril:(Ro-Ril)/(N-1):Ro],[ril dr_dRil]);
   Rl = Rl(:,1);
   rl = Yl(:,1);
   lamda_theta_l = rl./Rl;
   lamda_r_l = Yl(:,2);
%%%%%%%%%%%%%%%%%%FIGURES%%%%%%%%%%%%%%%%%%%%
figure
plot(rl,lamda_theta_l,rl,lamda_r_l)
end
```

C.6 HYDROGEL DEFORMATION DATA FIT (DEFECT CASE)

```
%%%This m-file will fit constitutive parameters for various strain-%%%energy functions
to the experimental gradient data measured for a %%%PEGDA hydrogel with a central
defect.
function [neohook, moonriv, fung, delfino, rivsaw] = gradientfit()
%%%%%%%%%%%%%%%%%%%%GIVEN%%%%%%%%%%%%%%%%%%%%%%%%%%%%%%%%%%%%%%%%%%%%%%%%%%%%%%%%
Rdata = xlsread('gel analysis.xlsx', 'N3:N16'); %Unstretched radial data points.
n = size(Rdata);
Ri = Rdata(1); %Unstretched inner radius of defect (mm)
Ro = Rdata(n);%Outer radius (mm).
   %Note: this doesn't affect graph shapes... only the domain space.
rdata800 = xlsread('gel analysis.xlsx', 'AX3:AX16');
   %Radial position data for 800 steps motion of stepper motor
   rdata800error = xlsread('gel analysis.xlsx', 'AY3:AY16');
   ri800= rdata800(1);
   rdata800b = rdata800(2:n-1);
   rdata800berror = rdata800error(2:n-1);
lambda_theta_data800 = xlsread('gel analysis.xlsx', 'AZ3:AZ16');
   lambda_theta_data800error = xlsread('gel analysis.xlsx', 'BA3:BA16');
lambda_r_data800 = xlsread('gel analysis.xlsx', 'BB4:BB15');
   lambda_r_data800error = xlsread('gel analysis.xlsx', 'BC4:BC15');
lambda_z_data800 = xlsread('gel analysis.xlsx', 'BD4:BD15');
   lambda_z_data800error = xlsread('gel analysis.xlsx', 'BE4:BE15');
%%%%%%%%%%%%%%%%%%%%%%%%%%SOLVER%%%%%%%%%%%%%%%%%%%%%%%%%%%%%%%%%%%%%%%%%%%%%%%%%%
%NEOHOOKEAN FIT
startn = [1 ri800];
[neohook, Errorsumn] = fminsearch(@sumfctnn, startn)
   function [Summationn] = sumfctnn(c)
      c1 = c(1);
      ri = c(2);
      function dy = neohookeq12(x,y)
         trr = 2*c1*(y(2)^2 - 1);
         ttheta = 2*c1*((y(1)/x)^2 - 1);
         dtrr_dlambdatheta = 0;
         dtrr_dlambdar = 4*c1*y(2);
         dy = zeros(2,1);
         dy(1) = y(2); % = r' = dr/dR
         dy(2) = ((y(2)/y(1))*(ttheta - trr) + dtrr_dlambdatheta*((y(1)/x) -
y(2))*(1/x))/dtrr_dlambdar ;
            % = r'' = d2r/dR2
            %Eq. 12, David&Humphrey, 2004
      end
      dr_dRi = 1;
      [Rn Yn]=ode45(@neohookeq12,Rdata,[ri dr_dRi]);
      rn = Yn(:,1);
```

```
        lambda_theta_n = Yn(:,1)./Rn;
        lambda_r_n = Yn(:,2);
        Summationn = sum((lambda_theta_n - lambda_theta_data800).^2) +
sum((lambda_r_n(2:n-1) - lambda_r_data800).^2);
    end
%MOONEY-RIVLIN FIT
startm = [1 1 ri800];
[moonriv,Errorsumm] = fminsearch(@sumfctnm, startm)
   function [Summationm] = sumfctnm(c)
       c1 = c(1);
       c2 = c(2);
       ri = c(3);
       function dy = moonriveq12(x,y)
           trr = 2*c1*(y(2)^2 - 1) + 2*c2*((y(2)*y(1)/x)^2 - 1);
           ttheta = 2*c1*((y(1)/x)^2 - 1) + 2*c2*((y(2)*y(1)/x)^2 - 1);
           dtrr_dlambdatheta = 4*c2*(y(2)^2)*y(1)/x;
           dtrr_dlambdar = 4*c1*y(2) + 4*c2*y(2)*(y(1)/x)^2;
           dy = zeros(2,1);
           dy(1) = y(2); % = r' = dr/dR
           dy(2) = ((y(2)/y(1))*(ttheta - trr) + dtrr_dlambdatheta*((y(1)/x) -
y(2))*(1/x))/dtrr_dlambdar ;
               % = r'' = d2r/dR2
               %Eq. 12, D&H 2004
       end
       dr_dRi = abs(sqrt((c1+c2)/(c1 + c2*(ri/Ri)^2)));
       [Rm Ym]=ode45(@moonriveq12,Rdata,[ri dr_dRi]);
       rm = Ym(:,1);
       lambda_theta_m = rm./Rm;
       lambda_r_m = Ym(:,2);
       Summationm = sum((lambda_theta_m - lambda_theta_data800).^2) +
sum((lambda_r_m(2:n-1) - lambda_r_data800).^2);
   end

%FUNG FIT
startf = [1 1 1 ri800];
[fung,Errorsumf] = fminsearch(@sumfctnf, startf)
    function [Summationf] = sumfctnf(cs)
       c = cs(1);
       c1 = cs(2);
       c2 = cs(2); %This forces isotropy.
       c3 = cs(3);
       ri = cs(4);
       function dy = fungeq12(x,y)
           Q = (c1/4)*(y(2)^2 - 1)^2 + (c2/4)*((y(1)/x)^2 - 1)^2 + (c3/4)*(y(2)^2 -
1)*((y(1)/x)^2 - 1);
           trr = (y(2)^2)*(c/2)*exp(Q)*(c1*(y(2)^2 - 1) + c3*((y(1)/x)^2 - 1));
           ttheta = ((y(1)/x)^2)*(c/2)*exp(Q)*(c3*(y(2)^2 - 1) + c2*((y(1)/x)^2 - 1));
           dtrr_dlambdatheta = (y(2)^2)*(c/2)*exp(Q)*[(2*c3*y(1)/x) + (c2*((y(1)/x)^2 -
1)*(y(1)/x) + c3*(y(2)^2 - 1)*(y(1)/x))*(c1*(y(2)^2 - 1) + c3*((y(1)/x)^2 - 1))];
           dtrr_dlambdar = (y(2)^2)*(c/2)*exp(Q)*[(2*c1*y(2)) + (c3*((y(1)/x)^2 - 1)*y(2) +
c1*(y(2)^2 - 1)*y(2))*(c1*(y(2)^2 - 1) + c3*((y(1)/x)^2 - 1))] + y(2)*c*exp(Q)*(c1*(y(2)^2 -
1) + c3*((y(1)/x)^2 - 1));
           dy = zeros(2,1);
```

```
        dy(1) = y(2); % = r' = dr/dR
        dy(2) = ((y(2)/y(1))*(ttheta - trr) + dtrr_dlambdatheta*((y(1)/x) -
y(2))*(1/x))/dtrr_dlambdar ;
            % = r'' = d2r/dR2
            %Eq. 12, D&H 2004
    end
    dr_dRi = abs(sqrt(1-(c3/c1)*((ri/Ri)^2-1))); %Eq. 16, David & Humphrey 2004
    [Rf Yf]=ode45(@fungeq12,Rdata,[ri dr_dRi]); %R = [Ri:(Ro-Ri)/n:Ro];
%Y = [y(1)                                    %y(2)] = [r dr/dR]
    rf = Yf(:,1);
    lambda_theta_f = rf./Rf;
    lambda_r_f = Yf(:,2);
    Summationf = sum((lambda_theta_f - lambda_theta_data800).^2) +
sum((lambda_r_f(2:n-1) - lambda_r_data800).^2);
  end
%%%DELFINO FIT
startd = [1 1 ri800];
[delfino,Errorsumd] = fminsearch(@sumfctnd, startd)
  function [Summationd] = sumfctnd(cs)
    a = cs(1);
    b = cs(2);
    ri = cs(3);
    function dy = delfinoeq12(x,y)
        expterm = (b/2)*(y(2)^2 + (y(1)/x)^2 - 2);
        trr = a*y(2)^2*exp(expterm) - a;
        ttheta = a*(y(1)/x)^2*exp(expterm) - a;
        dtrr_dlamdatheta = a*(y(1)/x)^2*exp(expterm)*b*y(1)/x;
        dtrr_dlamdar = 2*a*y(2)*exp(expterm) + a*y(2)^2*exp(expterm)*b*y(2);
        dy = zeros(2,1);
        dy(1) = y(2); % = r' = dr/dR
        dy(2) = ((y(2)/y(1))*(ttheta - trr) + dtrr_dlamdatheta*((y(1)/x) -
y(2))*(1/x))/dtrr_dlamdar ;
            % = r'' = d2r/dR2
            %Eq. 12, D&H 2004
    end
        function [zero] = delfinoBC(lamdar)
        zero = (lamdar^2)*exp((b/2)*(lamdar^2 + (ri/Ri)^2 - 2)) - 1;
        end
    range = [0 1.5];
    dr_dRi = fzero(@delfinoBC,range);
    [Rd Yd]=ode45(@delfinoeq12,Rdata,[ri dr_dRi]);
    rd = Yd(:,1);
    lambda_theta_d = rd./Rd;
    lambda_r_d = Yd(:,2);
    Summationd = sum((lambda_theta_d - lambda_theta_data800).^2) +
sum((lambda_r_d(2:n-1) - lambda_r_data800).^2);
  end
%%%RIVLIN-SAWYERS FIT
startrv = [1 1 1 ri800];
[rivsaw,Errorsumrv] = fminsearch(@sumfctnrv, startrv)
  function [Summationrv] = sumfctnrv(cs)
    c1 = cs(1);
    c2 = cs(2);
```

```
      c3 = cs(3);
      ri = cs(4);
      function dy = rivsaweq12(x,y)
          trr = 2*c1*(y(2)^2 - 1) + 2*c2*((y(2)*y(1)/x)^2 - 1) + 4*c3*((y(2)*y(1)/x)^4 -
(y(2)*y(1)/x)^2);
          ttheta = 2*c1*((y(1)/x)^2 - 1) + 2*c2*((y(2)*y(1)/x)^2 - 1) + 4*c3*((y(2)*y(1)/x)^4 -
(y(2)*y(1)/x)^2);
          dtrr_dlambdatheta = 4*c2*(y(2)^2)*y(1)/x + 4*c3*(4*(y(2)^4)*(y(1)/x)^3 -
2*(y(2)^2)*y(1)/x);
          dtrr_dlambdar = 4*c1*y(2) + 4*c2*y(2)*(y(1)/x)^2 + 4*c3*(4*(y(2)^3)*(y(1)/x)^4 -
2*y(2)*(y(1)/x)^2);
          dy = zeros(2,1);
          dy(1) = y(2); % = r' = dr/dR
          dy(2) = ((y(2)/y(1))*(ttheta - trr) + dtrr_dlambdatheta*((y(1)/x) -
y(2))*(1/x))/dtrr_dlambdar ;
              % = r'' = d2r/dR2
              %Eq. 12, D&H 2004
      end
       bc = [2*c3*(ri./Ri)^4 0 c1+(c2-2*c3)*(ri/Ri)^2 0 -c1-c2];
       rts = roots(bc);
       rt_location = 0.1 < rts & rts < 1.1;
       rt = rts(rt_location);
       dr_dRi = max(rt);
       [Rrv Yrv]=ode45(@rivsaweq12,Rdata,[ri dr_dRi]);
       rrv = Yrv(:,1);
       lambda_theta_rv = rrv./Rrv;
       lambda_r_rv = Yrv(:,2);
       Summationrv = sum((lambda_theta_rv - lambda_theta_data800).^2) +
sum((lambda_r_rv(2:n-1) - lambda_r_data800).^2);
  end
%%%%%%%%%%%%%%%%%FIGURES%%%%%%%%%%%%%%%%%%%
figure
hold on
plot(rn,lambda_theta_n,rm,lambda_theta_m,'--',rf,lambda_theta_f,':',rd,lambda_theta_d,'-
.',rrv,lambda_theta_rv,'-
..',rdata800,lambda_theta_data800,'o',rn,lambda_r_n,rm,lambda_r_m,'--
',rf,lambda_r_f,':',rd,lambda_r_d,'-.',rrv,lambda_r_rv,'-..')
   legend('Neo-Hookean','Mooney-Rivlin','Fung','Delfino','Rivlin-Sawyers','Data'),
xlabel('Radial Position(mm)'), ylabel('Stretch Ratio'), title('Data Fits')
   axis([0 35 0.9 1.2])
errorbar(rdata800,lambda_theta_data800,lambda_theta_data800error,'o')
errorbar(rdata800b,lambda_r_data800,lambda_r_data800error,'o')
herrorbar(rdata800,lambda_theta_data800,rdata800error,'o')
herrorbar(rdata800b,lambda_r_data800,rdata800berror,'o')
end
```

C.7 STRETCH PROFILES FOR HYDROGEL EXPERIMENT (DEFECT CASE)

```
%%% This file will plot experimental stretch data and
%%% constitutive model fit for a 3D hydrogel with central defect.
function [delfino] = gradientplots()
%%%%%%%%%%%%%%%%%%%%GIVEN%%%%%%%%%%%%%%%%%%%%%%%%%%%%%%%%%%%%%%%%%%%
Rdata = xlsread('gel analysis.xlsx', 'N3:N16');
n = size(Rdata);
Ri = Rdata(1); %Unstretched inner radius of defect (mm)
Ro = Rdata(n);%Outer radius (mm). Set as radial value of outermost experimental data
point.
   %This doesn't affect graph shapes... only the domain space.
rdata600 = xlsread('gel analysis.xlsx', 'X3:X16');
   %600 refers to 600steps motion of stepper motor.
   ri600= rdata600(1);
   rdata600b = rdata600(2:n-1);
lambda_theta_data600 = xlsread('gel analysis.xlsx', 'Y3:Y16');
lambda_r_data600 = xlsread('gel analysis.xlsx', 'Z4:Z15');
lambda_z_data600 = xlsread('gel analysis.xlsx', 'AA4:AA15');
rdata700 = xlsread('gel analysis.xlsx', 'AK3:AK16');
   ri700= rdata700(1);
   rdata700b = rdata700(2:n-1);
lambda_theta_data700 = xlsread('gel analysis.xlsx', 'AL3:AL16');
lambda_r_data700 = xlsread('gel analysis.xlsx', 'AM4:AM15');
lambda_z_data700 = xlsread('gel analysis.xlsx', 'AN4:AN15');
rdata800 = xlsread('gel analysis.xlsx', 'AX3:AX16');
   ri800= rdata800(1);
   rdata800b = rdata800(2:n-1);
lambda_theta_data800 = xlsread('gel analysis.xlsx', 'AZ3:AZ16');
lambda_r_data800 = xlsread('gel analysis.xlsx', 'BB4:BB15');
lambda_z_data800 = xlsread('gel analysis.xlsx', 'BD4:BD15');
%%%%%%%%%%%%%%%%%%%%%%%%%%SOLVER%%%%%%%%%%%%%%%%%%%%%%%%%%%%%%%%%%%%
%MOONEY-RIVLIN FIT
c1 = 1.6674;
c2 = 0.3965;
results =[];
for ri = [ri600,ri700,ri800];
   dr_dRi = abs(sqrt((c1+c2)/(c1 + c2*(ri/Ri)^2)));
   [Rm Ym] = ode45(@moonriveq12,Rdata,[ri dr_dRi]);
   results = [results Rm Ym];
end
R_600 = results(:,1);
r_600 = results(:,2);
lambda_theta_600 = r_600./R_600;
lambda_r_600 = results(:,3);
lambda_z_600 = 1./(lambda_theta_600.*lambda_r_600);
R_700 = results(:,4);
r_700 = results(:,5);
```

```
lambda_theta_700 = r_700./R_700;
lambda_r_700 = results(:,6);
lambda_z_700 = 1./(lambda_theta_700.*lambda_r_700);
R_800 = results(:,7);
r_800 = results(:,8);
lambda_theta_800 = r_800./R_800;
lambda_r_800 = results(:,9);
lambda_z_800 = 1./(lambda_theta_800.*lambda_r_800);
%%%%%%%%%%%%%%%%%FIGURES%%%%%%%%%%%%%%%%%%
figure
subplot(1,3,1)
plot(r_600,lambda_theta_600,r_600,lambda_r_600,r_600,lambda_z_600,rdata600,lamb
da_theta_data600,'o',rdata600b,lambda_r_data600,'o',rdata600b,lambda_z_data600,'o')
   legend('Lambda_theta','Lambda_r','Lambda_z'), xlabel('Radial Position(mm)'),
ylabel('Stretch Ratio'), title('600 steps')
subplot(1,3,2)
plot(r_700,lambda_theta_700,r_700,lambda_r_700,r_700,lambda_z_700,rdata700,lamb
da_theta_data700,'o',rdata700b,lambda_r_data700,'o',rdata700b,lambda_z_data700,'o')
   legend('Lambda_theta','Lambda_r','Lambda_z'), xlabel('Radial Position(mm)'),
ylabel('Stretch Ratio'), title('700 steps')
subplot(1,3,3)
plot(r_800,lambda_theta_800,r_800,lambda_r_800,r_800,lambda_z_800,rdata800,lamb
da_theta_data800,'o',rdata800b,lambda_r_data800,'o',rdata800b,lambda_z_data800,'o')
   legend('Lambda_theta','Lambda_r','Lambda_z'), xlabel('Radial Position(mm)'),
ylabel('Stretch Ratio'), title('800 steps')
figure
subplot(1,3,1)
plot(r_600,lambda_theta_600,r_700,lambda_theta_700,r_800,lambda_theta_800,rdata6
00,lambda_theta_data600,'o',rdata700,lambda_theta_data700,'o',rdata800,lambda_thet
a_data800,'o')
   legend('600','700','800'), xlabel('Radial Position(mm)'), ylabel('Stretch Ratio'),
title('Circumferential Stretch')
subplot(1,3,2)
plot(r_600,lambda_r_600,r_700,lambda_r_700,r_800,lambda_r_800,rdata600b,lambda_
r_data600,'o',rdata700b,lambda_r_data700,'o',rdata800b,lambda_r_data800,'o')
   legend('600','700','800'), xlabel('Radial Position(mm)'), ylabel('Stretch Ratio'),
title('Radial Stretch')
subplot(1,3,3)
plot(r_600,lambda_z_600,r_700,lambda_z_700,r_800,lambda_z_800,rdata600b,lambda
_z_data600,'o',rdata700b,lambda_z_data700,'o',rdata800b,lambda_z_data800,'o')
   legend('600','700','800'), xlabel('Radial Position(mm)'), ylabel('Stretch Ratio'),
title('Out-of-plane Axial Stretch')
end
```

C.8 SUBROUTINE FOR NEO-HOOKEAN CONSTITUTIVE FIT

```
function dy = neohookeq12(x,y)
c = 0.9733;
trr = 2*c*(y(2)^2 - 1);
ttheta = 2*c*((y(1)/x)^2 - 1);
dtrr_dlambdatheta = 0;
dtrr_dlambdar = 4*c*y(2);
dy = zeros(2,1);
dy(1) = y(2); % = r' = dr/dR
dy(2) = ((y(2)/y(1))*(ttheta - trr) + dtrr_dlambdatheta*((y(1)/x) - y(2))*(1/x))/dtrr_dlambdar
;
   % = r'' = d2r/dR2
   %Eq. 12, D&H 2004
end
```

C.9 SUBROUTINE FOR MOONEY-RIVLIN CONSTITUTIVE FIT

```
function dy = moonriveq12(x,y)
   c1 = 1.6674;
   c2 = 0.3965;
   trr = 2*c1*(y(2)^2 - 1) + 2*c2*((y(2)*y(1)/x)^2 - 1);
   ttheta = 2*c1*((y(1)/x)^2 - 1) + 2*c2*((y(2)*y(1)/x)^2 - 1);
   dtrr_dlambdatheta = 4*c2*(y(2)^2)*y(1)/x;
   dtrr_dlambdar = 4*c1*y(2) + 4*c2*y(2)*(y(1)/x)^2;
   dy = zeros(2,1);
   dy(1) = y(2); % = r' = dr/dR
   dy(2) = ((y(2)/y(1))*(ttheta - trr) + dtrr_dlambdatheta*((y(1)/x) -
y(2))*(1/x))/dtrr_dlambdar ;
      % = r'' = d2r/dR2
      % Eq. 12, D&H 2004
end
```

C.10 SUBROUTINE FOR FUNG CONSTITUTIVE FIT

```
function dy = fungeq12(x,y)
   c = 1.1617;
   c1 = 1.3684;
   c2 = 1.3684;
```

```
    c3 = 0.391;
    Q = (c1/4)*(y(2)^2 - 1)^2 + (c2/4)*((y(1)/x)^2 - 1)^2 + (c3/4)*(y(2)^2 - 1)*((y(1)/x)^2 - 1);
    trr = (y(2)^2)*(c/2)*exp(Q)*(c1*(y(2)^2 - 1) + c3*((y(1)/x)^2 - 1));
    ttheta = ((y(1)/x)^2)*(c/2)*exp(Q)*(c3*(y(2)^2 - 1) + c2*((y(1)/x)^2 - 1));
    dtrr_dlambdatheta = (y(2)^2)*(c/2)*exp(Q)*[(2*c3*y(1)/x) + (c2*((y(1)/x)^2 - 1)*(y(1)/x)
+ c3*(y(2)^2 - 1)*(y(1)/x))*(c1*(y(2)^2 - 1) + c3*((y(1)/x)^2 - 1))];
    dtrr_dlambdar = (y(2)^2)*(c/2)*exp(Q)*[(2*c1*y(2)) + (c3*((y(1)/x)^2 - 1)*y(2) +
c1*(y(2)^2 - 1)*y(2))*(c1*(y(2)^2 - 1) + c3*((y(1)/x)^2 - 1))] + y(2)*c*exp(Q)*(c1*(y(2)^2 -
1) + c3*((y(1)/x)^2 - 1));
    dy = zeros(2,1);
    dy(1) = y(2); % = r' = dr/dR
    dy(2) = ((y(2)/y(1))*(ttheta - trr) + dtrr_dlambdatheta*((y(1)/x) -
y(2))*(1/x))/dtrr_dlambdar ;
        % = r'' = d2r/dR2
        %Eq. 12, D&H 2004
end
```

C.11 SUBROUTINE FOR RIVLIN-SAWYERS CONSTITUTIVE FIT

```
function dy = rivsaweq12(x,y)
c1 = 0.873;
c2 = 1.8479;
c3 = -0.6325;
trr = 2*c1*(y(2)^2 - 1) + 2*c2*((y(2)*y(1)/x)^2 - 1) + 4*c3*((y(2)*y(1)/x)^4 -
(y(2)*y(1)/x)^2);
ttheta = 2*c1*((y(1)/x)^2 - 1) + 2*c2*((y(2)*y(1)/x)^2 - 1) + 4*c3*((y(2)*y(1)/x)^4 -
(y(2)*y(1)/x)^2);
dtrr_dlambdatheta = 4*c2*(y(2)^2)*y(1)/x + 4*c3*(4*(y(2)^4)*(y(1)/x)^3 -
2*(y(2)^2)*y(1)/x);
dtrr_dlambdar = 4*c1*y(2) + 4*c2*y(2)*(y(1)/x)^2 + 4*c3*(4*(y(2)^3)*(y(1)/x)^4 -
2*y(2)*(y(1)/x)^2);
dy = zeros(2,1);
dy(1) = y(2); % = r' = dr/dR
y(2) = ((y(2)/y(1))*(ttheta - trr) + dtrr_dlambdatheta*((y(1)/x) - y(2))*(1/x))/dtrr_dlambdar ;
  % = r'' = d2r/dR2
  %Eq. 12, D&H 2004
end
```

C.12 SUBROUTINE FOR DELFINO CONSTUTIVE FIT

```
function dy = delfinoeq12(x,y)
a = 1.0507;
```

```
b = 0.6561;
expterm = (b/2)*(y(2)^2 + (y(1)/x)^2 - 2);
trr = a*y(2)^2*exp(expterm) - a;
ttheta = a*(y(1)/x)^2*exp(expterm) - a;
dtrr_dlambdatheta = a*(y(1)/x)^2*exp(expterm)*b*y(1)/x;
dtrr_dlambdar = 2*a*y(2)*exp(expterm) + a*y(2)^2*exp(expterm)*b*y(2);
dy = zeros(2,1);
dy(1) = y(2); % = r' = dr/dR
dy(2) = ((y(2)/y(1))*(ttheta - trr) + dtrr_dlambdatheta*((y(1)/x) - y(2))*(1/x))/dtrr_dlambdar
;
   % = r'' = d2r/dR2
   %Eq. 12, D&H 2004
end
```

C.13 THIN-WALL TUB E DEFORMATION ANALYSIS

```
%%%This code follows thin-shell theory to calculate deformations of a %%%tube wall
with a rigid glass insert, during various levels of tube %%%inflation.
function [] =tube_displacement()
%%%GIVEN%%%%%%%%%%%%%%%%%%%%%%%%%%%%%%%%%%%%%%%%%%%%%
%%%%%%%%%%%%%%%%%%%%%%%%%%%%%%%%%%%%%
Ro = 2.625; %undeformed outer radius of tube (in mm)
Ri = 2.2; %undeformed outer radius of tube (in mm)
H = Ro - Ri; %tube thickness far from rigid insert (in mm)
Ri = Ro - H; %undeformed inner radius (in mm)
z_actual = 0:.0001:5; %Actual longitudinal position (in mm)
z = z_actual./Ro; %axial position normalized by outer radius
n = length(z_actual);
stepsize = z_actual(n)/(n-1);
z_long = z_actual(2:n-1);
ri_insert = 3; %inner radius of tube over rigid insert (in mm)
h_insert = -ri_insert + abs(sqrt(ri_insert^2 - H^2 + 2*Ro*H)); %thickness of tube over
insert (in mm)
ro_insert = ri_insert + h_insert; %outer radius of tube over rigid insert (in mm)
Pdia = 0; %Diastolic Intraluminal Pressure (in mmHg)**this value doesn't matter to final
solution.
Psys1 = -102; %Systolic Intraluminal Pressure (in mmHg)
Psys2 = -204;
E = 6255; %Elastic modulus (in mmHg)
%Sidenote: Only ratio of pressure:E matters to solution. If far-field deformation is
measured, these pressures can be varied until desired deformation is achieved. Also,
pressures are given as negative since radial direction is positive inward (following
Gibson derivation [1965].
%%%Baseline
Profile%%%%%%%%%%%%%%%%%%%%%%%%%%%%%%%%%%%%%%%%%%%%%%
%%%%%%
%Diastolic pressure, with rigid insert
```

```
k = sqrt(3*Ro/(2*H));
particular_soln = Pdia*Ro/(E*H);
c = ((ro_insert - Ro)/Ro) + particular_soln;
w = particular_soln - c*cosh(k*z).*cos(k*z) - c*cosh(k*z).*sin(k*z) + c*sinh(k*z).*cos(k*z)
+ c*sinh(k*z).*sin(k*z);
w_actual = Ro*w; %in mm
ro_diastolic = Ro - w_actual; %radial position profile
h_diastolic = ro_diastolic - abs(sqrt(ro_diastolic.^2 + H^2 - 2*Ro*H));
ri_diastolic = ro_diastolic - h_diastolic;
circ_strain_diastolic = -w_actual./Ro;
   der1_dia = diff(w_actual)./stepsize;
   der2_dia = diff(der1_dia)./stepsize;
   h_diastolic_long = h_diastolic(2:n-1);
long_strain_diastolic = -der2_dia.*(-h_diastolic_long/2);
%%%10 percent
stretch%%%%%%%%%%%%%%%%%%%%%%%%%%%%%%%%%%%%%%%%%%%%%%%%%%
%%%%%%%%%%%%%%
%Systolic pressure1, with rigid insert
k = sqrt(3*Ro/(2*H));
particular_soln = Psys1*Ro/(E*H);
c = ((ro_insert - Ro)/Ro) + particular_soln;
w = particular_soln - c*cosh(k*z).*cos(k*z) - c*cosh(k*z).*sin(k*z) + c*sinh(k*z).*cos(k*z)
+ c*sinh(k*z).*sin(k*z);
w_actual = Ro*w; %in mm
ro_sys1 = Ro - w_actual; %radial position profile
h_sys1 = ro_sys1 - abs(sqrt(ro_sys1.^2 + H^2 - 2*Ro*H));
circ_strain_sys1 = -w_actual./Ro;
   der1_sys1 = diff(w_actual)./stepsize;
   der2_sys1 = diff(der1_sys1)./stepsize;
   h_sys1_long = h_sys1(2:n-1);
long_strain_sys1 = -der2_sys1.*(-h_sys1_long/2);

%%%20 percent
stretch%%%%%%%%%%%%%%%%%%%%%%%%%%%%%%%%%%%%%%%%%%%%%%%%%%
%%%%%%%%%%%%%%%%
k = sqrt(3*Ro/(2*H));
particular_soln = Psys2*Ro/(E*H);
c = ((ro_insert - Ro)/Ro) + particular_soln;
w = particular_soln - c*cosh(k*z).*cos(k*z) - c*cosh(k*z).*sin(k*z) + c*sinh(k*z).*cos(k*z)
+ c*sinh(k*z).*sin(k*z);
w_actual = Ro*w; %in mm
ro_sys2 = Ro - w_actual; %radial position profile
h_sys2 = ro_sys2 - abs(sqrt(ro_sys2.^2 + H^2 - 2*Ro*H));
circ_strain_sys2 = -w_actual./Ro;
   der1_sys2 = diff(w_actual)./stepsize;
   der2_sys2 = diff(der1_sys2)./stepsize;
   h_sys2_long = h_sys2(2:n-1);
long_strain_sys2 = -der2_sys2.*(-h_sys2_long/2);
%%%STRAIN
CALCULATIONS%%%%%%%%%%%%%%%%%%%%%%%%%%%%%%%%%%%%%%%%%%%%%%%%
%%%%%%%%%%%%%%%%%%%%%%%%
Wcap_sys1 = ro_sys1 - ro_diastolic;
Wcap_sys2 = ro_sys2 - ro_diastolic;
```

```
circ_strain_Wcap_sys1 = (circ_strain_sys1 - circ_strain_diastolic)./(circ_strain_diastolic
+ 1);
long_strain_Wcap_sys1 = (long_strain_sys1 -
long_strain_diastolic)./(long_strain_diastolic + 1);
circ_strain_Wcap_sys2 = (circ_strain_sys2 - circ_strain_diastolic)./(circ_strain_diastolic
+ 1);
long_strain_Wcap_sys2 = (long_strain_sys2 -
long_strain_diastolic)./(long_strain_diastolic + 1);
circ_stretch_sys1 = circ_strain_Wcap_sys1(2:n-1) + 1;
long_stretch_sys1 = long_strain_Wcap_sys1 + 1;
phi_sys1=asind(real(sqrt((1-long_stretch_sys1.^2)./(circ_stretch_sys1.^2 -
long_stretch_sys1.^2))));
circ_stretch_sys2 = circ_strain_Wcap_sys2(2:n-1) + 1;
long_stretch_sys2 = long_strain_Wcap_sys2 + 1;
phi_sys2=asind(real(sqrt((1-long_stretch_sys2.^2)./(circ_stretch_sys2.^2 -
long_stretch_sys2.^2))));
circ_stretch = circ_stretch_sys1(n-2)
%%%FIGURES%%%%%%%%%%%%%%%%%%%%%%%%%%%%%%%%%%%%%%%
%%%%%%%%%%%%%%%%%%%%%%%%%%%%%%%%%%
figure
plot (z_actual, ro_diastolic, z_actual, ro_sys1, z_actual, ro_sys2)
title('Deformed Tube Profiles'),
ylabel('Tube Wall Radial Position (mm)'), xlabel('Longitudinal Position (mm)'),
legend('Baseline', '10% Strain', '20% Strain')
figure
plot(z_actual, circ_strain_diastolic, z_actual, circ_strain_sys1, z_actual,
circ_strain_Wcap_sys1)
hold on
plot(z_long, long_strain_diastolic,'--', z_long, long_strain_sys1,'--', z_long,
long_strain_Wcap_sys1,'--')
title('Circumferential & Axial Strains'),
ylabel('Strain'), xlabel('Axial Position (mm)'), legend('Dia Circ.', 'Sys1 Circ.', 'Sys1 Wcap
Circ.', 'Dia Axial.', 'Sys1 Axial', 'Sys1 Wcap Axial')
figure
plot(z_long, circ_stretch_sys1, z_long, circ_stretch_sys2)
hold on
plot(z_long, long_stretch_sys1,'--', z_long, long_stretch_sys2,'--')
title('Circumferential & Longitudinal Strains'),
ylabel('Strain'), xlabel('Longitudinal Position (mm)'), legend('10% Circ.', '20% Circ.', '10%
Long.', '20% Long.')
figure
plot(z_long, phi_sys1, z_long, phi_sys2)
title('Angle of Minimal Stretch'), xlabel('Axial Position (mm)'), ylabel('Angle from Axial
Direction (degrees)')
end
```